Sede Amministrativa: Università degli Studi di Padova

Dipartimento di Scienze Cardiologiche, Toraciche e Vascolari

CORSO DI DOTTORATO DI RICERCA IN: Medicina Specialistica "G.B. Morgagni"
CURRICOLO: Neuroscienze
CICLO: XXX

Facio-scapulo-humeral dystrophy: clinical follow-up and role of chromosome X inactivation in female patients

-

SHP2: a novel therapeutic target in MuSK-myasthenia

Coordinatore: Ch.ma Prof. Annalisa Angelini
Supervisore: Ch.ma Prof. Elena Pegoraro

Dottorando: Michelangelo Cao

Acknowledgements

To my supervisor, Professor Elena Pegoraro, for encouraging me “to add a little bit of love and passion” to my work.

To Professor Angela Vincent, for reminding me to think and use my brain.

To Professor David Beeson, for his quiet and reassuring presence.

To Judith, Saif, Pedro, An, Mirela, Richard, Hakan, Susan, and David for being friends instead of just colleagues.

To Dr. Adriana Gagliardi, for having taught me the importance of a broken shell.

To Bobo, for being close despite the distance.

To Mauro and Susanna, for having kept a door open… through which I invaded their home with all my stuff.

To Simon and Irmgard, for still having the patience to listen to my crazy photographic projects.

To Cinzia and Sara, for the ether intoxication.

To Simone and Daniela, for the comfort of an enthusiastic bungalow (oh yeah).

To the Fulvia because, in spite of all the odds, she made it!

To Leila, for learning how to bark in English.

To Mum, for having given me a dream which to believe in.

To the little China girl, for making me happy.

Foreword

This thesis is formed of two different pieces of work and which represent the evolution of my scientific interest during the last three years of studies. The first part consists of a clinical follow-up of facio-scapulo-humeral dystrophy patients and, in a manner, closes a circle that began long time ago when I visited for the first time the same patients for my undergraduate thesis. In the meantime, I started to be interested in laboratory work and this led me to do some basic research projects. As a first bench experience, under the supervision of Professor Elena Pegoraro at my home University of Padova, I selected a cohort of female FSHD patients, most of them already included in the previous follow-up study, and tried to characterise the chromosome X inactivation pattern in order to analyse its role as a genetic modifier for the disease.

During the last years of my residency in Neurology, I was involved in the management of the myasthenia gravis unit of my Department. It was an important and formative experience that started my interest in the disorders of the neuromuscular junction. This, combined with my desire to explore more basic research, led me away from Padova and to Oxford. There, under the expert supervision of Professors Angela Vincent and David Beeson, I have carried out the second project of this thesis on MuSK myasthenia gravis, studying the *in vitro* activity of a potential new therapy able to counteract the pathogenic effects of MuSK antibodies.

These years have been absolutely amazing as I widened my knowledge and perspectives thanks to all the extraordinary people I collaborated with. This thesis would not have been possible without their help and support and I am honoured to have collaborated with each one of them.

Table of contents

- **Part II**

List of Tables

Part I

Part II

List of Figures

Part I

Part II

Part I

Facio-scapulo-humeral dystrophy: clinical follow-up and role of chromosome X inactivation in female patients

Abstract

Facio-scapulo-humeral dystrophy (FSHD) is an autosomal dominant muscular dystrophy characterized by high prevalence and clinical variability. It involves facial muscles, shoulder girdle and, in most severe cases, the lower limbs. Over 95% of patients have a contraction of D4Z4 repeated units on chromosome 4q35 that causes hypomethylation of the region and the overexpression of a toxic factor, *DUX4*. In about 5% of patients, called FSHD2, D4Z4 hypomethylation is due to mutations of *SMCHD1*, a gene involved in the inactivation of chromosome X during embryotic development. The aim of this study was to evaluate the clinical progression of FSHD over a 5-year follow-up using the Clinical Severity Score (CSS), a scale previously validated by the Italian Network for FSHD. Furthermore, considering the role of *SMCHD1* in the epigenetic control of the chromosome X and the differences in severity between genders, the inactivation pattern of the chromosome X was analysed in order to test whether it could represent a genetic modifier of the disease.

The sample consisted of 55 FSHD patients (29 males and 26 females) from the Neuromuscular Centre of Padova. All subjects carried a pathological D4Z4 fragment between 17-40 Kb. Patients who had been evaluated with CSS at T0 were re-evaluated after an average period of 5 years (T1). The score of each muscle region, the total CSS and the MRC score were recorded and compared between T0 and T1.

Chromosome X inactivation was analysed in 38 FSHD1 and 4 FSHD2 females measuring the degree of methylation of the CAG repeated sequence of the androgen receptor gene. Genomic DNA was digested with methylation-sensitive restriction enzymes (*Hpa*II and *Hha*I), amplified by PCR and finally genotyped. 48 healthy individuals were studied as controls and X inactivation patterns were correlated to muscle impairment measured by CSS.

After 6 years of follow-up, the mean CSS difference between T0 and T1, and MRC score at biceps, triceps and tibialis anterior reached significance only in the probands group. There was no difference at shorter follow-up times or between relatives. Disease progression appeared independent of the size of D4Z4 fragment and no differences were found between genders. X-inactivation pattern was normally distributed in patients and controls. There was a moderate linear

correlation between the percentage of X-inactivation and the severity of the shoulder girdle involvement, but not with any other muscle groups.

In conclusion, FSHD symptoms progress slowly over time and, although CSS represents a valuable tool for patient assessment, it lacks sensitivity for the detection of subtle clinical modifications even over a five-year period. Therefore, its use in follow-up appears to be limited. Moreover, the X inactivation pattern in FSHD patients mirrors the normal distribution observed in healthy females and correlates only modestly with the severity of the disease. These latter findings suggest that different genetic regulators are involved in the full phenotypic expression of the disease, and make evaluation of potential therapies difficult.

Chapter 1
Introduction

Facio-scapulo-humeral muscular dystrophy (FSHD – OMIN #158900 - #158901) is one of the most common dystrophies of adulthood. It is inherited with autosomal dominant transmission with a variable severity in its phenotypic expression and clinical severity. The pathological mechanisms that cause FSHD have not been completely unravelled yet and only in recent years has a new pathogenic molecular model, able to explain the disease course and its clinical phenotype, been proposed. These novel insights in the pathogenic pathways of FSHD might be able to lead towards a deeper understanding of its pathophysiology and, hopefully, to new therapeutic approaches.

1.1) Epidemiology

Facio-scapulo-humeral dystrophy, known also as Landouzy-Dejerine syndrome from the names of the French neurologists who described it firsts in 1885, is one of the most common muscular dystrophies of adulthood, second only to myotonic dystrophy. Its incidence corresponds to 10 new cases per 100.000 population per year (Orphanet), but the variability of its phenotypic expression and the presence of paucisymptomatic patients are likely to mean that this is an underestimate.

FSHD has an autosomal dominant inheritance with a penetrance of 95% by the end of the third decade (Lunt et al, 1989; Padberg et al, 2004) although it varies significantly with respect to the genotype of each patient (Ricci et al, 2013). Both genders are affected, but females seem to have a slower progression of the disease, milder phenotype and a higher incidence of asymptomatic carriers compared to males (Zatz et al, 1998; Tonini et al, 2003; Ricci et al, 2013). Most of the cases described in the literature are familial and only 10% are sporadic suggesting that FSHD does not reduce significantly the fertility of the patients or their reproductive function in general.

1.2) Clinical features

FSHD involves selectively and asymmetrically the muscles of the face, that close the eyelids and move the lips (orbicularis oculi and oris respectively), and the proximal scapular girdle. In the most severe cases, there is also an impairment

of the lower limb that starts from the distal legs and progresses proximally with late involvement of the pelvic girdle.

The disease presents a high inter- and intra-family variability with respect to onset, progression and severity of the symptoms. Most frequently, the onset is in the second or third decade but some rare and most severe cases have symptoms at the moment of birth with widespread weakness and hypotonia (congenital FSHD forms).

The orbicular muscles of the face are impaired in the first stage of the disease with weakness in closing eyelids, moving lips and puffing up cheeks (Figure 1A). Generally, muscles of the inferior part of the face are more frequently involved compared to those of the upper part. Symptoms of facial impairment consist of lagophthalmos, that causes an incomplete closure of the eyelids during sleep, inability to whistle and an overall reduction in facial mimicry. Facial weakness affects about 90% of patients but due to mild and symmetrical involvement, patients are often not aware of it (Mul et al, 2016).

The shoulder girdle involvement has been reported in about 80% of FSHD patients (Wang and Tawill, 2016) and the first sign of impairment usually consists of an asymmetric detachment of the scapula from the back (winging scapula, Figure 1B). This is due to the weakness of the trapezius and the dentatus anterior and causes a progressive difficulty in the abduction of the arms. The winging scapula can be observed in the standing rest posture and enhanced by the abduction and flexion of the arm (Figure 1C). The selective muscular hypotrophy determines the characteristic “sloping” shape of the shoulders together with the straight clavicle. Symptoms related to the impairment of the shoulder girdle consists in difficulties to raise the arms above the head and to lift weights. From the shoulder girdle, the weakness spreads to the proximal part of the upper limb involving the biceps and triceps brachii and sparing the deltoid and the distal muscles.

Involvement of the legs and the pelvic girdle usually occur during the later stages of the disease and affect about 20% of patients (Mul et al, 2016). These have an inverse distribution pattern compared to the upper limbs. The muscular weakness starts distally with impairment of the tibialis anterior causing a characteristic foot drop during gait (steppage). Only in the most severe forms of the disease is the pelvic girdle involved causing anserine gait and hyperlordosis

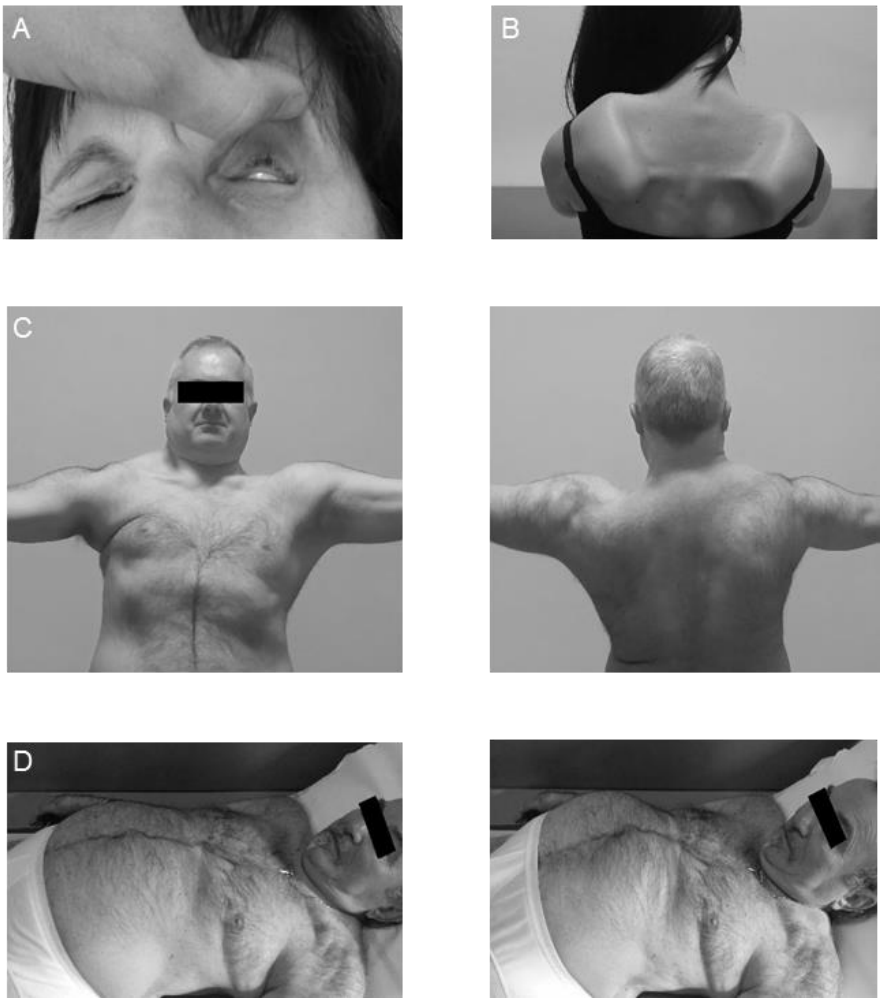

Figure 1. Phenotypic features of FSHD. In A: weakness of orbicularis oculi. In B: severe asymmetric winging scapula. In C: asymmetric winging scapula with impairment of arm abduction. In D: Beevor's sign. The flexion of the head on the chest causes the umbilicus to rise along the mid-line for at least 1 cm.

posture. In these patients, there is an important impairment of both balance and ambulation with necessity to use a wheelchair in some cases.

With respect to the trunk muscles, the inferior rectus abdominis is selectively involved while the superior is usually spared. This asymmetrical impairment of the abdominal muscles causes the characteristic Beevor's sign: the patient is asked to flex his head on the chest from the supine position maintaining, at the same time, the shoulders on the bed. In case of abdominal muscle weakness, the umbilicus will rise upwards along the median line by at least 1 cm (Figure 1D).

Respiratory function is generally normal in FSHD. A restrictive respiratory deficit has been rarely described in very severe patients with a long lasting history of disease and seems to be related to secondary modifications of the shape of the

rib cage more than a direct involvement of the respiratory muscles (Kilmer et al, 1995; Wohlgemuth et al. 2004).

The extraocular muscles, the bulbar district and the heart are selectively spared (Tawill et al. 2006). With respect to cardiac involvement, FSHD patients have been reported to have a higher frequency of atrial tachiarrythmia and alteration in the conduction system although they rarely cause clinical symptoms (Stevenson et al, 1990; Trevisan et al, 2006).

There are some extramuscular signs that, if present in association with the characteristic muscular involvement, could sustain the diagnosis of FSHD. Between 25% and 60% of patients have an acoustic neusosensitive deficit that involve high frequencies. Patients usually are not aware of this impairment but it is easily assessed by an audiometric test (Gieron et al, 1985; Balatsouras et al, 2007). A severe hypoacusis has been described in some cases with juvenile onset (Chen et al. 2013).

The involvement of the ocular retina has a variable frequency. Up to 40% of the patients have retinal microaneurisms and telangiectasia, detectable by fluorescent angiography, in the absence of symptomatic visual deficits (Padberg et al, 1995). In rare cases, retinal involvement can evolve into an exudative retinopathy with characteristica similar to those of Coat's syndrome. This is a severe complication that could result in detachment of the retina and loss of sight or even complete blindness (Statland et al. 2013).

The Central Nervous System can also be affected. Cognitive impairment associated with generalised epilepsy has been described in neonatal patients (Chen et al, 2013). In the more frequent adult forms, brain MRI scans showed slight not-specific alterations concerning the white matter together with hypotrophy of the primary frontal motor cortex on the left side of the brain. None of these changes correspond to detectable signs or symptoms in the patients (Quarantelli et al, 2006).

With respect to the prognosis, disease progression is generally very slow and there is no reduction in life span. On the other hand, in those patient with an early onset, there is relevant impairment of muscle function and, therefore, quality of life can be markedly reduced. About 20% of patients require the wheelchair before the age of 50 (Statland et al, 2013).

The diagnosis is based on the clinical symptoms according to the pattern of muscular involvement and it is confirmed by molecular analysis. Blood tests and other instrumental and histological examinations are not essential to address the correct diagnosis. The blood level of Creatine Kinase (CK) is usually raised by up to 3-5 folds of the normal value. A raised CK level over 1000 U/L is unusual in FSHD and suggests a different diagnosis (Lunt and Harper, 1991). Electromyography shows mild myopathic changes with a concomitant polyneuropathy.

Among all the instrumental tests, muscular magnetic resonance (MR) seems to be the most useful for both diagnosis and clinical follow-up. The Relaxation Time 1 (T1) and Short-tau inversion recovery (STIR) weighted MR images are able to highlight the typical asymmetric involvement of the shoulder girdle and the distal leg that mirrors the muscular weakness observed during the clinical evaluation of the patient. STIR weighted images show that muscle inflammation represents the first detectable change before a rapid substitution of the muscle fibres with fibro-adipose tissue. RMN studies allowed to identify the most involved muscles (specifically the semimembranosus, gluteus minimus, biceps femoris, and the rectus abdominis) and those which are selectively spared (iliopsoas and obturator) (Tasca et al, 2016). Moreover, RMN scans are more sensitive compared to clinical evaluation to detect early signs of involvement in previously healthy muscles. Therefore, RMN could be helpful in detecting paucisymptomatic carriers of the mutations among the population of relatives of the proband (Leung et al, 2015).

1.3) Muscular histopathology

In patients affected by FHSD, the muscle biopsy shows nonspecific and chronic myopathic changes. There is an increase of fibre size variability and central nuclei, with the concomitant presence of atrophic fibres together with normotrophic or hypertrophic ones (Figure 2A). In the most severe cases with early onset and long lasting disease, there is a marked increase of the connective tissue and adipose substitution typical for dystrophic abnormalities (Figure 2B).

Typically, there is no sign of denervation or necrosis, but the expression of proteins related to development such as the foetal myosin isoform and MHC class I suggests the presence of regenerative fibres among the atrophic ones. The high

variability observed within the fibres could be related to the type of muscle sampled. However, there is no correlation between the clinical severity and the histopathologic changes detectable as muscles with substantial weakness can have only minor abnormalities in the muscle biopsy (Dubowitz et al, 2007).

Up to 40% of the biopsies of FSHD patients have a mononuclear inflammatory reaction of the endomysium and, less often, the perivascular areas (Padberg et al,1982). In some cases, the severity of this immune reaction could be confused with a primary inflammatory myopathy (Rothstein et al. 1971). Usually, the immune infiltrate consists mainly of CD8+ T cells and some CD4+ T cells along the blood vessels. There is no inflammatory invasion inside the muscle cells and immune-mediate necrosis has not been observed (Arahata et al, 1995; Frisullo et al, 2011).

Apoptosis seems to be the main cause of cell death in FSHD pathogenesis and could be related to activation of caspase 3, and expression of bax and bcl-2 (Sandri et al, 2001).

Nowadays, considering the typical phenotypic features, the existence of highly sensitive molecular analysis, and the nonspecific histological findings, the role of the muscle biopsy in FSHD diagnosis is limited. Therefore, muscle biopsy should be performed only in those cases with atypical clinical characteristics and when the molecular test results are negative.

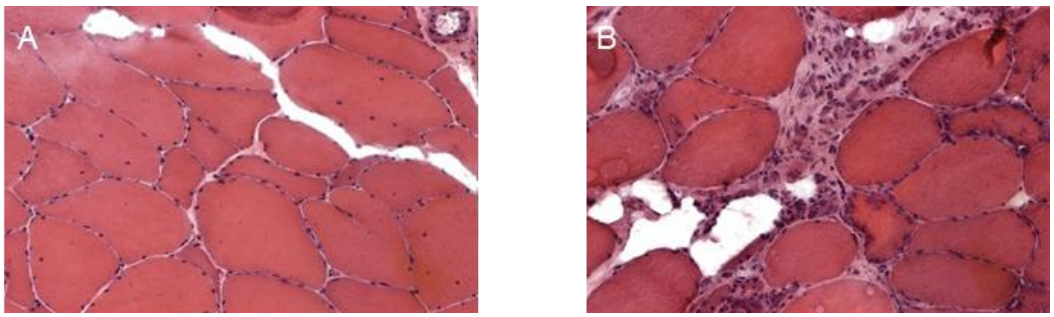

Figure 2. FSHD muscle biopsy features. In A: increased fibre size variability and presence of central nuclei. In B: increased fibre size variability with angulated atrophic fibres and fibro-adipose substitution. H&E x200.

1.4) Molecular genetic

First linkage studies, performed in the 1990s, showed an association of FSHD with the subtelomeric region of the chromosome 4 (4q35) (Upadahyaya et al, 1990; Wijmenga et al, 1990). This is a highly polymorphic region rich in sequences recognised by the restriction enzyme *Eco*RI. The fragment obtained after enzymatic restriction contains the region called D4Z4 that, in healthy individuals, has 12-100 copies of a tandem repeat sequence of 3.3 Kbs. Each tandem repeat is rich in GC and has strict similarities with LSau sequences that are characteristic of heterochromatin. Therefore, under physiological conditions, this region is silenced for genetic transcription because of its highly methylated status.

The molecular probes used to identify the D4Z4 locus in the Fluorescent in situ hybridisation (FISH) assay also identified other associations with different chromosomes, in particular Chr 10 and Y (Hewitt et al, 1994; Winokur et al, 1994). Further linkage analyses did not confirm these results suggesting a cross-reaction of the probes with other sequences similar to the D4Z4 region of 4q35(Gilbert et al. 1995).

Inside each tandem repeat of the D4Z4 region there is an open reading frame (ORF) for the gene *Double Homeobox 4* (*DUX4*), a retrogene that encodes for a transcriptional factor made by two homeobox domains (Hewitt et al, 1994; Gabriels et al, 1999). *DUX4* is normally expressed during the first stages of the embryotic development and then is silenced once the cellular differentiation is complete. In the adult, it remains actively expressed only in testicular tissue. The physiological role of *DUX4* is to regulate the activity of retrotrasposomes and other several genes implicated in cellular differentiation and in the regulation of the immune system (Geng et al, 2012). The first two exons of *DUX4* are inside every tandem repeat but the remaining coding sequences are located downstream of D4Z4. Therefore, only the *DUX4* located in the last tandem repeat is able to generate a full functional transcript (Lemmers et al, 2012).

Additional genetic studies ravelled the presence of two different haplotypes in the subtelomeric region of chromosome 4q, called 4qA and 4qB (Lemmers et al, 2002), evenly distributed among the population. These two variants differ in several minor polymorphisms located in different parts of the D4Z4 (either proximally, distally and inside the tandem repeats). However, the most important

region is the distal one as it contains, in the 4qA haplotype, a pLAM sequence with a polyadenylation signal. This sequence is absent in the 4qB variant. A strong association with the disease has been confirmed only for the 4qA polymorphism (Thomas et al, 2007). In addition to these two main haplotypes, 9 other minor polymorphisms have been reported, but only a few of them (known as 159, 161 and 168) seem to be significantly correlated with FSHD and they always require the combined presence of the major haplotype 4qA (Lemmers et al, 2007; Spurlock et al, 2010).

Further clues to the likely roles of the different haplotypes in the pathogenic mechanisms of the disease come from the translocation analyses between chromosome 10 and 4. The D4Z4 tandem repeats of the 4q35 have a high degree of homology, up to 98%, with 10q26. These two loci have a high frequency of reciprocal translocation but, downstream the tandem repeat, the region in 10q26 lacks the entire haplotype A, that remains characteristic of the chr. 4q35. Mutations of 10q26 are not associated with FSHD. These data suggest that, considering the similarities of the two chromosome regions, only the particular configuration of the different haplotypes on chromosome 4 is able to trigger the pathological mechanisms that cause the disease (van Deutekom et al, 1996; Lemmers et al, 1998; Lemmers et al, 2010).

The homology between the D4Z4 and the region on 10q26 requires a complex protocol in order to identify only the sequences of the chromosome 4. Samples undergo double digestion with two different restriction enzymes: the first digestion is done by *Eco*RI while the second by *Bln*I. The latter is able to cut specifically the sequences of the chromosome 10q leaving intact the D4Z4 fragment from 4q (Deidda et al, 1996). After the enzymatic restriction, the final stage of the genetic analysis consists of pulse-field electrophoresis (PFGE) to identify the size of D4Z4 fragment and the number of tandem repeats.

95% of FSHD patients carry a D4Z4 fragment shorter than 38 Kb that corresponds to a number of tandem repeats lower than 10. A D4Z4 fragment with a size between 38 and 41 Kb (10 – 11 tandem repeats) is considered borderline (Wijmenga et al, 1994; Van Deutekom et al, 1993; Upadhyaya et al, 1997). Monosomy of 4q is not associated with the disease and it is necessary to show at least 1 tandem repeat to have a clinical manifestation of FSHD (Tupler et al, 1996).

Initially, the first molecular studies focused on the identification of a specific gene located near the D4Z4 region, on the assumption that the depletion of the tandem repeat could determine a dysregulated expression. It was observed that in the presence of a pathological D4Z4 contraction there was a corresponding reduction in the methylation degree of the entire region (de Greef et al, 2007). DNA methylation of cytosine residues is one of the most relevant epigenetic modification that regulates gene expression. Methylated genes are usually silenced due to a closed chromatin conformation (heterochromatin) that avoid the binding of the transcription complex to the DNA helix. In FSHD, the reduction of methylation degree due to D4Z4 contraction, is thought to induce a conformational change of the chromatin (from heterochromatin to euchromatin) with the suppression of gene silencing. Several genes located upstream of the 4q35 region, such as *FRG1*, *FGR2* and *ANT1*, has been identified and proposed as potential candidates in the pathogenicity of the disease (Van Deutekom et al, 1996, Gabellini et al, 2002, Rijkers et al, 2004). However, none of them has been confirmed to be dysregulated nor to have a significant pathogenic effect. Although the overexpression of *FRG1* is associated with the development of a muscular dystrophy in an animal model, this activation does not occur in FSHD patients compared to the control population (Jiang et al, 2003; Winokur et al, 2003).

The recent identification of the gene *DUX4* inside the D4Z4 tandem repeats and the association of the disease with the haplotype 4qA have contributed significantly to the formulation of the current and most recognised pathogenic hypothesis. The contraction of the D4Z4 fragment determines the reduction in methylation of the entire region with a consequent relaxation in the chromatin status. Therefore, gene expression is reactivated with an enhanced transcription of *DUX4*, previously silenced. However, in order to allow the correct expression of *DUX4*, the contraction of the D4Z4 fragment is not sufficient but the sequences downstream of the tandem repeats must contain also the third exon of *DUX4* and the pLAM polyadenylation sequence of the 4qA haplotype. Only if all these conditions are fulfilled, could the expression of the *DUX4* gene of the last tandem repeat generate a complete and stable mRNA with an efficient protein translation (Lemmers et al, 2010, Lemmers et al, 2012) (Figure 3A, B).

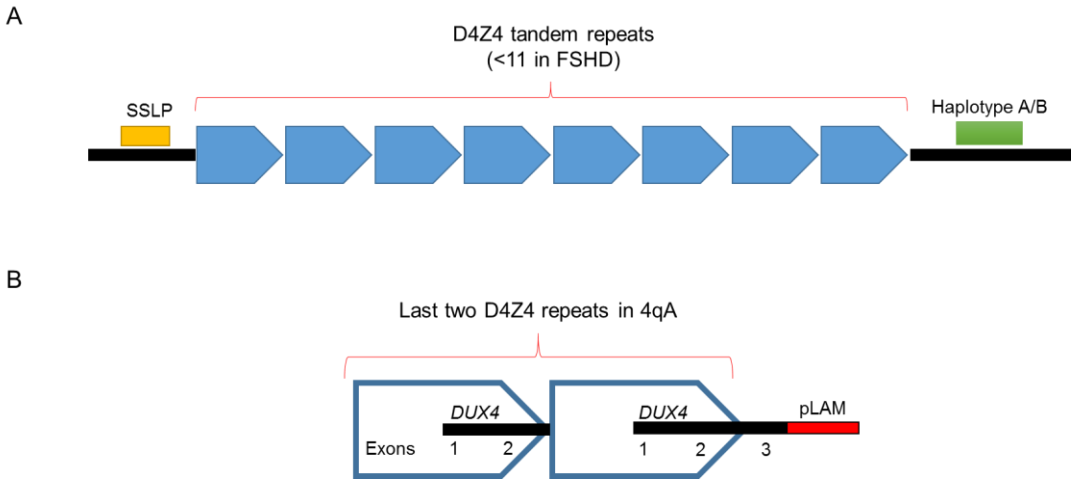

Figure 3. Schematic representation of the subtelomeric region 4q35. In A: structure of the D4Z4 locus formed by several tandem repeats. Upstream and downstream of the D4Z4 there are the SSLP polymorphisms and the haplotypes 4qA/B respectively. A number of tandem repeats lower than 11 is considered pathological and has been associated with FSHD. In B: each tandem repeat contains the first two exons of *DUX4*. The third *DUX4* exon and the polyadenylation sequence pLAM are present only in the haplotype A and they are needed for the expression and stabilisation of the *DUX4* transcript. In the presence of the permissive haplotype 4qA, the contraction of the D4Z4 fragment seems to determine the hypomethylation of the whole region with the consequent overexpression of *DUX4*, leading to toxicity and cell death through apoptosis.

The overexpression of *DUX4* should cause a toxic effect on the muscle due to the activation of different pathways leading to cell damage and apoptosis. Under physiological conditions, *DUX4* has a role in the differentiation of the muscle tissue and its overexpression determines the transcription of several genes involved in the post-transcriptional processes of proteins, such as splicing factors and ubiquitin ligase, and mediators of the inflammatory response (Geng et al, 2012). *In vitro* studies on myoblasts collected from FSHD biopsies showed an increase in the expression of the transcriptional factor *PITX1* mediated by *DUX4* (Dixit et al, 2007) and p53 induced apoptosis has also been reported (Kowaljow et al, 2007; Wallace et al, 2011). The apoptosis phenomenon could be related to the induction of the differentiation programme on the adult muscle by *DUX4* (Endo et al. 1998). Moreover, the alteration of the protein expression pattern caused by the abnormal transcription of splicing and ubiquitin proteins could determine protein catabolism and muscular atrophy. Finally, the activation of other regulator proteins, such as DEFB103, could reduce myoblast regeneration and antigen

tolerance with the induction of local inflammatory reaction observed in some muscular biopsies (Geng et al, 2012; Semple et al, 2011).

However, expression studies of *DUX4* on muscle biopsies have given controversial results. Snider and colleagues reported that *DUX4* RNA was detected in all individuals carrying a permissive allele, regardless of their clinical phenotype. However, only subjects expressing a full length splicing variant of DUX4 (DUX4-fl) have been reported to express the phenotype whereas shorter splicing variants (DUX4-s) do not seem to be correlated with clinical symptoms. In a different study, however, DUX4-fl was not detectable in some FSHD patients with full phenotype expression while a minority of unaffected individuals expressed DUX4-fl, even though they did not have contracted D4Z4 fragment (Jones et al, 2012).

Other epidemiologic evidences further challenged the supposed indispensable role of *DUX4* in the pathogenic development of FSHD. The Italian Consortium for FSHD have found that the genetic signatures of FSHD (such as the presence of a permissive 4qA haplotype and the D4Z4 fragment contraction) are present in more than 1% of the unaffected population (Scionti et al, 2012). Moreover, some patient with classical phenotypes carry a non-permissive 4qB haplotype whilst some relatives of FSHD patients who do not show any clinical sign of the disease, still have an increased expression of *DUX4*. These observations suggest that the actual pathogenic model is far from comprehensive and further mechanisms of damage, independent of *DUX4*, are necessary for the development of the disease (Jones et al, 2012).

1.5) FSHD2

Between 5% and 10% of FSHD patients do not have a pathological contraction of D4Z4 fragment. These patients called FSHD2, are phenotypically indistinguishable from those who carry the D4Z4 contraction. Most of FSHD2 patients present as sporadic cases, but both dominant and recessive inheritance have been reported in familial cases (de Greef et al, 2010). In FSHD2, the D4Z4 region has a normal size and number of tandem repeats but, similarly to FSHD1, is significantly hypomethylated. (de Greef et al, 2007). As previously described above, in addition to the impairment of methylation degree, FSHD2 also requires the presence of a permissive 4qA haplotype on at least one chromosome 4 to be

manifested. This suggests that both FSHD1 and FSHD2, despite the original cause of D4Z4 hypomethylation, have a common final pathogenesis (de Greef et al, 2009).

Next Generation Sequencing analyses in FSHD2 families showed, in some, an association with heterozygous mutations on the gene *Structural Maintenance of Chromosomes Flexible Hinge Domain Containing 1* (*SMCHD1*) located on the chromosome 18p11.32. *SMCHD1* is a physiological regulator of CpG methylation and plays a significant role in epigenetic silencing of chromosome X during the embryogenesis (Blewitt et al, 2008; Gendrel et al, 2012). *SMCHD1* is able to bind and maintain the heterochromatinic status of the D4Z4 repeats. In FSHD2, detrimental mutations of *SMCHD1* cause the loss of its binding with D4Z4 tandem repeats with consequent chromatin relaxation and derepression of *DUX4* (Lemmers et al, 2012).

Some FSHD patients with a particularly severe phenotype have been reported to carry both the contraction of D4Z4 and *SMCHD1* mutations. Therefore, *SMCHD1* could play an important role as a genetic modifier of the disease (Sacconi et al, 2013; Larsen et al, 2015).

1.6) Genotype-phenotype correlations

Several studies have tried to find correlations between the size of D4Z4 fragment and the severity of FSHD clinical symptoms. The deletion of the entire D4Z4 region from both chromosomes is not lethal and, as mentioned above, the presence of at least one tandem repeat is necessary in order to have expression of the phenotype (Tupler et al, 1996). Some studies pointed out that the smaller the size of D4Z4 fragment, the earlier the age of onset and loss of ambulation (Zatz et al, 1995; Lunt et al, 1995). In particular, a number of tandem repeats <3 determine an infantile onset of the disease, sometimes just after birth, together with extramuscular involvement such as cognitive impairment, epilepsy, Coat's syndrome and severe hypoacusis (Chen et al, 2013). With respect to D4Z4 fragments with a higher residual number of tandem repeats, the correlation with the severity of clinical expression is still controversial, as different studies showed incongruous results (Tawill et al, 1996; Butz et al, 2003; Tonini et al, 2003).

Although FSHD is inherited with autosomal dominant transmission, there is evidence suggesting different expression of the phenotype between males and

females. A higher number of asymptomatic females have been reported to carry pathological D4Z4 mutations and, in general, females show slower disease progression compared to males (Zatz et al, 1998). A recent study showed that the differences between the two genders in terms of age of onset and severity of symptoms are significant only during the female fertile period. On the other hand, males and females have the same phenotype expression during pre-puberty and post-menopause, suggesting an important role of female hormones as a protective factor in the development of symptoms (Ricci et al, 2013).

Patients who carry the D4Z4 mutation in mosaic usually have a milder phenotype or are completely asymptomatic according to the percentage of muscle cells that have inherited the mutation (Lemmers et al, 2004).

Controversial evidences have been reported regarding the expression severity in the presence of compound heterozygous (double fragment). Some studies showed that the presence of two pathogenic D4Z4 fragments did not result in an increased severity of symptoms (Wohlgemuth et al, 2003; Tonini et al, 2004). However, other reports pointed out an increased percentage of symptomatic patients and a more severe phenotype in patients who are compound heterozygous (Scionti et al, 2012).

Conversely to other inherited diseases associated with alterations in tandem repeats, FSHD does not show the phenomenon of anticipation. In first studies, this phenomenon was suggested on the evidence that the offsprings of FSHD patient seemed to be more severe compared to their parents (Zatz et al, 1995). However, futther studies did not confirm this preliminary hypothesis (Flaningan et al, 2001) and, moreover, there is no evidence of an instability of the D4Z4 tandem repeat that could explain anticipation of the symptoms towards generations.

1.7) Therapy

There is no pharmacological treatment able to cure or stop the progression of FSHD. An early study with prednisolone, performed on patients with an inflammatory reaction in the muscle biopsy, showed a brief and unsustained benefit with a mild improvement of muscle strength (Munsat et al, 1972). A further trial with the administration of steroids for 12 consecutive weeks did not show any improvement or significant modification of the symptoms (Tawill et al, 1997). An oral β2 agonist (albuterol) was tested in two different trials (Kissel et

al. 2001, Van der Kooi et al. 2004) but again did not have any significant improvement except for a mild increase in the muscular trophism.

Following the new insights on the molecular pathogenic mechanisms responsible for the development of the disease, there are novel potential molecules that could be specifically targeted with a more pharmacological compound in order to reduce *DUX4* expression. However, at the moment, we do not have any drugs able to modify or regulate the conformation of the chromatin required to silence the genes overexpressed in FSHD. Moreover, this kind of compound would increase significantly the high risk of tumours. On the other hand, the pathways downstream of *DUX4* are not established enough to develop a specific treatment. The development of micro-RNAs able to block the activity of the messenger RNA of *DUX4*, altering its splicing and reducing its stability, appears to be the most viable and safe way to achieve a pharmacological treatment (Tawil et al, 2014). A recent *in vitro* study showed that siRNAs directed against *DUX4* coding region, 3′UTR, and *DUX4* promoter were effective in reducing both DUX4 and DUX4-target gene expression and in initiating epigenetic silencing of *DUX4* expression (Lim et al, 2015). Moreover, morpholino oligonucleotides that specifically target the pLAM sequence significantly decreased expression of several *DUX4* target genes (Chen et al, 2016). These findings are encouraging and raise the possibility that RNA-based therapies may be effective in future FSHD treatment.

Physiotherapy remains one of the most important therapeutic approaches for FSHD patients, due to its effectiveness in slowing down disease progression and in maintaining muscular trophism. There is evidence that a mild aerobic exercise, if performed regularly, is able to reduce fatigue and prolong physical tolerance (Olsen et al. 2005). Other therapies include orthopaedic aids, useful in ameliorating ambulatory performance and, only in a few selected cases, the fixation of the scapula in order to reduce the limitation of arms abduction.

Aims of the study

Facio-Scapulo-Humeral muscular dystrophy is characterised by a high variability in its phenotype expression. Moreover, despite its inheritance through autosomal dominant transmission that would imply a similar expression in both genders, important differences have been reported in disease severity between males and females.

Considering the variability in phenotypic expression and the lack of reliable tools to predict the progression of the disease, in the first part of the study, the FSHD cohort of Padova was evaluated at 5 years from the first visit. A clinical evaluation scale, named CSS (Clinical Severity Score), created and validated in 2007 by the Italian Network for FSHD, was used to test and quantify the muscular involvement of the patients in both the first (T0) and second evaluations (T1). Therefore, the first aim of my study was to quantify the progression and the residual muscular function of FSHD patients and, at the same time, to verify the sensitivity and the utility of the CSS as a reliable tool in the clinical follow-up.

The second part of the study was focused on the identification of possible genetic modifiers of the disease. *SMCHD1* mutations have been proven to be responsible for a large proportion of FSHD2 cases and to increase FSHD1 severity in patients who carry a concomitant D4Z4 contraction. *SMCHD1* is also known to play a significant role in the epigenetic silencing of chromosome X in the early phases of female embryonic development. For these reasons, I tested for *SMCHD1* mutations in the patients who were negative in a previous D4Z4 analysis to study the inactivation pattern of chromosome X in FSHD1 and FSHD2 females in order to see whether it could represent a genetic modifier of the disease.

Chapter 2
Materials and Methods

2.1) Patient population

For the follow-up study, FSHD patients were selected among those who were first evaluated between 2008 and 2013. 55 cases were identified, including 23 probands (42%) and 32 relatives (58%). All of them carried a pathological D4Z4 fragment, ranging between 19 and 40 Kbs. The probands consisted of 14 males (41%) and 9 females (39%) while, in the relatives, there were 15 males (47%) and 17 females (53%). The relatives group was further subdivided between "symptomatic" (n=13; 40.6%) and "asymptomatic" (n=19; 59%). Both the first (T0) and the follow-up (T1) evaluations were performed by the candidate minimising the inter-observer bias.

SMCHD1 mutations and D4Z4 methylation analyses were performed in 9 patients (4 males and 5 females) presenting typical FSHD features and previously found negative for the D4Z4 contraction.

With respect to the chromosome X inactivation study, the 42 FSHD female patients whose DNA was available were studied. 38 of them were FSHD1, carrying a D4Z4 fragment with a range between 19 and 40 Kbs. Two patients were compound heterozygous with a reduced D4Z4 fragment in both alleles. The remaining 4 patients were FSHD2 with pathogenic mutations in *SMCHD1*. The average age of FSHD1 patients were 51 ± 15 years, while FSHD2 patients were 49 ± 21 years. 48 healthy individuals, with an average age of 38 ± 14, were used as controls.

2.2) Clinical evaluation of the patients

The Clinical Severity Score (CSS), a scale created and first validated by the Italian Network for FSHD in 2007 (Lamperti et al, 2010), was used to quantify disease severity and to compare the two clinical evaluations in a standardised manner.

The CSS consists in an objective clinical examination of the patient and evaluates all the 6 major muscular districts involved in FHSD (face, shoulder girdle, proximal arm, pelvic girdle, distal leg and abdominal muscles) in a

quantitative and functional way. The strength of each muscle is quantified by the Medical Research Council (MRC) score.

The function of the facial muscles is evaluated asking the patient to perform specific facial movements such as closing eyes, puff out cheeks and protrude lips. The ability of the patient to do all the different actions is classified as "normal", "partial" or "abolished" depending on the degree of complete the movement required in the presence and in the absence of the examiner's resistance.

The function of the shoulder girdle is evaluated through the patient's ability to abduct the upper limbs in the frontal plane with a complete extension of the arms. The function is considered normal if the patients are able to clap their hands over their head. A complete but abnormal function is defined by the necessity to use compensatory actions to fulfil the task such as flexing the elbows or rotating forward the shoulders. If the patient is not able to complete the movement, the score would depend on the degree of arm abduction (higher or lower than 45°).

The ability to rise from a chair and to climb 4 steps are the movements evaluated for the pelvic girdle function. The score will be given according to the necessity of support and to the time needed (cut-off of 12 seconds) to complete the different actions.

The function of the lower limbs is evaluated through the observation of the gait, the ability to walk on both tiptoes and heels and the necessity to use the wheelchair with either manual or electric control.

The strength of several muscles is tested by the MRC score. The following muscles of upper and lower limbs are evaluated: biceps and triceps brachii, arm extrarotators, fingers' flexors and extensors, wrist's flexors and extensors, quadriceps femoris, and tibialis anterior.

The involvement of the abdominal musculature is evaluated by the presence or absence of the Beevor's sign (upward movement of the umbilicus on the median line when the patient rises his head on the chest in supine position).

Finally, the presence of winging scapula, asymmetrical hypotrophy, sloping shoulders, and straight clavicula are considered in the final evaluation of the patient.

The results of the score of each muscule region are then added together in order to obtatin a final comprehensive mark corresponding to the Clinical Severity Score - *CSS*. Thus the final score is calculated as following:

1) *facial waekness*:

0: no weakness;

1: partial ability to do at least one of the following tasks:

- to close eyes
- to protrude lips
- to puff out cheeks

2: severe weakness. Unable to do at least one of the previous tasks.

2) *Scapular girdle involvement*:

0: no invovement

1: mild involvement with no limitation of arm abduction

2: arm abduction > 45

3: arm abduction ≤45°

3) *Upper limbs involvement*:

0: no involvement

1: at least two muscles affected with MRC >3

2: at least two muscles with MRC ≤3

4) *Legs involvement*

0: no involvement

1: unable to walk on tiptoes or heels (only one task impaired)

2: unable to walk on tiptoes and heels (two tasks impaired)

5) *Pelvic girdle involvement*

0: no involvement

1: able to walk and to climb stairs without support but abnormally/ because of posterior leg muscle hypotrophy

2: able to walk unaided, to climb stairs or to stand up from a chair with support

3: able to walk unaided but unable to stand up from a chair or to climb stairs without support/ more than 12 seconds

4: able to walk with support

5: wheelchair bound

6) *Abdominal muscle involvement*

0: no involvement

1: presence of Beevor's sign

The final score varies from 0 to a maximum of 15 points. A score equal to 0 corresponds to the complete absence of symptoms. A score between 1 and 4 indicates a mild form of the disease while a score between 5 and 10 is consistent with a moderate impairment. Finally, a severe disease reaches a CSS of 11-15.

The CSS was used to standardise the evaluation of all the patients of the study.

2.3) Molecular analyses

Genetic analyses for the detection and methylation degree of D4Z4 fragment, 4qA and 4qB haplotypes, and for *SMCHD1* mutations were performed by the Miogen laboratory at the University of Modena and Reggio Emilia by the group of Professor Rossella Tupler, and at the Centre de référence des maladies neuromusculaires of Nice by the group of Professor Sabrina Sacconi. The following methods were previously described (Scionti et al 2012; Lemmers et al, 2012) and are reported here in order to provide the laboratory details underlying the clinical follow-up and the characterization of FSHD2 patients of this study.

Genomic DNA from each patient was extracted from peripheral blood leucocytes using standard techniques and then digested by the restriction enzymes *Eco*RI, *Eco*RI*/Bln*I and *Xap*I (p13E-11 probe). Digested DNA samples were separated using pulse-field gel electrophoresis (PFGE) in a 1% agarose gel. To estimate the dimension of the D4Z4 fragment size, 7 µg of digested DNA were hybridised with the probe p13E-11 and subjected to electrophoresis in 0.4% agarose gel for 45-48 hours at 35 V together with a marker of 8-48 Kb (Bio-Rad). In order to identify the chromosomal origin of D4Z4 (chr. 4 vs chr. 10), DNA samples underwent a second enzymatic digestion with the restriction enzyme *Not*I and were then hybridised with the probe B31. The digested fragments were then identified by autoradiography or the Typhoon Trio® system (GE Healthcare).

The haplotypes 4qA and 4qB were studied by PFGE followed by Southern blot and hybridisation of 7 µg DNA, previously digested with the restriction enzyme *Hind*III, with radioactive probes for the sequences of 4qA/4qB. The chromosome

attribution of the two haplotypes was performed evaluating the dimension of the fragment after enzymatic digestion with *Eco*RI, as previously described.

For the identification of the simple sequence length polymorphisms (SSLPs) and the pLAM SNP (AT(T/C)AAA) sequence, adjacent to the D4Z4 tandem repeats, the single D4Z4 alleles, separated by linear electrophoresis from DNA samples, were digested by *Eco*RI. The SSLP sequence was then determined by PCR amplification using specific oligonucleotides (forward primer 5'-GGTGGAGTTCTGGTTTCAGC-3' marked with hexachlorofluorescein [HEX], reverse primer 5'-CCTGTGCTTCAGAGGCATTTG-3').

The pLAM sequence analysis was performed through PCR amplification using specific oligonucleotides (forward primer 5'-ACGCTGTCTAGGCAAACCTG-3', reverse primer 5'-TGCACTCATCACACAAAAGATG-3'). The differences between the size of SSLPs and pLAM sequences were determined using the program ABI Prism 3130 Genetic Analyzer.

To study the degree of methylation of the D4Z4 region, genomic DNA underwent double enzymatic digestion by restriction enzymes *Eco*RI and *Bgl*I, run overnight at 37ºC and finally purified through specific PCR column extraction. Once the purified DNA sample was obtained, it was further digested with the enzyme *Fse*I for 4 hours, separated by 0.8% agarose gel and probed with a radioactive p13E-11 probe on Southern blot. The radioactive signal of the probes was quantified by Image Quant software. The % ratio of the radioactive signal values between the methylated fragments of 4061 bps and the non-methylated fragments of 3387 bps corresponds to the proportion of methylated *Fse*I sites.

SMCHD1 analysis was performed using either Sanger mutational analysis or Southern blot deletion assay. The mutational analysis was done by performing the Sanger sequencing on all the 48 exons of the gene using intronic primers and annealing sequences of at least 50 nucleotides from donator or acceptor splice sites. 5' and 3' non-coding sequences were not included. The genomic sequence of *SMCHD1* was obtained by Ensemble (build 37) [GRCh37:18:2655286:2805615]. The pathogenicity of SMCHD1 mutation was predicted by SIFT and GVGD Align software.

Deletions of the *SMCHD1* gene were studied using a hybridisation method based on the Southern blot technique. 5 µg of genomic DNA were digested by the restriction enzymes *Eco*RV o *Bam*HI (MBI ferments) followed by 2 cycles of

PFGE on 0.85% agarose gel at 8.5V for 16 hours. The time-lapse between the cycles was increased progressively from 1 second to 2 seconds in the final stages. PFGE was performed in 0.5xTBE buffer supplemented with 150 ng/ml ethyl bromide at 20°C. Southern blot was hybridised overnight at 65°C with a cDNA probe of *SMCHD1* that binds all the 48 exons of the gene, and then washed three time for 10 minutes in SSC and 0.1% SDS at 65°C. The blots were finally developed and analysed with Image Quant® software (Molecular Dynamics).

2.4) Chromosome X inactivation analysis

This part of the study and the related laboratory techniques were performed and developed directly by the candidate. The methylation status of the CAG repeated sequences of the androgen receptor (AR) gene was used to determine the pattern of chromosome X inactivation as it correlates with the methylation of the entire chromosome (Allen et al, 1992).

About 15 ml of blood were collected in EDTA tubes from the patients and DNA was extracted from peripheral leucocytes by phenol-chloroform method. An equivalent amount of lysis buffer (0.77 M NH_4Cl, 46 mM $KHCO_3$) was added to the samples and then spun at 4000 rpm for 15 min in order to lyse the erythrocytes. Supernatant was discharged and the whole procedure was repeated other two times until the pellet became clearer. In order to lyse the leucocytes, the pellet was incubated with to a second lysis buffer (100 mM NaCl, 25 mM EDTA, 500 µl 20% SDS, 1 mg/ml Proteinase K) and mechanically destroyed by pipetting. After overnight incubation at 37ºC, an equal volume of phenol, saturated with 0.1 M TrisHCl, was added to the samples and followed by mixing and spinning at 4000 rpm for 15 min. The surpernant was removed and another equal volume of phenol was added repeating the last steps 5 times. Two times of the original volume of 100% ethanol were added to the solution together with 1 µl of 4 M ammonium acetate, followed by gently shaking to precipitate the DNA. After spinning at 3000 rpm for 5 min, the 100% ethanol was carefully removed and 500 µl of 70% ethanol were added to the DNA. Finally, after the last spinning at 4000 rpm for 15 min, the 70% ethanol solution was removed and the DNA pellet left to air-dry before dissolve it in 500 µl of sterile water.

The methylation analyses were performed on two DNA samples of 100 ng/µl. One DNA sample was restricted for 2 hours at 37°C with 10 U of two different

methylation sensitive restriction enzymes, *HpA*II and *HhA*I. The second sample was incubated under the same condition without the restriction enzymes. In order to stop the action of the restriction enzymes, samples were incubated at -20ºC for at least one hour. Finally, in order to purify the DNA, 30 µl of phenol-chloroform were added to the samples, spun at 15000 rpm for 2 minutes and then washed twice with 80 µl of ether. Purified DNA samples were amplified through semi-quantitative PCR (forward primer 5'-TCCAGAATCTGTTCCAGAGGCGTG-3', reverse primer 5'-GCTGTGAAGGTTGCTGTTCCTCAT-3'). Efficacy of PCR amplification was tested by electrophoresis of the samples in 2% agarose gel. Finally, the samples were genotyped with capillary electrophoresis (ABI 3100 DNA Sequencer, Applied Biosystems, Foster City, CA). Peak Scanner® software was used to analyse genotyping results.

To obtain the methylation degree of the two X chromosomes, the ratio between the height of the peaks of each restricted alleles was compared to those of the non-restricted alleles. Chromosome X inactivation was considered skewed if the ratio between the peaks was greater than 80% (Amos-Landgraf et al, 2006).

2.5) Statistical analysis

In the follow-up study, Student's t was used to compared independent groups with variables with normal distribution while ANOVA multiple comparison was used when the groups were more than two. Ordinal variables were analysed by Mann Whitney U test while non-correlated variables by χ^2. For repeated values with normal distribution (T0 – T1), repeated measures ANOVA analysis was performed in ordert to compare the three different groups (probands, asymptomatic and symptomatic relatives). One-way ANOVA was used to test the difference between ordinal variables at T0 and T1 among the three groups. In case of positivity, single group couples were further analysed by Mann-Whitney U test. Correlations between the D4Z4 size and all the other variables were tested through Spearman's rho as the dimension of D4Z4 did not show a normal distribution. The Saphiro-Wilk test was used in the chromosome X inactivation study to analyse whether the population of patients and controls were normally distributed. Correlations between the percentage of X inactivation, total CSS and the scores of each muscle district were tested through Spearman's rho. Statistical significance was set at $p<0.05$.

Chapter 3

Results

3.1) Clinical follow-up

A total of 55 patients were recruited for the follow-up study. They were divided in 23 probands (42%) and 32 relatives (58%), all of them carrying a pathological D4Z4 fragment. The number of males (29) was not significantly different from those of the females (26) (p=0.31). At the first visit, the average age of the probands was 45.5±15 years and it was comparable to the age of the relatives (44±17 years). The whole population was subdivided into three groups: probands, symptomatic and asymptomatic relatives.

We compared the MRC score of every muscle, and the partial and total Clinical Severity Score (CSS) at the time of the first (T0) and the second (T1) evaluation between each patients' groups. Differences between genders and possible correlations between the size of D4Z4 were also analysed.

At the first visit, conducted at T0, all the 23 probands were symptomatic by definition. In the group of relatives, 13 (40.63%) showed clinical signs of FSHD and this difference between the two groups was statistically significant (p<0.0001). The size of D4Z4 fragment were uniformly distributed and no significant difference were found between the probands and the relatives (p=0.61) (Table 1).

D4Z4 fragment size (Kb)	Probands		Relatives		Tot
	N	%	N	%	
19	1	4.3%	1	3.1%	2
21	2	8.7%	1	3.1%	3
23	1	4.3%	3	9.4%	4
24	1	4.3%	2	6.2%	3
26	2	8.7%	8	25.0%	10
27	1	4.3%	2	6.2%	3
30	3	1.3%	0	0.0%	3
32	1	4.3%	1	3.1%	2
33	5	21.7%	3	9.4%	8
35	2	8.7%	2	6.2%	4
36	1	4.3%	3	9.4%	4
38	2	8.7%	3	9.4%	5
40	1	4.3%	3	9.4%	4
Tot	23	42%	32	58%	55

Table 1. D4Z4 fragment size distribution in the groups of probands and their relatives.

The average age at onset in the probands (29.7±17.15 years) was lower compared to the symptomatic relatives (31.6±14 years), but this difference did not reach significance (p=0.73) (Figure 4). As expected, the average duration of disease was higher in the probands (15.7±15 years) compared to the symptomatic relatives (5.6±5.4 years) (p<0.05) (Figure 5).

At T0, the average CSS was 5.4, 2.6, and 0.8 in the groups of probands, symptomatic, and asymptomatic relatives respectively. The result of the Kruskal-Wallis test showed that the CSS was significantly higher in the probands' group compared to both groups of relatives (p<0.0001), and as expected, symptomatic relatives had a higher CSS than the asymptomatic relatives (p<0.01) (Figure 6).

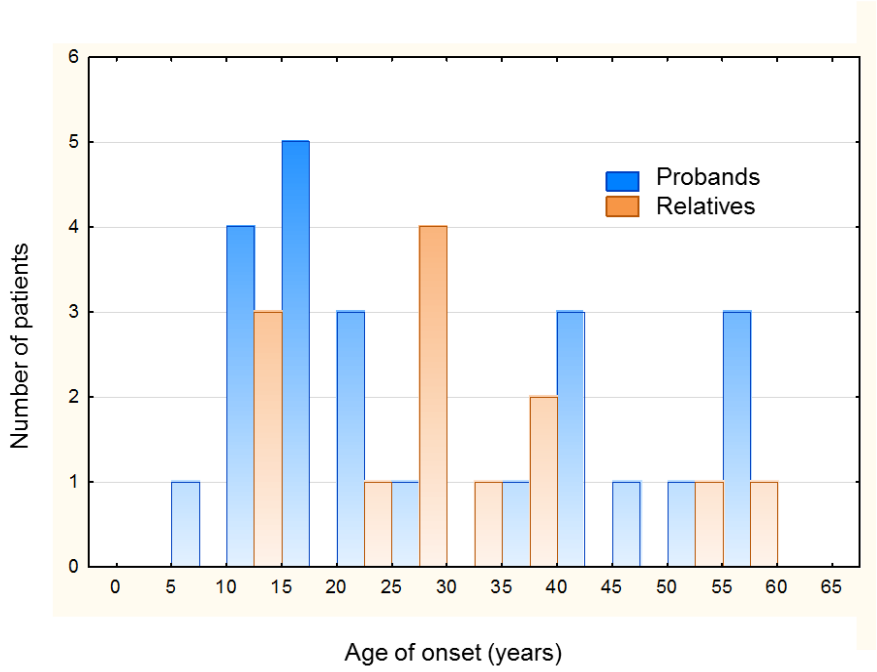

Figure 4. Distribution of the age of disease onset in the groups of probands and their relatives. Probands had an earlier onset on average compared to their relatives, but this difference did not reach significance (p=0.73; Mann Witney test).

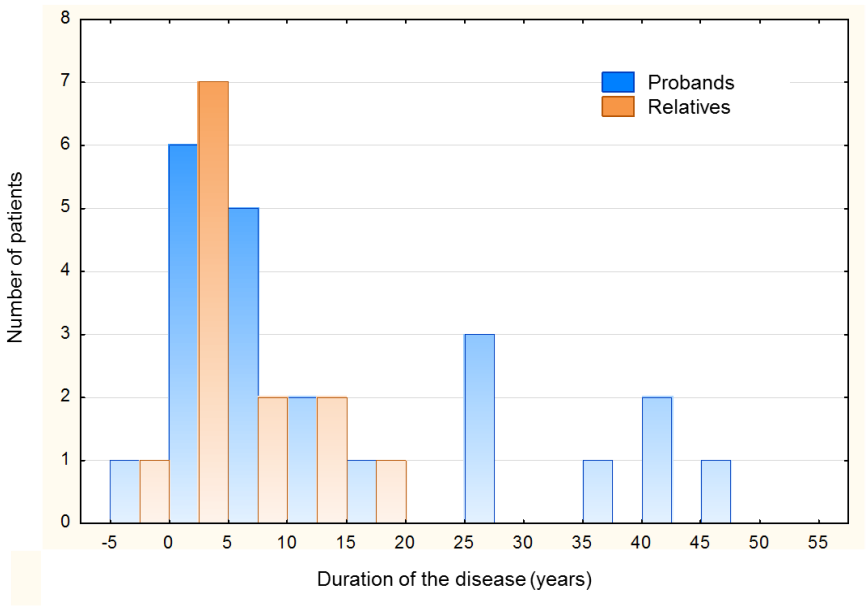

Figure 5. Distribution of disease duration in the groups of probands and their relatives. Probands had a significantly longer disease compared to their symptomatic relatives ($p<0.05$; Mann Witney test).

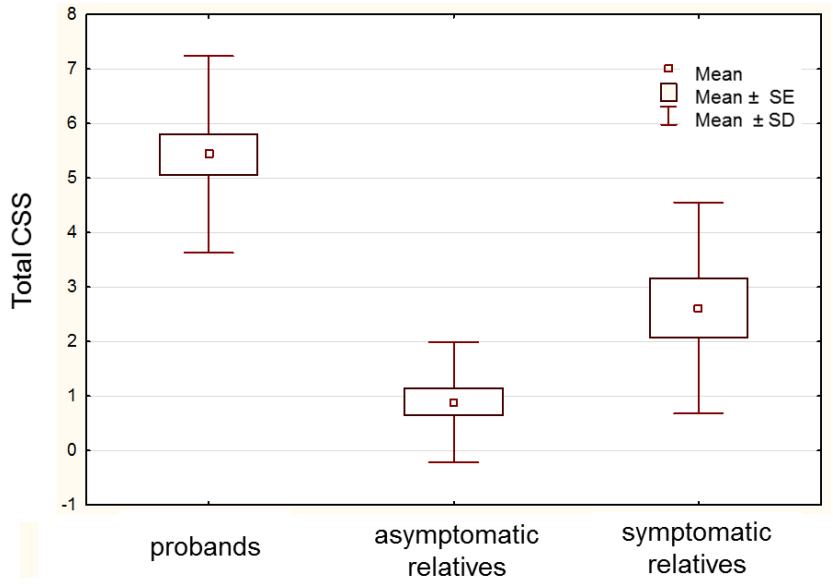

Figure 6. Total CSS values in the groups of probands, asymptomatic, and symptomatic relatives. Total CSS was significantly higher in the probands compared to both groups of relatives ($p<0.0001$; One-way ANOVA). Within the relatives, as expected, the symptomatic individuals had a higher CSS compared to the asymptomatic subjects ($p<0.01$; One-way ANOVA).

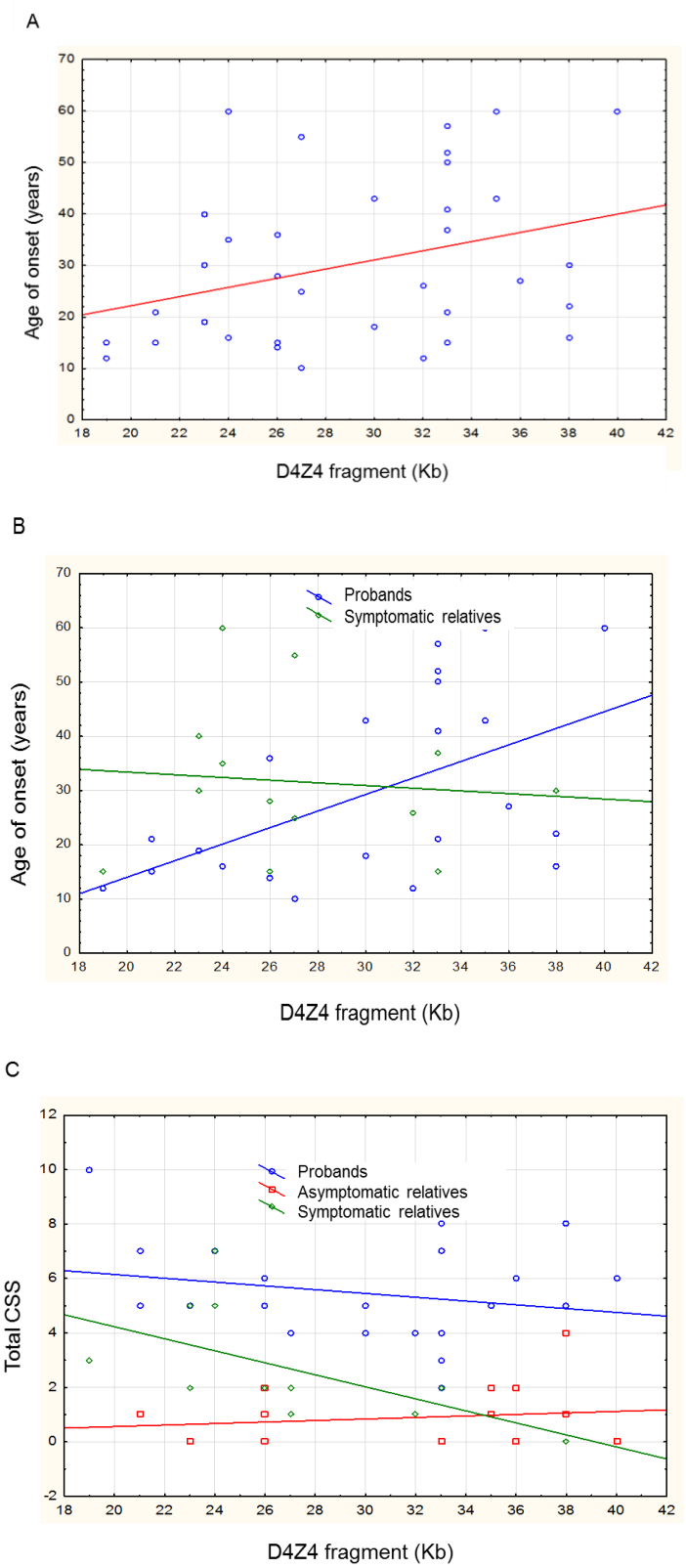

Figure 7. Correlations between D4Z4 size, age of onset and total CSS. In A: significant correlation between D4Z4 fragment size and age of onset of the symptoms among all the symptomatic patients (probands and relatives) (Spearman's rho=0.36, $p<0.05$). In B: analysing separately the probands from the symptomatic relatives, the onset-D4Z4 correlation was maintained only in the group of probands (Spearman's rho=0.58, $p<0.01$). In C: significant inverse correlation between D4Z4 size and total CSS only within the groups of symptomatic relatives (Spearman's rho= -0.72, $p<0.01$).

Considering all the symptomatic patients, the age of onset of the disease proportionally correlated with the size of D4Z4 fragment (Rho=0.36, $p<0.05$) (Figure 7A), ie. early onset corresponded to a smaller D4Z4 fragment. However, once the analysis was repeated separating the probands from the symptomatic relatives, the onset-D4Z4 correlation was maintained only within the probands (Rho=0.58, $p<0.01$) (Figure 7B). Finally, within the group of symptomatic relatives there was an inverse correlation with smaller D4Z4s associated with higher scores (Rho= -0.72, $p<0.01$) (Figure 7C).

All the patients were evaluated after 5.35 ± 1.27 (median value: 5.8; range 3-7 years). Figure 8 shows patients' distribution according to the time lapse between the evaluations at T0 and T1. The majority of patients (31) were re-evaluated after 6 or 7 years from the first visit.

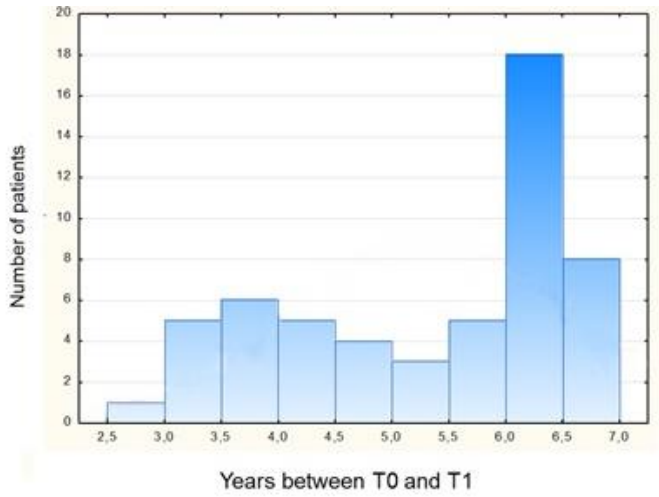

Figure 8. Distribution of the average follow-up period between T0 and T1 in the patients' cohort. The highest number of patients (31/55) were re-evaluated between 6 and 7 years after the first visit.

With respect to the whole cohort of patients, the CSS worsened significantly during the two evaluations starting from a score of 3.2 ± 2.5 at T0 and reaching 3.9 ± 3.2 at T1 ($p<0.01$). However, analysing separately the three groups, the significance was maintained ($p<0.001$) only among the probands while the relatives did not show any significant worsening ($p=0.29$) (Figure 9A). Then, the analysis was restricted to the 31 patients with the longest interval between the two evaluations (6-7 years) and, as seen before, only in the probands' group the disease showed a significant progression ($p<0.05$) (Figure 9B).

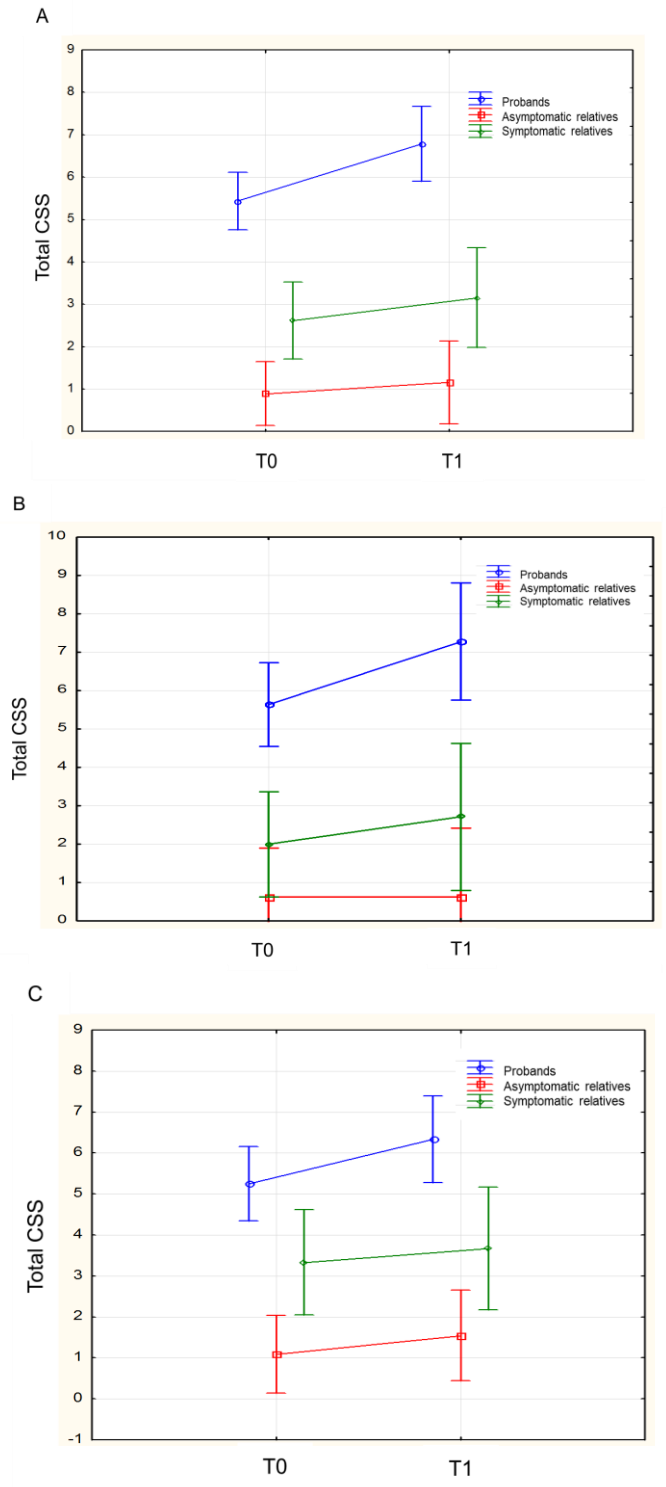

Figure 9. Disease progression measured by total CSS at T0 and T1 in the groups of probands (blue), symptomatic (green), and asymptomatic (red) relatives. In A: analysing the whole population (n=55) for the entire period of follow-up, the CSS worsened significantly between T0 and T1 only within the probands while the relatives did not show any significant worsening ($p<0.001$; repeated measures ANOVA). In B: a similar result was observed analysing separately the subjects (n=31) with the longer follow-up period ($p<0.05$; repeated measures ANOVA). In C: no significant differences were found analysing the cohort of patients (n=24) with a follow-up of 3-5 years in each group ($p=0.78$; repeated measures ANOVA).

The separate analysis of the remaining 24 patients with a time interval between T0 and T1 of 3-5 years did not show any significant difference among the three groups (p=0.78) (Figure 9C). No correlation was found between the size of the D4Z4 fragment and the degree of worsening, measured as the difference between the total CSS at T0 and T1 (Rho= -0.15, p=0.26) (Figure 10).

Correlation analysis was performed also between the values at T0 and T1 of the MRC score of each muscle tested (biceps brachii, triceps brachii, fingers flexors and extensors, wrist flexors and extensors, quadriceps, tibialis anterior) and the CSS of every muscle group included in the evaluation protocol (face, upper and lower limb girdles, distal legs and abdomen). The MRC scores of triceps brachii, biceps brachii and tibialis anterior were weaker at T1 compared to T0. Tables 2 and 3 show the MRC and CSS values for each muscle group tested at T0 and T1.

On the other hand, only the pelvic girdle was significantly more impaired in the analysis of the single muscular districts evaluated by CSS. Consistently with the previous findings, only the group of the probands resulted worsened in the correlation analysis on tibialis anterior and pelvic girdle compared to the groups of relatives (Table 4 and Figure 11).

No significant differences were found between the progression of the disease between males (14) and females (9) in the probands' group (Table 5).

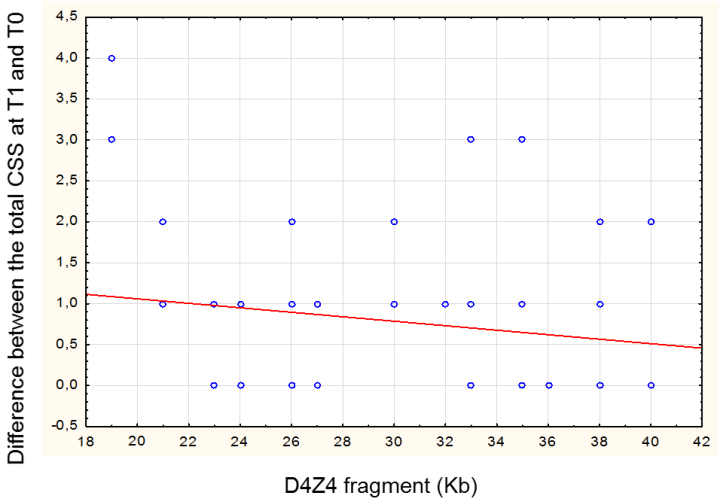

Figure 10. Correlation analysis between D4Z4 fragment size and progression of the disease. No correlation was found between the D4Z4 fragment size and the progression of the disease measured by the difference between the total CSS at T1 and T0 (Spearman's rho= -0.15, p=0.26).

Muscle	Probands (mean MRC score)	Asymptomatic relatives (mean MRC score)	Symptomatic relatives (mean MRC score)
Triceps brachii (left)	4.65 ± 0.411	4.92 ± 0.25	4.76 ± 0.388
Triceps brachii (right)	4.58 ± 0.51	4.86 ± 0.32	4.80 ± 0.38
Biceps brachii (left)	4.84 ± 0.35	5.0 ± 0.00	4.88 ± 0.21
Biceps brachii (right)	4.82 ± 0.32	4.97 ± 0.11	4.96 ± 0.13
Quadriceps (left)	4.89 ± 0.52	5.00 ± 0.00	4.92 ± 0.27
Quadriceps (right)	4.78 ± 0.65	5. 00 ± 0.00	5.00 ± 0.00
Tibialis anterior (left)	3.97 ± 1.00	4.81 ± 0.41	4.50 ± 0.95
Tibialis anterior (right)	3.93 ± 1.24	5.00 ± 0.00	4.57 ± 0.75
Extensor digitorum (left)	4.95 ± 0.20	4.89 ± 0.31	4.96 ± 0.13
Extensor digitorum (right)	4.93 ± 0.31	4.89 ± 0.31	4.96 ± 0.13
Extensor carpi (left)	5.00 ± 0.00	5.00 ± 0.00	5.00 ± 0.0
Extensor carpi (right)	5.00 ± 0.00	5.00 ± 0.00	5.00 ± 0.00
Flexor digitorum (left)	4.95 ± 0.20	5.00 ± 0.00	5.00 ± 0.00
Flexor digitorum (right)	5.00 ± 0.00	5.00 ± 0.00	5.00 ± 0.00
Flexor carpi (left)	4.97 ± 0.10	5.00 ± 0.00	5.00 ± 0.00
Flexor carpi (right)	4.96 ± 0.10	5.00 ± 0.00	5.00 ± 0.00
Muscular group	Mean CSS value	Mean CSS value	Mean CSS value
Face	0.95 ± 0.36	0.47 ± 0.51	0.92 ± 0.27
Scapular girdle	1.73 ± 0.54	0.05 ± 0.22	0.53 ± 0.51
Upper arms	1.00 ±0.42	0.15 ± 0.37	0.38 ± 0.50
Distal leg	0.69 ± 0.70	0.10 ± 0.31	0.23 ± 0.438
Pelvic girdle	0.69 ± 0.63	0.10 ± 0.45	0,30 ± 0.63
Abdomen	0.43 ± 0.50	0.00 ± 0.00	0.23 ± 0.43

Table 2. Mean MRC scores of each muscle and mean CSS values for each muscle group measured in the groups of probands, asymptomatic, and symptomatic relatives at T0.

Muscle	Probands (mean MRC score)	Asymptomatic relatives (mean MRC score)	Symptomatic relatives (mean MRC score)
Triceps brachii (left)	4.19 ± 0.63	4.78 ± 0.41	4.65 ± 0.42
Triceps brachii (right)	4.19 ± 0.44	4.76 ± 0.42	4.53 ± 0.51
Biceps brachii (left)	4.54 ± 0.39	4.97 ± 0.11	4.76 ± 0.33
Biceps brachii (right)	4.56 ± 0.52	4.94 ± 0.15	4.84 ± 0.31
Quadriceps (left)	4.69 ± 0.73	5.00 ± 0.00	5.0 ± 0.00
Quadriceps (right)	4.76 ± 0.65	5.00 ± 0.00	5.00 ± 0.00
Tibialis anterior (left)	3.28 ± 1.35	4.81 ± 0.47	4.42 ± 0.90
Tibialis anterior (right)	3.19 ± 1.34	4.92 ± 0.25	4.34 ± 1.14
Extensor digitorum (left)	4.97 ± 0.10	4.89 ± 0.31	4.96 ± 0.13
Extensor digitorum (right)	5.00 ± 0.00	4.89 ± 0.31	5.00 ± 0.00
Extensor carpi (left)	5.00 ± 0.00	5.00 ± 0.00	5.00 ± 0.00
Extensor carpi (right)	5.00 ± 0.00	5.00 ± 0.00	5.00 ± 0.00
Flexor digitorum (left)	5.00 ± 0.00	5.00 ± 0.00	5.00 ± 0.00
Flexor digitorum (right)	5.00 ± 0.00	5.00 ± 0.00	5.00 ± 0.00
Flexor carpi (left)	4.97 ± 0.10	5.00 ± 0.00	5.00 ± 0.00
Flexor carpi (right)	4.97 ± 0.10	5.00 ± 0.00	5.00 ± 0.00
Muscular group	Mean CSS value	Mean CSS value	Mean CSS value
Face	1.13 ± 0.344	0.52 ± 0.51	1.00 ± 0.40
Scapular girdle	1.78 ± 0.51	0.10 ± 0.31	0.61 ± 0.50
Upper arms	0.95 ± 0.36	0.26 ± 0.45	0.53 ± 0.51
Distal leg	1.00±0.67	0.15 ± 0.50	0.30 ± 0.48
Pelvic girdle	1.34±1.22	0.10 ± 0.45	0.38 ± 0.76
Abdomen	0.56 ± 0.50	0.00 ± 0.00	0.30 ± 0.48

Table 3. Mean MRC scores of each muscle and mean CSS for each muscle group measured in the groups of probands, asymptomatic, and symptomatic relatives at T1.

Muscle	Probands		Asymptomatic relatives		Symptomatic relatives		One-way ANOVA	Mann Whitney		
	Mean	**SD**	**Mean**	**SD**	**Mean**	**SD**		P vs A	P vs S	A vs S
Triceps brachii (left)	-0.45	0.58	-0.13	0.32	-0.11	0.36	0.034	0.045	0.08	1.00
Triceps brachii (right)	-0.39	0.47	-0.10	0.31	-0.26	0.43	0.045	0.014	0.40	0.36
Biceps brachii (left)	-0.30	0.36	-0.02	0.11	-0.11	0.21	0.007	0.003	0.18	0.40
Biceps brachii (right)	-0.26	0.54	-0.02	0.11	-0.11	0.30	0.04	0.017	0.27	0.62
Quadriceps (left)	-0.19	0.55	0.00	0.00	0.07	0.27	0.03	0.06	0.25	0.73
Quadriceps (right)	-0.02	0.10	0.00	0.00	0.00	0.00	0.50			
Tibialis anterior (left)	-0.69	0.71	0.00	0.28	-0.07	0.34	0.0001	0.0006	0.006	0.90
Tibialis anterior (right)	-0.73	0.63	-0.07	0.25	-0.23	0.63	0.0003	0.0002	0.02	0.76
Extensor digitorum (left)	0.02	0.23	0.00	0.00	0.00	0.00	1.00			
Extensor digitorum (right)	0.06	0.31	0.00	0.00	0.03	0.13	0.52			
Extensor carpi (left)	0.00	0.00	0.00	0.00	0.00	0.00	1.00			
Extensor carpi (right)	0.00	0.00	0.00	0.00	0.00	0.00	1.00			
Flexor digitorum (left)	0.04	0.20	0.00	0.00	0.00	0.00	0.45			
Flexor digitorum (right)	0.00	0.00	0.00	0.00	0.00	0.00	1.00			
Flexor carpi (left)	0.00	0.00	0.00	0.00	0.00	0.00	1.00			
Flexor carpi (right)	0.00	0.00	0.00	0.00	0.00	0.00	1.00			
Muscular group										
Face	0.17	0.38	0.05	0.22	0.07	0.27	0.42			
Shoulder girdle	0.04	0.20	0.05	0.22	0.07	0.27	0.91			
Upper arms	-0.04	0.20	0.10	0.31	0.15	0.37	0.11			
Distal legs	0.30	0.55	0.05	0.22	0.07	0.27	0.09			
Pelvic girdle	0.65	0.88	0.00	0.00	0.07	0.27	0.0004	0.0008	0.04	0.73
Abdomen	0.13	0.34	0.00	0.00	0.07	0.27	0.26			

Table 4. Differences of MRC scores and CSS between T1 and T0 for each muscle in the groups of probands, asymptomatic, and symptomatic relatives. In red are highlighted the muscles that showed a significant worsening during the period of follow-up.

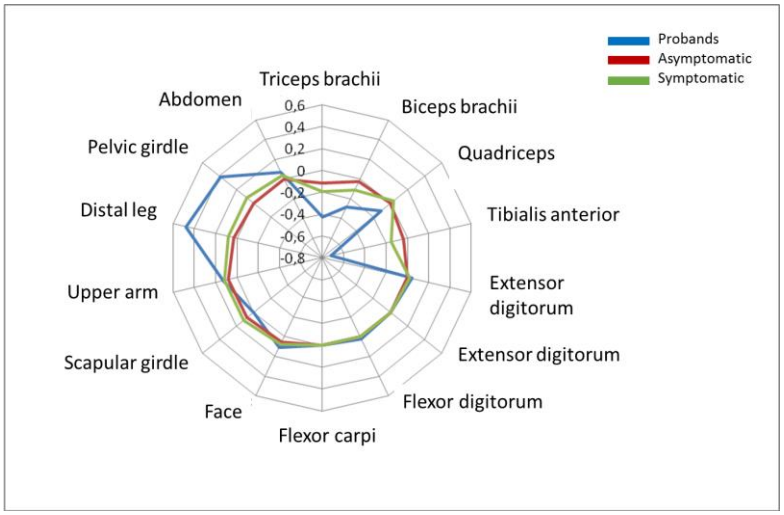

Figure 11. Percentages of variation of the scores for each muscle (on the right of the diagram) and muscle group (on the left of the diagram) between T0 and T1 for each group (proband: in blue; asymptomatic relatives: in red; symptomatic relatives: in green). Probands had the highest variations among the three groups in the strength of triceps brachii, biceps brachii, and tibialis anterior ($p<0.05$, $p<0.05$ and $p<0.0001$ respectively; One-way ANOVA) and an increase in the scores of distal leg (NS) and pelvic girdle ($p<0.001$; One-way ANOVA) measured by CSS.

Muscle	Mean (difference between T1 e T0)		P	SD	
	F	**M**		**F**	**M**
Triceps brachii (left)	-0.50	-0.42	0.781	0.43	0.67
Triceps brachii (right)	-0.33	-0.42	0.650	0.35	0.54
Biceps brachii (left)	-0.38	-0.25	0.380	0.33	0.37
Biceps brachii (right)	-0.50	-0.10	0.089	0.66	0.40
Quadriceps (left)	-0.33	-0.10	0.355	0.82	0.28
Quadriceps (right)	-0.05	0.00	0.220	0.16	0,00
Tibialis anterior (left)	-0.66	-0.71	0.880	0.43	0.87
Tibialis anterior (right)	-0.55	-0.85	0.277	0.46	0.71
Extensor digitorum (left)	0.00	0.03	0.733	0.00	0.30
Extensor digitorum (right)	0,00	0.10	0,435	0.00	0.40
Extensor carpi (left)	0.00	0.00		0.00	0.00
Extensor carpi (right)	0.00	0.00		0.00	0.00
Flexor digitorum (left)	0.00	0.07	0.435	0.00	0.26
Flexor digitorum (right)	0.00	0.00		0.00	0.00
Flexor carpi (left)	0.00	0.00		0.00	0.00
Flexor carpi (right)	0.00	0.00		0.00	0.00
Muscular group					
Face	0.22	0.14	0.642	0.44	0.36
Shoulder girdle	0.00	0.07	0.435	0.00	0.26
Upper arms	0.00	-0.07	0,435	0.00	0.26
Distal legs	0.11	0.42	0.189	0.33	0.64
Pelvic girdle	0.77	0.57	0.596	0.97	0.85
Abdomen	0.11	0.14	0.834	0.33	0.36

Table 5. Differences of MRC scores and CSS between T1 and T0 of all the patients divided according to their gender.

3.2) Methylation status of the D4Z4 alleles and SMCHD1 mutational analyses in patients with normal D4Z4 fragment size.

Molecular analyses of *SMCHD1* mutations, and the size and methylation degree of the D4Z4 fragment were performed at the Centre de référence des maladies neuromusculaires of Nice by the group of Professor Sabrina Sacconi.

Eight patients (4 males and 4 females) with normal D4Z4 fragment size and typical FSHD clinical features were investigated for the methylation status of both D4Z4 alleles and for mutations on *SMCHD1* gene. In addition, the analysis of the dimension of the D4Z4 fragment was repeated in order to avoid false negative results in the first molecular analysis. Indeed, three patients were positive in the second test showing a pathogenic D4Z4 fragment. Among the other 6 patients, 2 had normal D4Z4s (in size and methylation) and no mutations were detected in *SMCHD1*. In the remaining 4 patients (1 male and 3 females), the D4Z4 fragment was significantly hypomethylated (*Fse* < 25%) and different pathogenic mutations were identified in *SMCHD1*. Moreover, the haplotype analysis showed the presence of the permissive haplotype 4qA161 in all the FSHD2 patients studied.

Clinical features of these 4 patients differed in clinical severity and course of disease. Patient 1 (V.R.) had the onset of her symptoms at the age of 45 with a progressive impairment of the shoulder girdle. The course of her disease has been mild with a very slow progression of the weakness. In fact, at the time of the evaluation, 12 years from the onset, she had only a mild involvement of the facial and proximal upper limb muscles (CSS=3). A missense *SMCHD1* mutation (chr18:2760707G>A; p.Met1468Ile) was identified. Patient 2 (C.D.) had a more severe course with earlier onset (26 years) at the shoulder girdle and a more aggressive progression of muscle weakness. At the time of the evaluation he was 66 (40 years of disease history) and showed severe impairment during ambulation and arm abduction (CSS=10). This patient was found to carry a deletion of *SMCHD1* (chr18:2732494_2732497delAGTA) that caused a splicing alteration with the formation of an abnormal final transcript. Patient 3 (B.M.) had onset at 25 years with impairment of the shoulder girdle followed by a slow progression of symptoms. At the time of this study, 25 years from the onset, the patient showed moderate weakness of the proximal upper limb muscles and initial ambulatory impairment (CSS=6). In this patient a single base pair deletion in *SMCHD1* (chr18:2775841_2775841delG; Arg1762Leu fs*53), causing the formation of an

Proband	Gender	Disease duration (years)	CSS score	*SMCHD1* mutation	D4Z4 fragment
1 (V.R.)	F	11	3	chr18:2760707G>A	normal
2 (C.D.)	M	40	10	chr18:2732494_2732497delAGTA	normal
3 (B.M.)	F	27	6	chr18:2775841_2775841delG ; Arg1762Leu fs*53	normal
4 (M.R.)	F	10	9	chr18:2718234G>T	36 kb

Table 6. Clinical and genetic features of FSHD2 patients.

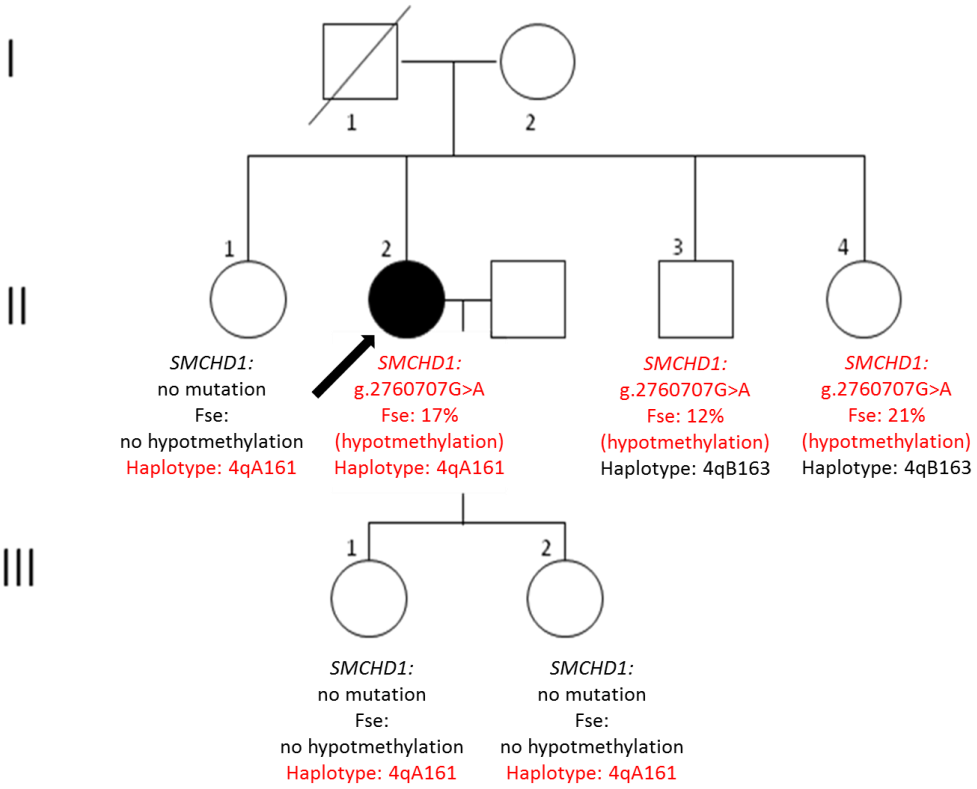

Figure 12. Genealogical tree patient #1's family. In red are highlighted the pathological findings for each member of the family. Only in the proband (II;2 - arrow) the mutation of *SMCHD1* is inherited together with a permissive haplotype 4qA161 and, consequently, the disease is expressed. All the other relatives lack of at least one pathogenic feature (II;3 and II;4 have the mutation in *SMCHD1* and a non-permissive haplotype while III;1 and III;2 have the permissive haplotype but not the mutation in *SMCHD1*) preventing the expression of the phenotype.

early stop codon after 53 triplets, was detected. Finally, the forth patient (M.R.) differed from the other four as she carried a splicing mutation in *SMCHD1* (chr18:2718234G>T) combined with a pathological contraction of D4Z4 (36 Kb). This patient had a late onset of the disease (60 years) but the progression was particularly fast as, just after 10 years, her impairment was severe and widespread (CSS=10).

Table 6 summarises the clinical features and the *SMCHD1* mutations identified in the patients described above.

The methylation status of the D4Z4 alleles and *SMCHD1* mutational analyses were also performed in all the first-degree relatives (1 brother, 2 sisters and 2 daughters) of patient 1 (V.R.). Her relatives were completely asymptomatic at the evaluation. One of the sisters and both the daughters of the patient inherited the permissive haplotype 4qA161 but none of them were positive for SMCHD1 mutations nor for D4Z4 hypomethylation. The brother and the other sister of the patient had the same *SMCHD1* mutation (chr18:2760707G>A; p.Met1468Ile) and, consequently, showed D4Z4 hypomethylation. However, both of them had a non-permissive 4qB163 haplotype. Figure 12 shows the genealogical tree of patient 1's family and the corresponding results of the molecular analysis.

3.3) Chromosome X inactivation pattern in the female FSHD population

The 41 females were from the FSHD cohort of Padova. 38 of them were FSHD1, carrying a D4Z4 fragment with a range between 19 and 40 Kbs. Two patients were compound heterozygous presenting a reduced D4Z4 fragment in both 4qA regions. The remaining three patients, were the FSHD2 females who carried pathogenic mutations in *SMCHD1*, already identified in the previous part of the study. The average age of FSHD1 patients was 51 ± 15 years, while FSHD2 patients were 49 ± 21. 48 healthy individuals, with an average age of 38 ± 14, were used as a control population. All patients were clinically evaluated, at the moment of the sample, using the FSHD Clinical Severity Score (CSS). Table 7 shows the clinical features of the patients included in this part of the study.

The methylation status of the CAG repeated sequences of the androgen receptor (AR) gene was used to define the pattern of chromosome X inactivation, because it correlates with the methylation degree of the entire chromosome. Genomic DNA sequence of the AR gene was digested by two different restriction

enzymes (*HpA*II and *HhA*I). These enzymes selectively cut the methylated cytosines on the AR gene. After digestion, according to the methylation degree of the AR alleles, DNA was not able to be amplified by PCR. Therefore, the methylation degree of the AR gene has an inverse correlation with the PCR amplification. As a control, a non-digested DNA was used. To verify the efficacy of PCR amplification, DNA samples were run on 2% agarose gel (Figure 13).

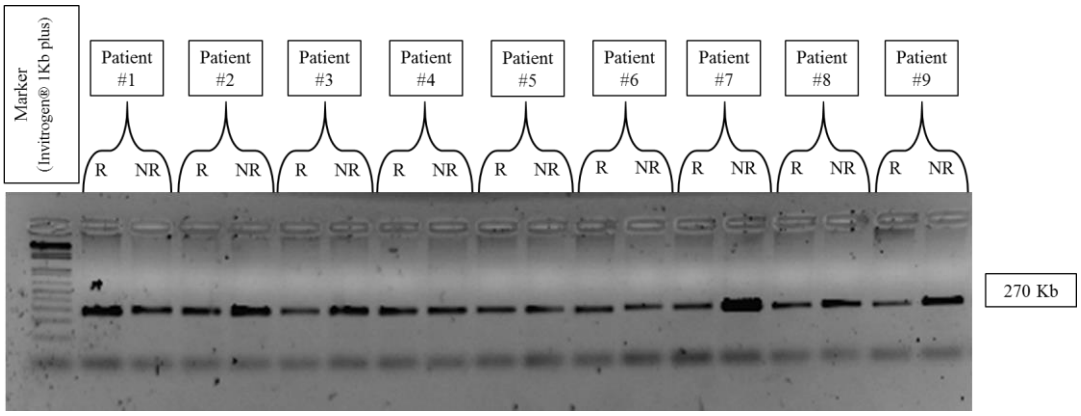

Figure 13. Electrophoresis in 2% agarose gel of the DNA samples of patients 1-9 after restriction and PCR amplification. The gel was done to verify the effectiveness of PCR amplification in order proceed to genotype sequencing. R = restricted sample; NR= non restricted sample.

The amplified samples were genotyped with capillary electrophoresis and analysed by Peak Scanner® software. The area of each peak calculated by the software corresponds to the amplification of the single allele and, therefore, it is inversely correlated to the methylation degree of that allele. Raw data were normalised to the genotyping results from the alleles of genomic DNA not exposed to enzymatic digestion. The inactivation pattern was considered skewed if the ratio between the percentage inactivation of each AR gene was greater than 80%. Methylation degree and X inactivation pattern were then related to the severity of muscle impairment according to the scores of the single muscle groups and to total CSS. Figure 14 shows three different examples of the results of genotype peak analysis with the pattern of a skewed X inactivation (A), a random inactivation (B) and two homozygous AR alleles (C). The results of the genotype analyses of AR alleles (with and without enzymatic restriction) of each patient and control are shown in table 8 and 9 respectively.

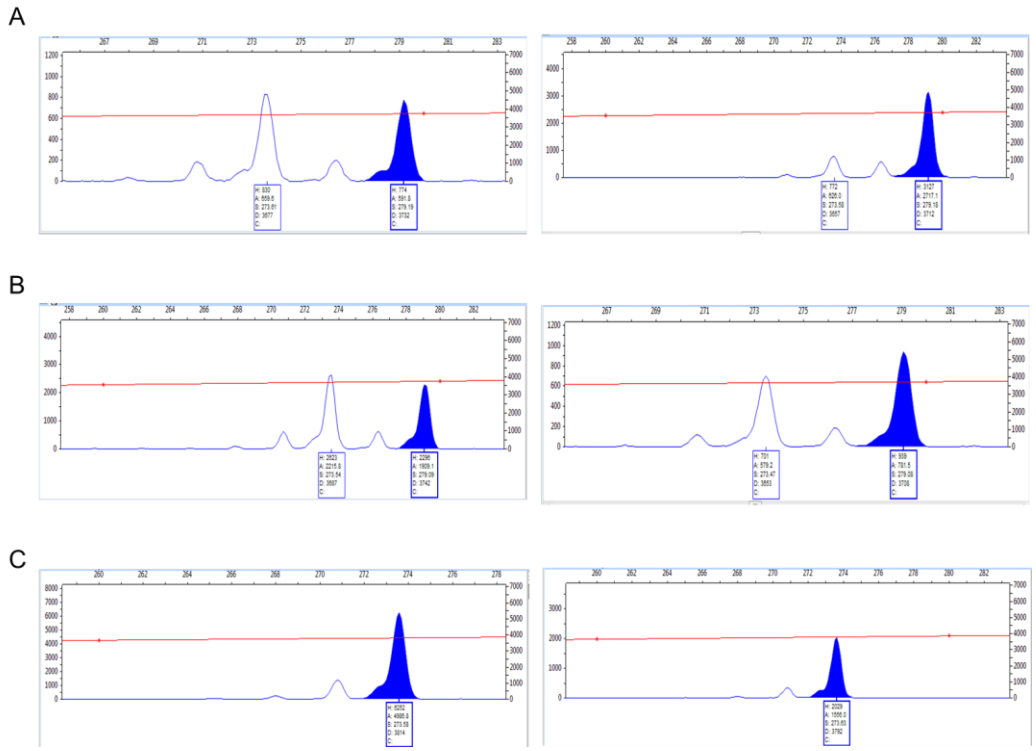

Figure 14. Genotype analyses of the CAG repeats in the first exon of the androgen receptor (*AR)* gene. On the left are shown the two AR alleles not digested by the restriction enzymes: on the right DNA was digested with the methylation-sensitive *HpaII* and *HhaI* restriction enzymes prior PCR amplification. PCR products, both before and after digestion, were electrophoresed on an ABI automated sequencer, and peak heights and area were analysed. In A: skewed X inactivation pattern where a peak of one allele is almost completely digested and therefore not amplified by PCR. The remaining peak corresponds to the inactive, methylated allele. In B: random X inactivation pattern where the ratio between the height of the two peaks is similar before and after enzymatic digestion. In C: homozygous (CAG)n in the *AR* gene where the two peaks overlap with each other.

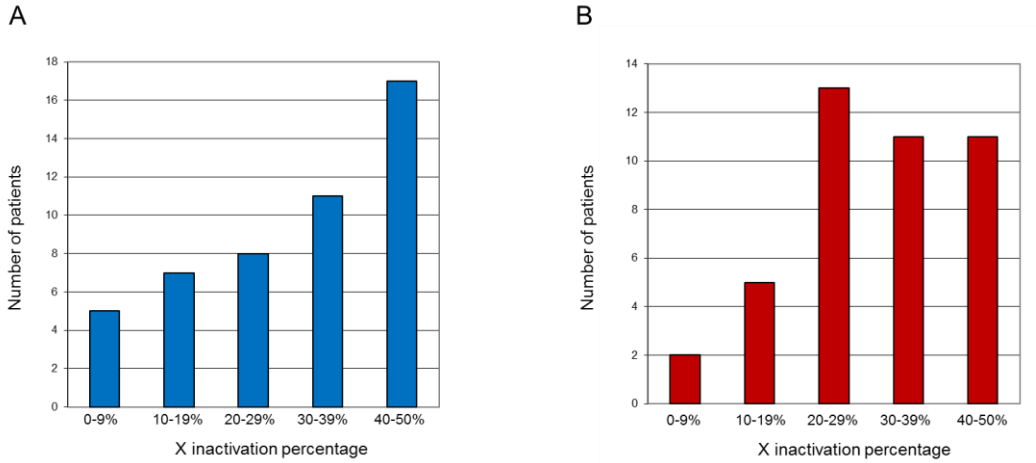

Figure 15. Distribution of the X inactivation pattern in patients (A) and controls (B). Both populations have a normal distribution of the values of the percentages of chromosome X inactivation (patients: W=0.95906, p=0.3311; controls: W=0.96008, p=0.1487; Saphiro-Wilk test).

6 controls and 5 patients were homozygous for AR and were excluded from the analysis as it is impossible to distinguish the methylation degree between the two homozygous alleles. 28 patients presented a random inactivation pattern while the remaining 9 were skewed. Of those, one patient was affected by FSHD2. 35 controls were randomly inactivated whilst 7 were skewed. Both populations of patients ($W = 0.95906$, $p = 0.3311$) and controls ($W = 0.96008$, $p = 0.1487$) showed a normal distribution of X chromosome inactivation pattern with skewed values corresponding to the tail of the curve (Figure 15).

Finally, it was important to assess whether the X inactivation pattern correlated with the severity of the phenotype among the patient populations. A moderate linear correlation ($rho = 0.574$) was found between the percentage of X inactivation and the severity of the shoulder girdle involvement; the group with a skewed X inactivation had a shoulder girdle score significantly lower than the random X inactivation group ($p< 0.01$) (Figure 16A). No further significant differences were found in the other muscle groups although a trend was emerging between the abdominal muscle involvement, the total CSS scores and the percentage of X inactivation (Figure 16B, C). A significant inverse correlation ($rho = -0.405$) was found between the total CSS and the size of D4Z4 fragment (Figure 16D). The FSHD2 patients were not analysed in a covariate analysis due to the low number of individuals but their degree of inactivation was randomly distributed.

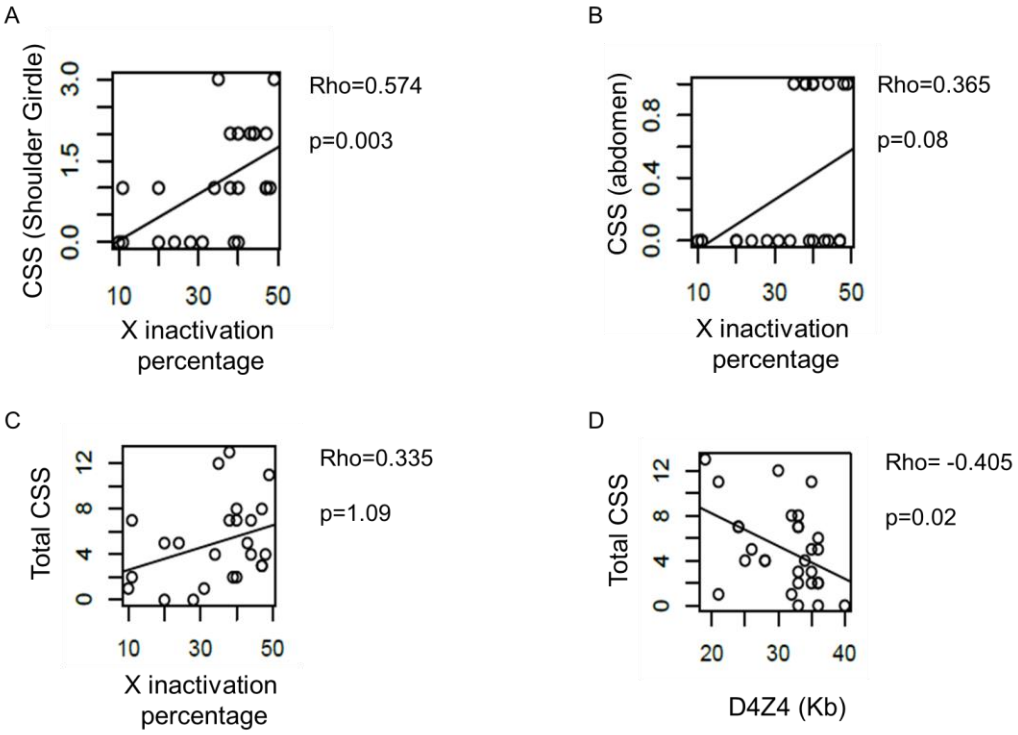

Figure 16. Correlations among the percentages of X inactivation, the CSS in different muscular districts and the D4Z4 size. In A: moderate linear correlation (Spearman's rho=0.574) between the percentage of X inactivation and the severity of the shoulder girdle involvement. In the patients with a skewed X inactivation, the CSS of the shoulder girdle was significantly lower compared to the patients with a random inactivation ($p<0.01$; Mann Witney test). In B and C: linear correlation trend among the abdominal muscle involvement, the total CSS and the percentage of X inactivation. In D: significant inverse correlation (Spearman's rho= -0.405) between the total CSS and the size of D4Z4 fragment.

			Clinical Severity Score (CSS)						
Patients	Age of onset	Age at the sample	Face	Arm abduction	Proximal upper limb	Distal leg	Pelvic girdle	Abdo-men	Total
1	asympt.	63	0	0	0	0	0	0	0
2	35	73	2	1	2	2	5	1	13
3	52	57	1	2	1	1	1	1	7
4	13	29	2	3	1	1	3	1	11
5	31	52	1	1	1	2	2	0	7
6	59	63	0	1	2	1	0	0	4
7	50	60	1	2	1	2	2	0	8
8	39	45	1	1	0	0	1	1	4
9	48	51	1	1	0	0	1	0	3
10	60	67	1	1	1	1	2	1	7
11	21	46	1	2	1	2	1	1	8
12	23	54	1	2	1	0	0	0	4
13	29	30	1	0	0	0	0	0	1
14	asympt.	45	1	0	0	0	0	0	1
15	60	67	1	1	1	1	1	0	5
16	14	27	2	2	1	0	0	0	5
17	57	65	0	1	1	1	0	0	3
18	37	41	1	0	1	0	0	0	2
19	16	42	1	2	1	1	1	1	7
20	asympt.	38	0	0	0	0	0	0	0
21	83	84	1	0	0	1	3	0	5
22	18	33	1	0	1	0	0	0	2
23	55	63	1	0	1	0	0	1	3
24	asympt.	70	0	1	0	0	2	0	3
25	asympt.	35	1	1	0	0	0	0	2
26	53	63	2	2	1	1	2	0	8
27	49	69	1	2	1	2	2	1	9
28	40	65	1	1	1	1	2	0	6
29	50	79	1	3	2	1	2	0	9
30	29	35	0	0	1	0	0	0	1
31	asympt.	14	0	0	0	0	0	0	0
32	66	67	1	0	1	0	0	0	2
33	10	24	0	3	2	2	4	1	12
34	25	51	1	3	1	1	2	0	8
35	60	65	1	2	2	2	2	0	9
36	45	56	1	0	1	0	0	0	2
37	11	18	1	2	1	0	0	0	4
38	18	64	1	2	0	0	1	0	4
39	67	72	2	2	2	1	4	0	11
40	asympt.	53	0	0	0	0	0	0	0
41	27	32	1	2	1	0	1	1	6
42	61	62	1	0	0	1	0	0	2

Table 7. Clinical features of FSHD female patients included in the chromosome X inactivation study. Age of onset, age at the sample, scores of each muscle group and total CSS are shown.

		Restricted		Non restricted			
Patients	D4Z4 (Kb)	AR allele 1 height	AR allele 2 height	AR allele 1 height	AR allele 2 height	Inactivation of one AR alleles (%)	X inactivation pattern
1	33	743	1687	1200	1056	28	Random
2	19	2288	1217	2051	1811	62	Random
3	33	1315	889	943	798	56	Random
4	21	2454	1731	1053	780	51	Random
5	33	1208	4500	4384	1964	11	Skewed
6	28	523	223	1167	981	66	Random
7	32	1275	855	1620	1206	53	Random
8	28	856	786	854	733	48	Random
9	35	1219	1039	1838	1393	47	Random
10	24	5714	2880	1597	1183	60	Random
11	33	3120	3503	3216	2413	40	Random
12	34	2707	2311	949	636	44	Random
13	32	1380	2393	2218	1710	31	Random
14	21	508	1815	1255	496	10	Skewed
15	35	2276	676	1216	1440	80	Random
16	26	2564	2723	7112	5800	43	Random
17	33	1747	1592	1490	1224	47	Random
18	33	1788	1845	2252	1479	39	Random
19	24	482	597	254	194	38	Random
20	36	418	1274	2535	1902	20	Random
21	36	831	236	2646	2439	76	Random
22	35	651	919	901	838	40	Random
23	27	1803	798	2448	2292	68	Random
24	38	3459	694	2107	2452	85	Skewed
25	28	701	939	830	774	41	Random
26	20	772	3127	2623	2296	18	Skewed
27	33	2526	1834	2057	1980	57	Random
28	23	326	1040	2076	1662	20	Random
29	38	751	0	1825	2056	100	Skewed
30	35	725	3092	5690	4027	14	Skewed
31	33	168	1538	1527	1240	8	Skewed
32	36 and 38	257	1840	815	744	11	Skewed
33	30 and 36	2893	1472	1261	1208	65	Random
34	*SMCHD1*	353	264	275	154	43	Random
35	*SMCHD1* + 36	5871	1416	2065	1922	79	Random
36	*SMCHD1*	227	2909	1994	1716	6	Skewed
37	25	4349		5421		homozygous	N.D.
38	35	5403		3497		homozygous	N.D.
39	40	6932		5230		homozygous	N.D.
40	36	1239		156		homozygous	N.D.
41	36	2459		1117		homozygous	N.D.

Table 8. Results of the genotype analysis of AR alleles performed on restricted and non-restricted DNA samples from 41 FSHD female patients. When the ratio between the percentage inactivation of each AR allele was greater than 80%, the X inactivation pattern was considered skewed. 5 patients were homozygous for AR alleles and, therefore, was not possible to determine the percentage pattern.

	Restricted AR		Non restricted			
Controls	AR allele 1 height	AR allele 2 height	AR allele 1 height	AR allele 2 height	Inactivation of one AR alleles (%)	X inactivation pattern
1	2218	209	260	324	93	skewed
2	1067	348	1512	1406	74	random
3	516	975	354	230	26	random
4	620	1143	592	413	27	random
5	53	139	1398	1145	24	random
6	155	292	1974	3037	45	random
7	246	182	2102	1888	55	random
8	150	205	2167	1815	38	random
9	330	2482	2514	1941	9	skewed
10	1835	605	433	459	76	random
11	1368	2104	1074	619	27	random
12	1031	1558	122	57	24	random
13	2223	2076	312	270	48	random
14	2241	1072	5021	3937	62	random
15	510	905	457	517	39	random
16	1843	1325	553	418	51	random
17	339	827	624	528	26	random
18	760	303	753	517	63	random
19	301	290	446	293	41	random
20	1507	827	865	688	59	random
21	1069	1661	596	560	38	random
22	187	361	420	236	23	random
23	1168	560	505	422	64	random
24	1593	391	393	444	82	skewed
25	426	560	447	351	37	random
26	404	735	2546	1912	29	random
27	1311	325	318	308	80	random
28	2334	1291	1654	1518	62	random
29	4185	690	2177	2194	86	skewed
30	935	699	1280	1154	55	random
31	1157	255	1146	1058	81	skewed
32	330	1057	289	237	20	random
33	1482	545	642	332	58	random
34	196	106	734	857	68	random
35	592	588	745	620	46	random
36	431	1668	1586	776	11	skewed
37	263	175	1451	702	42	random
38	507	522	358	359	49	random
39	940	1349	756	528	33	random
40	619	119	509	455	82	skewed
41	219	282	232	169	36	random
42	657	621	990	357	28	random
43	1378		2324		homozygous	N.D.
44	2957		3204		homozygous	N.D.
45	5432		4396		homozygous	N.D.
46	945		734		homozygous	N.D.
47	7047		861		homozygous	N.D.
48	2373		3842		homozygous	N.D.

Table 9. Results of the genotype analysis of AR alleles performed on restricted and non-restricted DNA samples from 48 healthy controls. When the ratio between the percentage inactivation of each AR allele was greater than 80%, the X inactivation pattern was considered skewed. 6 individuals were homozygous for AR alleles and, therefore, was not possible to determine the inactivation pattern.

Chapter 4
Discussion

Facio-scapulo-humeral dystrophy is a complex disease characterised by high variability in phenotype expression that challenges our ability to foresee its course. A comprehensive pathogenic model, able to explain all the several discrepancies reported in literature, is still missing and, therefore, genotype-phenotype correlations are hard to estimate. The overexpression of *DUX4*, due to the contraction of D4Z4 and its selective hypomethylation, undoubtedly plays a significant role in disease pathogenesis but, at the same time, there is evidence suggesting that other alterations are required to trigger the process that leads to the manifestation of the disease.

Considering the variability in phenotypic expression and the lack of reliable tools to predict the progression of the disease, a clinical follow-up of the FSHD cohort of Padova was performed re-evaluating 55 patients, visited from 2008 to 2013, after an average time lapse of 5 years. The Clinical Severity Score (CSS) was used for the clinical assessment of the patients. The CSS is a specific scale validated in 2007 by the neuromuscular centre of Padova, in collaboration with the Italian Consortium for FSHD, a nation-wide network established to set up an Italian registry of FSHD patients and to investigate its genotype-phenotype correlations and pathogenic mechanisms. The CSS was created with the intent to provide a reliable and standardised protocol to use in clinical trials and epidemiological studies in which a uniform evaluation of the patients was required. However, its reliability and sensitivity were not previously tested in the follow-up of the patients.

The whole population was split into probands and relatives and the latters were further subdivided between symptomatic and asymptomatic subjects. At the time of the first evaluation (T0), less than half of the relatives (40%) had clinical symptoms although they carried the D4Z4 fragment of the probands. As expected, probands showed a more severe involvement, measured by CSS, and a lower age of onset compared to their relatives while the penetrance of the disease decreases among the relatives. As the degree of kinship increases, each relative carries a genetic background progressively less close to the proband. Therefore, although

relatives and probands have in common the same D4Z4 mutation, different genetic factors largely modulate the phenotypic expression of the disease.

The higher age of onset within the relatives could be partially explained by the fact that the proband, being more affected, was the first member of the family to be diagnosed. The other relatives usually have only mild involvement and tend to underestimate their symtpoms causing a delay in their detection and making it difficult to determine the correct date of onset.

With respect to the whole cohort of patients, the D4Z4 fragement showed a normal distribution ranging between 19 Kb and 40 Kb. Analysing the genotype-phenotype correlations, in the probands' group, the D4Z4 size was inversely correlated with the severity of the symptoms as the most affected patients carried the smallest D4Z4 fragment. On the other hand, this correlation was lost within the relatives. This could be due to the fact that the probands' CSS was more uniformely distributed and clustered around a score of 6. Conversely, in the relatives group, the phenotype expression was more variable with the consequent dispersal of CSS values and the loss of correlation between the severity and the D4Z4 fragment size.

The comparison of the CSS values between T0 and T1 showed that only the probands had a significant worsening of the disease. Disease progression was definitely slower within the relatives, and the CSS was not able to detect any significant differences. Noteworthy, those individuals who were asymptomatic at T0 did not express the disease over the entire period of the follow-up. The slow progression of the disease is further confirmed by the fact that, once the patients were clustered according to different follow-up periods, significant differences were found only in those subjects with the longest time lapse between T0 and T1 (more than 5 years). Males and females showed a similar pattern of disease progression.

With respect to the MRC scores of each muscle, there was a significant worsening in the strength of the biceps brachii, triceps brachii and tibialis anterior. However, in the CSS functional scale, only the pelvic girdle showed a significant progression of the impairment while arm abduction and involvement of facial and abdominal muscles were unchanged. It is worth noting that the worsening measured by the MRC score did not correlate with the loss of function measured by the CSS due to the lack of sensitivity of the latter. In fact, for the upper limb, a

MRC score > 3/5 or ≤ 3/5 represents the cut-off between a CSS of 1 and 2 where a score of "2" is the highest achievable. Therefore, for every MRC scores < 3/5, the CSS lack a corresponding level of worsening with a consequent loss of sensitivity. A similar threshold effect happens also when the MRC scores of the distal leg are compared to the function measured by the CSS. When the patients loose their ability to walk on both the heels and the tiptoes, any further worsening of the muscle strength measured by the MRC score does not modify any further the functional CSS value.

According to these results, the CSS seems to provide a detailed picture of the general impairment of the patient but the results are not reliable in the detection of subtle modification during the follow-up. Moreover, neither the size of the D4Z4 fragment nor gender were relevant in predicting the course of the disease.

It is likely that the contraction of the D4Z4 fragment is necessary to initiate the pathological mechanisms underlying FSHD but other, yet unknown, factors (both genetic and environmental) play a role in modulating disease progression. Moreover, although females have been reported to have a milder phenotype, they do not differ from males in disease progression suggesting that the genetic or hormonal factors that protect females from developing symptoms are no longer effective once the disease is triggered.

The second part of this study aimed to identify possible genetic modifiers that modulate the phenotypic expression of FSHD. The identification of FSHD2 patients with mutations in *SMCHD1* was particularly relevant. *SMCHD1* mutations have been reported to cause D4Z4 hypomethylation regardless of fragment contraction (Lemmers et al, 2012) and to be associated with more severe phenotypes when inherited together with an abnormal D4Z4 (Sacconi et al, 2013).

Among the FSHD population of Padova, 9 subjects with typical FSHD phenotype and a normal D4Z4 fragment were identified to be tested for *SMCHD1* mutations. The analysis of D4Z4 fragment size is not straightforward and, therefore, it was repeated in order to avoid false negatives. Indeed, 3 subjects among the 9 tested carried a previously undetected pathological D4Z4 fragment. Of the remaining 6 patients, 4 of them carried *SMCHD1* mutations and all the mutations detected showed pathogenic potential as they were associated with hypomethylation of the D4Z4 region. However, the molecular analyses of the first-degree relatives of one proband showed that mutations in *SMCHD1* are not

alone sufficient to cause the disease. In the family studied, the only member affected was the proband that carries the *SMCHD1* mutation combined with a permissive 4qA161 haplotype. All the other relatives, who were positive for the 4qB haplotype, were asymptomatic despite the presence of the same *SMCHD1* mutation and consequent D4Z4 hypomethylation. These results are consistent with the pathogenic model proposed by Lemmers and colleagues in 2010; they proposed that the D4Z4 hypomehtylation needs to be combined with a permissive 4qA haplotype to cause the toxic overexpression of *DUX4* and, therefore, the phenotypic expression of the disease. FSHD2 patients showed a similar phenotypic expression to the more common FSHD1, with similar variability among severity of symptoms, age of onset and disease progression. Of particular interest is the case of patient 5 who carried both D4Z4 fragment contraction and *SMCHD1* mutation. She had a late onset of the disease after menopause that could suggest a protective role of female hormones as previously hypothesised in recent reports (Ricci et al, 2013). However, the patient showed a fast progression reaching a high CSS (9) in less than a decade. It is reasonable to think that this unusal course of the disease is due to the combined action of the *SMCHD1* mutation and the D4Z4 fragment contraction. Although the number of the patients studied were not sufficient to make any statistical inference, these data are in agreement with reports in the literature and suggest that *SMCHD1* plays a significant role in the phenotype expression of FSHD. Therefore, its mutations should be searched for in all the patients negative for D4Z4 contraction and in those with a severe and fast progressive phenotype.

Considering that the impairment of genome methylation is one of the main causes of the disease, that *SMCHD1* is implied in chromosome X inactivation during embryogenesis, and that phenotypic differences have been frequently reported between genders, it was reasonable to suspect that some genetic modifiers could be located on chromosome X and their function impaired by an inbalanced inactivation of the chromosome itself. Therefore, the last part of the study focused on the assessment of chromosome X inactivation pattern in the FSHD female population.

The inactivataion of chromosome X is distributed as a continuous value, such as height and weight, and happens randomly in the healthy population. Consequently, a variable proportion of healthy individuals have a skewed X

inactivation that corresponds to different percentiles of the curve. The threshold at which the inactivation is considered skewed is arbitrary and, frequently, is set at 80% of the cells (Amos-Landgraf et al, 2006).

The FSHD female cohort of the study showed a normal distribution of the chromosome X inactivation and did not differ to the distribution observed in the healthy control population. Moreover, once the distribution of X inactivation was studied among the patient population, it did not correlate with the severity of the phenotype measured by the total CSS. Only the score of the shoulder girdle was lower among the patients with a skewed X inactivation compared to those with a random pattern. Both FSHD1 and FSHD2 cases were included in the analyses. The patients with *SMCHD1* mutations were only 4 and, although the number was not sufficient to reach any statistical significance, X inactivation was randomly distributed.

These results suggest that the impairment of methylation, in the pathogenesis of FSHD, is confined to the 4q35 region, further confirming that local rearrangements of the D4Z4 fragment are mainly involved. Therefore, the control of chromosome X methylation seems to be unaffected and inactivation happens randomly as in the healthy individuals. Moreover, it is important to note that *SMCHD1* acts in the final stages of the inactivation process (Blewitt et al, 2008) presumably once the chromosome to be inactivated has already been selected. The differences found in the symptom severity between patients with skewed and non-skewed inactivation are subtle although a slight trend is detectable, suggesting a more severe phenotype among those individuals with a chromosome X random inactivation. A higher number of patients is needed, however, to reach a final and more reliable conclusion regarding the possible role of the chromosome X inactivation as a genetic modifier of phenotype expression.

Conclusions

Although the diagnosis of facio-scapulo-humeral dystrophy is usually straightforward considering the characteristic clinical features, the prediction of the clinical course is hard to define due to the high variability of its phenotype expression. This should be taken into account in the evaluation of the prognosis and during the genetic counselling.

The follow-up study performed in the FSHD patients of Padova confirmed that the disease has, usually, a long slow progression over the years, independent of gender and of the D4Z4 fragment size. The proximal muscles of the upper limbs and the distal leg are the regions where the disease shows the greatest progression. The evaluation scale used, the Clinical Severity Score, was not sensitive enough in the detection of minor changes of muscle strength and, therefore, is not reliable for the follow-up of the patients. More sensitive tools, either clinical, instrumental or biochemical, or combined, are required in order to monitor the progression of the disease over time.

The identification of genetic modifiers represents another major aim for the understanding the phenotype expression and clinical course of FSHD. Mutations in *SMCHD1* were pathogenic in all the patients studied and also actively contributed to determine a more severe phenotype when inherited together with a D4Z4 fragment contraction. Moreover, the haplotype analyses of the FSHD2 patients further confirmed that a permissive genetic background is needed for the full development of the disease.

Finally, the chromosome X inactivation pattern appeared not to differ between healthy and affected females suggesting that the pathogenic mechanisms underlying the disease do not include? The methylation process of chromosome X during embryogenesis. Nonetheless, female patients with a skewed inactivation of chromosome X seem to have a milder phenotype, in particular regarding the involvement of the shoulder girdle. Therefore, a greater number of patients is needed to reach final conclusions for the role of chromosome X inactivation as genetic modifier of the disease.

Part II

SHP2: a novel therapeutic target in MuSK-myasthenia

Abstract

Muscle Specific Kinase antibody myasthenia gravis (MuSK-MG) is an autoimmune disease that impairs neuromuscular transmission leading to widespread muscle weakness and fatigability. Under physiological conditions, agrin activates the LRP4-MuSK complex, initiating a phosphorylation cascade that culminates with the clustering of acetylcholine receptors (AChRs). SH2 domain-containing phosphatase (SHP2) is a negative regulator of AChR clustering that inhibits MuSK phosphorylation. In MuSK-MG, (auto)antibodies against MuSK, mainly of the IgG4 subclass, block MuSK interaction with LRP4 and, therefore, its activation. The smaller population of MuSK IgG1-3 appear to act by a different mechanism. Although MuSK-MG is a treatable disease, a therapy that targets specifically its pathogenic mechanisms is still not available. The aim of this study was to confirm and extend preliminary findings that demonstrated the *in vitro* effects of a specific SHP2 inhibitor, NSC-87877, as a potential specific treatment for MuSK-MG.

Total IgG and IgG subclasses (IgG1-3, IgG4) were purified from plasma of 3 MuSK-MG patients. MuSK-Ab titres were measured by radioimmunoassay. To test the effects of NSC-87877 on MuSK phosphorylation and AChR clustering, C2C12 myotubes were used. The myotubes were incubated with increasing concentrations of NSC-87877 at different time intervals (from 15 to 360 minutes) using agrin and DMEM as positive and negative controls respectively. To test whether the drug was able to reverse the pathogenic effects of MuSK-Abs, myotubes were then exposed to agrin either with MuSK total IgG, IgG1-3 or IgG4, in the presence or absence of NSC-87877. MuSK expression and tyrosine phosphorylation were detected by western blotting, and the phosphorylation expressed as the ratio of the densitometry values of phospho-tyrosine MuSK to total MuSK. For AChR cluster quantification, myotubes were labelled with α-bungataroxin-594 followed by image acquisition and analysis with ImageJ software. For all experiments 20 images were scanned, coded, and the number of clusters > 5 μm counted using ImageJ.

In the absence of agrin, NSC-87877 caused a dose-dependent increase in both MuSK phosphorylation and AChR clustering, reaching a maximum at 100 μM, after 40 minutes of incubation. 100 μM NSC-87877 enhanced MuSK

phosphorylation in the presence of MuSK total IgG and purified IgG4 while no significant change was observed with purified IgG1-3. Nevertheless, MuSK total IgG and both subclass fractions caused the dispersal of AChR clusters (see also Koneczny et al, 2013), and NSC-87877 was able to reverse their pathological effects in all samples.

SHP2 inhibition by NSC-87877 induced MuSK phosphorylation and increased AChR clustering regardless of direct stimulation by agrin. Moreover, NSC-87877 effectively induced MuSK activation despite the inhibitory effects of MuSK IgG4 antibodies, and enhanced AChR clustering in the presence of all the different IgG subclasses. Therefore, irrespectively of the MuSK IgG subclass, SHP2 inhibition represents a potential therapeutic strategy in MuSK myasthenia and further studies should access its efficacy and reliability *in vivo*.

Chapter 1
Introduction

Myasthenia gravis is an autoimmune disease that impairs transmission at the neuromuscular junction. It is a heterogeneous disorder with respect to its clinical manifestations and pathogenic mechanisms. From a clinical point of view, its key features are distinct as they consist of fluctuating weakness in skeletal muscles which deteriorates during effort and improves with rest. On the other hand, the range of severity is wide, from mild and inconstant involvement of the ocular muscles to life-threatening respiratory impairment.

The disease is caused by antibodies directed against various proteins expressed at the neuromuscular junction. Symptoms and response to treatment vary partially according to which antibody is responsible for the disease. Therefore, identifying the antibody is a fundamental step not only for correct diagnosis but also to choose and administer the most effective therapy.

Myasthenia gravis is usually a treatable disease and the therapeutic options include steroids, immunosuppressant and immunomodulatory drugs. Although these treatments are often effective to control the symptoms, they lack specificity and might cause important side effects as they target the whole immune system. The purpose of this thesis was, therefore, to analyse the *in vitro* effects of a novel therapeutic strategy that could provide an additional and specific treatment for patients.

1.1) Epidemiology

Due to its heterogeneity in clinical and immunological aspects, it is difficult to make a precise estimation of the prevalence and incidence of myasthenia. If we consider the disease as a whole, a recent meta-analysis that pooled 55 studies performed between 1950 and 2007 in different countries around the world, showed an overall incidence rate of 5.3:1000000 population-year and a prevalence rate of 77.7 cases/1000000 population (Carr et al, 2010). It is worth noting that the prevalence has been rising over the last 40 years. This could be due to a more accurate diagnosis following the introduction of the radioimmunoassay to detect antibodies titres, to better health care of the patients and, finally, to more precise statistical analyses. There is also evidence that the incidence is increasing among

elderly people and this seems to be due only partially to a prolonged life expectancy (Pakzad et al, 2011; Phillips et al, 1996; Vincent et at, 2003; Matsui et al, 2009; Somnier et al, 2005).

The incidence of myasthenia differs significantly between males and females. Males present the peak of incidence after the age of 60, whilst females have a bimodal distribution with two different peaks, one during the fertile period between the second and third decade, the second after the menopause, at a similar age to men (Vincent et al, 2003; Carr et al, 2010; Heldal et al, 2009).

The variations in incidence and prevalence rates observed between the studies of the meta-analysis represent evidence of the heterogeneous background of myasthenia. Age of onset, gender and geographical distribution vary significantly according to HLA genotypes, thymus involvement and type of antibodies that sustain the disease. For example, in North America and Europe, *HLA-DR3* and *B8* alleles are strongly associated with early onset of the disease with thymic hyperplasia (Compston et al, 1980; Janer et al, 1999) while late-onset cases are weakly associated with *HLA-DR2* and *B7* (Giraud et al, 2008). *HLA-DR9* allele represents a risk factor for Asian people and they seem to have a higher incidence of infantile cases (onset <15 years) particularly in China and Japan (Chen et al, 1993; Matsuki et al, 1999; Yu et al, 1992; Zhang et al, 2007). With respect to the type of antibodies, myasthenia with antibodies against Muscle Specific Kinase (MuSK) often presents at a younger age with female predominance and its frequency decreases with distance from the equator (Sanders et al, 2003; Evoli et al, 2003; Guptil et al, 2011; Vincent et al, 2008).

1.2) Clinical features

Myasthenia gravis was first described as a distinct clinical entity in 1672 by Thomas Willis who reported the case of a woman with a fluctuating palsy of her limbs and tongue (Hughes, 2005). In his book "De anima Brutorum", Willis draws an accurate picture of the basic symptoms that characterise myasthenia writing that "*those who be in trouble with a scarcity of spirits, are able at first rising in the morning to walk, move their arms this way and that, or to lift up a weight with strength; but before noon, the stores of spirits which influenced the muscles being almost spent, they are scarce able to move hand or foot*".

The name myasthenia gravis was coined in late 19th century fusing the Greek words "*μῦς*" (muscle) and "*ἀσθένεια*" (weakness). The Latin adjective "*gravis*" was added in order to highlight the severity that in the past characterised the prognosis of the disease, almost inevitably fatal, when no treatment was available (Keesey, 2002).

Patients present a typical fluctuating weakness that involves different skeletal muscle groups. Muscle fatigue worsens with exercise and improves with rest, sometimes with full recovery. Therefore, symptoms are usually mild or even absent during the first hours after awakening and tend to worsen during the day with a characteristic circadian pattern. In over 85% of patients, the onset of the disease involves the extraocular muscles that control gaze movements (Grob et al, 2008). This causes diplopia and ptosis of the eyelids, often asymmetrical, exacerbated by activities that imply focus of the gaze such as reading, watching television or driving.

Within two years from an ocular onset, between 50% and 80% of the patients have generalisation of the weakness with limb and/or bulbar involvement (Antonio-Santos et al, 2008). If the symptoms remain confined to the ocular muscles for more than two years, is very unlikely that the disease will spread to other muscles (Kerty et al, 2014). In the generalised form, muscle weakness usually is symmetrical and more proximal than distal, although cases with prevalent distal and asymmetrical involvement have been reported (Rodolico et al, 2003; Nations et al, 1999). In a small percentage of cases (up to 15%), the impairment of the bulbar muscles represents the first manifestation of the disease causing life-threatening symptoms like dysphagia, dysarthria, dysphonia and dyspnea (Meriggioli et al, 2009). A quick diagnosis and prompt treatment are fundamental in these cases.

Myasthenia has a relapsing-remitting course. Exacerbations of the symptoms are due mainly to intermittent infections, concomitant treatments for other diseases (such as antibiotics, anticonvulsants, statins, anaesthetics, and antihypertensives), unplanned or too quick withdrawal of the therapy, pregnancy, or surgeries. A severe exacerbation that requires a prompt intubation of the airways due to the failure of respiratory muscles defines the myasthenic crisis (Bedlack et al, 2002). About 10-20% of the patients experience this kind of crises

at least once during their illness and up to 20% of them have a crisis as the first manifestation of myasthenia (Wendell et al, 2011).

The disease tends to progress to highest severity during the first 5 years after the onset and, in this period, crises are also more frequent. After this initial period, myasthenia usually stabilises in terms of of general symptomatology and exacerbations while permanent and spontaneous remission occurs in about 10% of the cases (Grob et al, 2008).

1.3) Quantification of clinical severity

According to the severity and distribution of muscle weakness, myasthenic patients are divided into the following five classes:

- Class I: Any ocular muscle weakness. May have weakness of eye closure. All other muscle strength is normal;
- Class II: Mild weakness affecting other than ocular muscles; may also have ocular muscle weakness of any severity;
  - IIa: Predominantly affecting limb, axial muscles, or both. May also have lesser involvement of oropharyngeal muscles;
  - IIb: Predominantly affecting oropharyngeal, respiratory muscles, or both. May also have lesser or equal involvement of limb, axial muscles, or both;
- Class III: Moderate weakness affecting other than ocular muscles; may have ocular muscle weakness of any severity;
  - IIIa: Predominantly affecting limb, axial muscles, or both. May also have lesser involvement of oropharyngeal muscles;
  - IIIb: Predominantly affecting oropharyngeal, respiratory muscles, or both. May also have lesser or equal involvement of limb, axial muscles, or both;
- Class IV: Severe weakness affecting other than ocular muscles; may have ocular muscle weakness of any severity;
  - IVa: Predominantly affecting limb, axial muscles, or both. May also have lesser involvement of oropharyngeal muscles;

- IVb: Predominantly affecting oropharyngeal, respiratory muscles, or both. May also have lesser or equal involvement of limb, axial muscles, or both;

- Class V: Defined by intubation, with or without mechanical ventilation, except when employed during routine postoperative management. The use of a feeding tube without intubation places the patient in class IVb.

This classification was introduced and validated by the Myasthenia Gravis Foundation of America (Jaretzki et al, 2000) and represents a quick and reliable system to categorise the patients for therapeutic research trials and, nowadays, is broadly used in the clinical practise.

1.4) Clinical subtypes

As mentioned above, myasthenia is a heterogeneous disease sustained by different pathogenic mechanisms. The classification of its different subtypes reflects this heterogeneity and takes into account epidemiology, thymic pathology and type of antibodies detected.

1.4.1) AChR-MG

The most common myasthenia subtype (80% of all cases) is caused by antibodies (abs) directed against the acetylcholine receptor (AChR). AChR-Ab positive myasthenia is usually classified into the following groups according to the age of onset and to the associated thymic pathology:

- Early-onset myasthenia: the onset is set before the age of 40-50, and females are more affected than males with a ratio of 3:1 (Meriggioli et al, 2009). Thymic follicular hyperplasia is a common feature and patients usually respond well to thymectomy. There is a strong association with *HLA-DR3*, *HLA-B8* and with other autoimmune diseases, especially thyroiditis (Compston et al, 1980; Klein et al, 2013) both in the patient and their families.
- Late-onset myasthenia: the age of onset is usually considered after 50 years, although this threshold could vary between different studies. Males are more affected than females (approx 1.5:1) and thymic pathology is rare (Aarli, 2008; Marx et al, 2013). Therefore, thymectomy is usually not indicated in

these patients. There is a weak association with *HLADR2*, *HLA-B7*, and *HLA-DRB1*15:01* (Compston et al, 1980).

- Thymoma-associated myasthenia: in this case the disease is considered paraneoplastic as it is sustained by the tumour that affects the thymus. It accounts for about 10-15% of all myasthenic patients (Grob et al, 2008) and virtually all of them have AChR antibodies. Frequently, antibodies against other muscle intracellular antigens (titin, ryanodine receptor) have been reported (Aarli et al., 1998, Marx et al., 1998) and antibodies against voltage-gated K+ channel (Kv1.4) have been associated with concomitant diagnosis of myocarditis (Suzuki et al, 2014). Antibodies against titin or ryanodine receptor are a frequent finding in late onset myasthenia while they have been detected rarely in early-onset forms. Therefore, the presence of these antibodies in young patients is highly suggestive for the presence of thymoma (Buckley et al, 2001). However, these antibodies are also found in late-onset MG with no detectable thymoma. The incidence of thymoma reaches the peak at the age of 50 and there is no gender predominance (Marx et al, 2013) while the presentation tends to be more severe compared to non-thymomatous forms.

1.4.2) MuSK-MG

MuSK is a transmembrane tyrosine kinase located at the muscular sarcolemma that is indispensable for the correct development and the maintenance of the high density of AChRs at the neuromuscular junction. Its role will be described in some detail below. Antibodies directed against MuSK were first described in a population of seronegative myasthenic patients by Hoch and colleagues in 2001. The original study suggested that MuSK-Abs were responsible for about 70% of all the seronegative cases, but more recent findings showed that this percentage depends greatly on the population studied with significant variations among the different cohorts (Vincent et al, 2005).

MuSK-MG represents an important subgroup and differs from the more common form with AChR-Abs in terms of epidemiology, muscle involvement and response to treatment. The disease affects mainly females in the third decade (Gutpill et al, 2011; Evoli et al, 2003) and is not commonly reported in elders or children (Pasnoor et al, 2010; Skjei et al, 2013). Considering the higher frequency

of the disease in the populations that live closer to the equator (Vincent et al, 2008), together with the *HLA-DQ5* association which is the same in different European centres (Niks et al, 2006, Bartoccioni et al, 2009; Alahgholi-Hajibehzad et al, 2013), environmental factors and genetic background both appear to play a significant role in the pathogenesis of MuSK-MG. From a clinical point of view, ocular muscles and limbs are often mildly affected compared to the bulbar muscles that are often severely impaired with high frequency of respiratory crises (Evoli, 2006; Gutpill et al, 2011). No association with thymic pathology has been reported so far and, therefore, thymectomy is not indicated (Marx et al, 2013).

1.4.3) LRP4-MG

Antibodies against the Low-density-lipoprotein Receptor-related Protein 4 (LRP4) have been detected in a variable proportion (2-27%) of patients without AChR or MuSK-Abs (Higuchi et al, 2011; Zhang et al, 2012; Pevzner et al, 2012). Different tests, including cell-based assay (CBA) and ELISA, were used to estimate the level of antibodies and this could explain part of the reason for the incidence variability in seronegative patients.

LRP4 is upstream MuSK in the AChR clustering pathway (see below) and mediates MuSK activation, but the pathogenicity of LRP4-antibodies in myasthenic patients is still a matter of debate. However, *in vitro* experiments showed that LRP4-antibodies are able to reduce agrin-dependent AChR clustering (Zhang et al, 2012; Pevzner et al, 2012) and a passive immunisation model had clinical and neurophysiological myasthenic features (Shen et al, 2013). Patients with detectable levels of LRP4-antibodies are usually females presenting with ocular symptoms or mild generalised involvement while the most severe cases often have double positivity with MuSK-Abs (Higuchi et al, 2011).

1.4.4) Seronegative myasthenia

Seronegative myasthenia (SNMG) is defined always by the absence of antibodies against well characterised antigens such as AChR, MuSK or LRP4 in patients who have clinical and neurophysiological features consistent with the diagnosis of myasthenia. Seronegative cases count for about 15% of all the patients and for roughly 50% of the pure ocular forms (Kerty et al, 2014). The introduction of a cell-based assay with rapsyn-induced clusters of the

acetylcholine receptor improved detection of AChR-Abs in patients who otherwise were negative in the traditional radioimmunoassays for AChR or MuSK antibodies (Leite et al, 2008; LRP4 was unknown at this time). Up to 66% of SNMG patients present these "low-affinity" AChR antibodies.

Subsequent to the definition of ACHR, MuSK and LRP4 as relevant antigens, several other proteins of the neuromuscular junction, such as agrin, cortactin or collagen Q, have been proposed as potential targets for antibodies in seronegative patients (Cossins et al, 2012; Gasperi et al, 2014; Gallardo et al, 2014, Zoltowska Katarzyna et al, 2015) and low titres of antibodies against agrin have been reported, but often co-existing with AChR or MuSK-Abs (Zhang et al, 2014). Despite the increasing number of reports, the specificities of these antibodies are unclear and their potential pathogenic effects unexplored.

1.5) Structure and physiology of the neuromuscular junction

The different subtypes of myasthenia gravis have in common an initial dysregulation of the immune system that leads to the production of autoantibodies against different antigens of the neuromuscular junction. AChR-Abs have been proven to be pathogenic causing the destruction and dispersal of the acetylcholine receptor clusters located on the muscle membrane in correspondence of the nerve terminal. In order to understand the pathogenic mechanisms that cause each form of myasthenia, is important to describe first the normal structure, development and physiology of the neuromuscular junction.

1.5.1) Principles of development of the neuromuscular junction and the agrin-LRP4-MuSK pathway

The neuromuscular junction is a chemical synapsis between the second motor nerve and the surface of skeletal muscle, using acetylcholine as the main neurotransmitter. Due to its accessibility and to the apparent simplicity of its connections, the neuromuscular junction represents a very well-studied and understood model of synaptic transmission.

The formation of the junction requires a complex signalling process, both spatially and temporally, between the motor neuron and the muscle myotubes. The end of this process results in the clustering of acetylcholine receptors on the postsynaptic side and a differentiated nerve terminal on the presynaptic one

(Burden, 2002). During embryonic development, the motor nerve, sprouting from the spinal anterior columns, targets the muscle fibres and starts the innervation preferentially where pre-patterned AChR clusters are expressed (Panzer et al, 2006; Flanagan-Steet et al, 2005). The axon of a single motor nerve innervates multiple muscle fibres generating large motor units. The final dimension of each motor unit is then determined by the intensity of the neural activity Wyatt et al, 2003; Chung et al, 2009).

Several proteins are involved in the maturation process and in the maintenance of the structure of the neuromuscular junction. Synaptic laminins are responsible, for example, for the correct relative positioning of each synaptic element (Nishimune et al, 2008). However, the most important role in both pre- and post-synaptic development of the synapsis is played by the agrin-LRP4-MuSK pathway that leads to the clustering of the AChR receptors (Figure 1). Agrin is a heparan-sulfate proteoglycan secreted into the synaptic cleft by the motor nerve terminal. Its receptor, LRP4, is located on the muscular sarcolemma (Glass et al., 1996; Zhang et al, 2008) and has specific effects on both sides of the junction. At first, LRP4 contributes to the pre-synaptic maturation of the nerve terminal increasing the clustering of acetylcholine vesicles through a retrograde signalling (Yumoto et al, 2012). Most importantly, LRP4 is the key intermediary protein that induces MuSK activation following agrin stimulation (Zhang et al, 2011). Both LRP4 and MuSK are transmembrane proteins that form a heteromeric tetramer on the muscular sarcolemma. LRP4 interacts with MuSK even in the absence of agrin and this basal interaction is sufficient to partially activate MuSK causing the pre-patterning of acetylcholine receptors in myotubes prior to innervation (Arber et al., 2002; Kummer et al., 2006). Since the innervation process starts where the pre-pattered AChR are located, the secretion of agrin by the motor nerve represents a fundamental step to strengthen the connection between the two sides of the junction, leading to the formation of mature AChR clusters and the establishment of a fully-operational neuromuscular synapse.

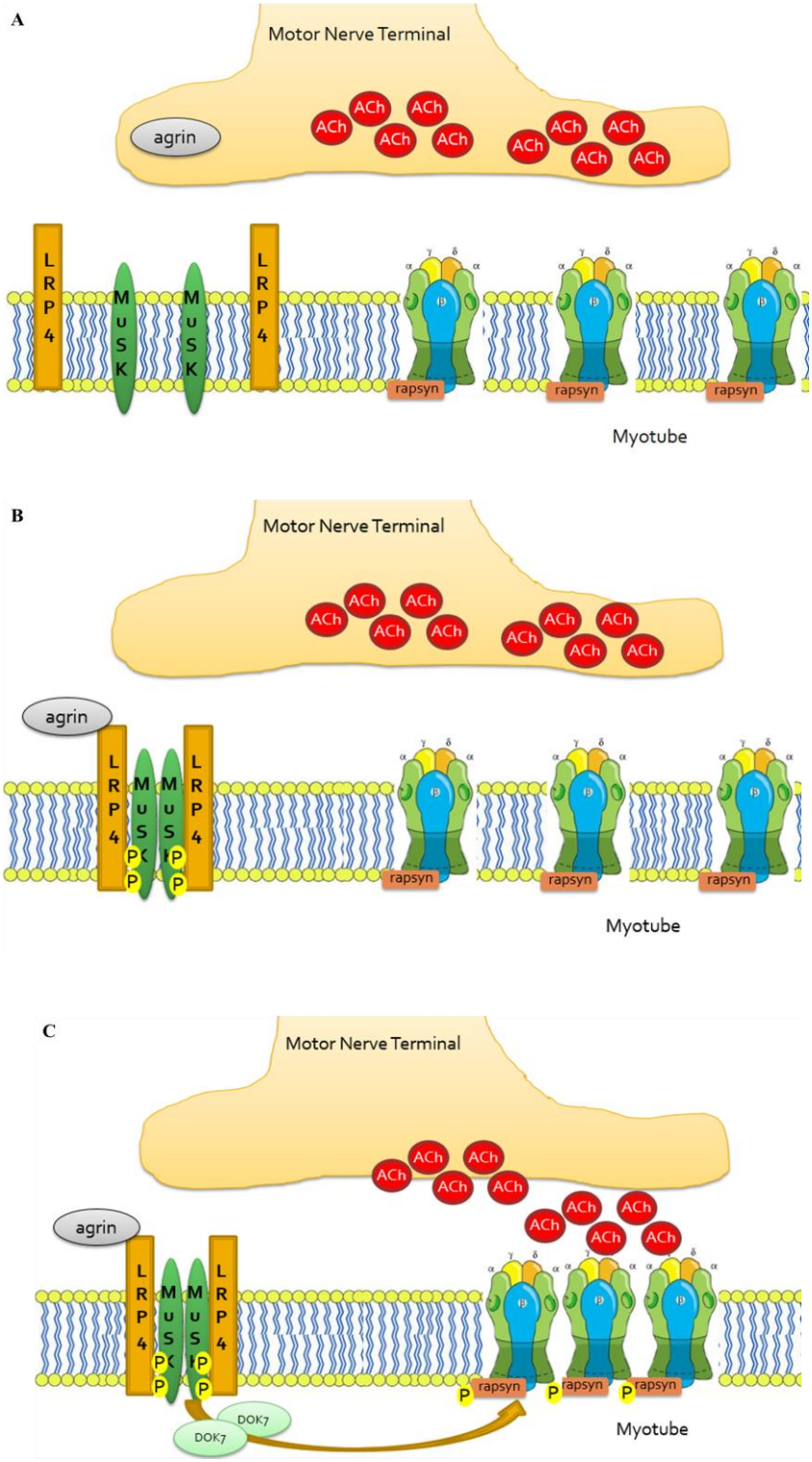

Figure 1. Schematic representation of the agrin-LRP4-MuSK-Dok7 clustering pathway. On the muscle sarcolemma, LRP4 and MuSK form a loose tetramer and AChRs are disperse (A). Once agrin is secreted by the motor nerve terminal into the synaptic cleft, it interacts with LRP4 inducing a conformational change in the LRP4-MuSK tetramer. MuSK is activated and starts an autophosphorylation loop (B). Finally, through the mediation of Dok7, the phosphorylation cascade is triggered and culminates in the activation of rapsyn and AChRs clustering (C). Aggregation of AChRs in clusters is fundamental for a fast and effective response to acetylcholine stimulation and, therefore, for the correct signalling at the neuromuscular synapsis.

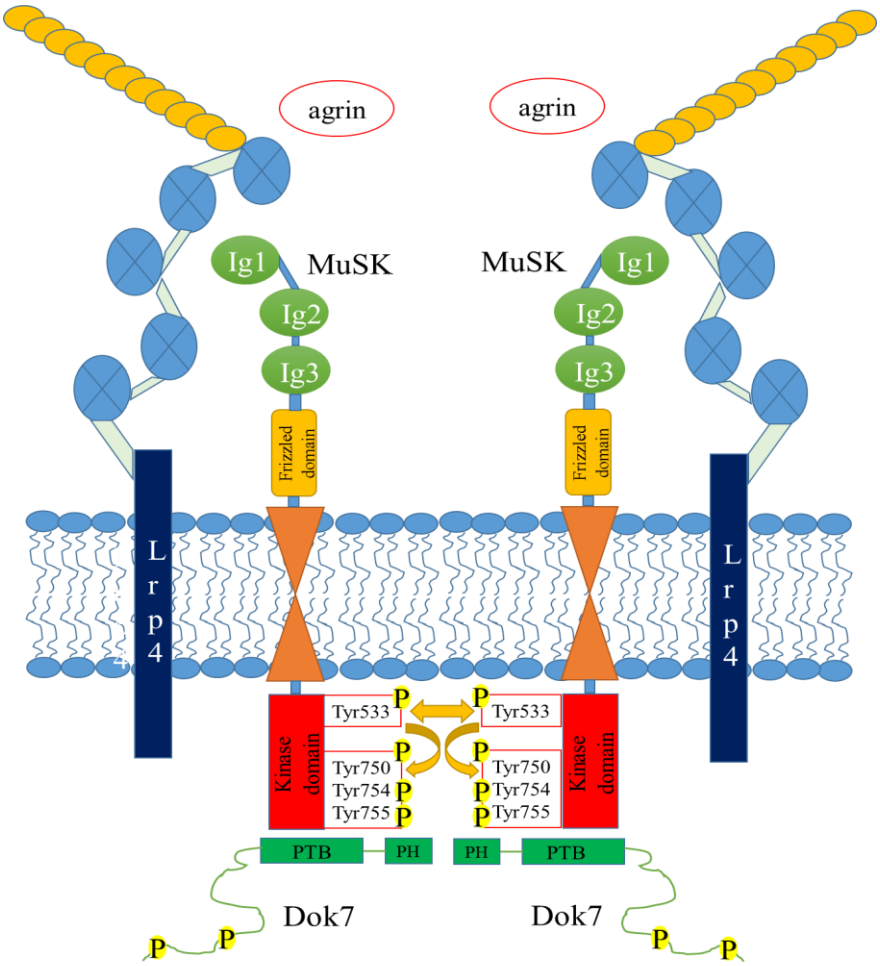

Figure 2. LRP4-MuSK-Dok7 structures and interactions. MuSK consists of an extracellular domain, a transmembrane helix, and an intracytoplasmic region. The extracellular part has three immunoglobulin-like domains (Ig1-3) and a cysteine-rich frizzled domain. The first immunoglobulin-like (Ig1) domain mediates the interaction with the extracellular region of LRP4. MuSK tyrosine kinase domain is located in the intracytoplasmic part of the protein and its juxtamembrane tyrosine residue 533 (Tyr533) starts the autophosphorylation of MuSK dimer. Other three tyrosine residues (Tyr750, Tyr754 and Tyr755) are then phosphorylated in an activation loop. To sustain MuSK activation, Dok7 is recruited and binds to Tyr 533 through its PTB domain. The PH domain mediates the dimerization of Dok7 and stabilises also MuSK dimer. MuSK and Dok7 activates each other this reciprocal activation starts the intracellular phosphorylation cascade that causes the clustering of the acetylcholine receptors.

The binding of agrin to the N-terminal of LRP4 induces a conformational change in the structure of the whole LRP4-MuSK tetramer that tightens the interaction of two molecules of MuSK (Zhang et al., 2011; Zong et al., 2012). This causes the autophosphorylation of the tyrosine residues located on the intracytoplasmic part of MuSK and the beginning of a phosphorylation cascade that determines the clustering of the acetylcholine receptors (Figure 1B, C).

MuSK is a complex protein consisting of three main parts: an extracellular domain, a transmembrane helix, and an intracytoplasmic region (Figure 2). The extracellular part has three immunoglobulin-like domains (Ig1-3) and a cysteine-rich frizzled domain. The first immunoglobulin-like (Ig1) domain is essential as it mediates the interaction with LRP4 and, together with the Ig2 domain, forms a dimer with another MuSK molecule (Zhang et al., 2011; Stiegler et al., 2006). A hydrophilic transmembrane helix connects the extracellular domains to the intracytoplasmic region that contains the tyrosine kinase. Within the first cytoplasmic juxtamembrane segment, there is a tyrosine residue 533 (Tyr533) which starts the autophosphorylation process that activates MuSK (Herbst and Burden, 2000). Three other tyrosine residues located in the kinase domain (Tyr750, Tyr754 and Tyr755) are then phosphorylated in an activation loop (Till et al, 2002).

In order to sustain MuSK activation, however, it is necessary to recruitan additional adaptor protein, docking protein 7 (Dok7). Dok7 presents two main consecutive domains, the N-terminal PH and the PTB, followed by a long unstructured region that contains two sites of tyrosine phosphorylation (Figure 2). The PTB domain binds directly to phosphorylated Tyr553 of MuSK while the PH domain mediates the dimerization of Dok7 and stabilises also MuSK dimer in order to promote trans-phosphorylation of Tyr750, Tyr754 and Tyr755 (Bergamin et al, 2010). The role of Dok7 is essential as it operates both upstream and downstream of MuSK. MuSK and Dok7 activate each other and this reciprocal activation starts the intracellular phosphorylation cascade that causes the clustering of the acetylcholine receptors.

1.5.2) Clustering of the acetylcholine receptors and transmission of the signal

The downstream parts of the pathway have been only partially defined. Following MuSK-Dok7 activation, several other adaptor proteins are

phosphorylated and activated, in particular Crk and Crk-L (Hallock et al, 2010), as well as other kinases, such as Abl (Finn et al, 2003), Scr (Mittaud et al, 2001), and GTpases of the Rho family (Weston et al, 2003). The whole cascade converges on the phosphorylation of the AChR subunits and rapsyn (Figure 1C), a structural protein that self-aggregates making a scaffold where the AChRs could anchor to the actin cytoskeleton and form mature dense clusters (Borges et al, 2001; Zuber et al, 2013; Lee et al, 2009).

The clustering of the acetylcholine receptors in a pretzel-like shape, that resembles the form of the nerve terminal, represents the final result of the activation of agrin-LRP4-MuSK-Dok7 pathway. Only clustered receptors are able to respond appropriately to the signal transmitted by the motor nerve terminal and determine muscle contraction. The acetylcholine receptor located on the muscular sarcolemma is a nicotine type ligand-gate ion channel. The adult receptor is formed by 5 subunits with a stoichiometry of α_2-β-δ-ε, while the fetal form presents a γ subunits instead of the ε one (Mishina et al, 1986). The subunits are disposed in a circle in order to create a central pore for the passage of the ions. Each subunit carries an extracellular domain, four transmembrane domains (TMD1-4) linked together with intracellular or extracellular loops, and an intracytoplasmic C-terminal end. The binding sites for acetylcholine are in the interface between the extracellular domains of the α−δ and α−ε subunits (Lee et al, 2009; Mukhtasimova et al, 2009).

The neurotransmitter acetylcholine is secreted in quantal amount into the synaptic cleft, as firstly suggested by Bernard Katz in 1966, as the nerve action potential reaches the nerve terminal causing the exocytosis of the ACh vesicles. Acetylcholine diffuses into the synaptic cleft and interacts with the receptors on the postsynaptic muscle membrane. When two acetylcholine molecules bind to the AChR, the receptor undergoes a conformational change that opens the channel allowing the entrance of cations, in particular Na^+, into the cell. The influx of cations causes a local depolarisation of the membrane, called the end plate potential (EPP) which then, if the stimulus is enough to reach the threshold of -50 mV (Slater, 2015), leads to the generation of an action potential. To ensure a fast and efficient transmission through the synapse, the AChR clustering pathway concentrates the receptors (up to 10000 AChRs per micron) on the muscle membrane opposed to the motoneuron terminal. AChRs density drops to less than

10 per micron just a few micrometers away from the junction. At this concentration, AChR receptors are too disperse and, therefore, are not able to sustain the transmission of the signal after the binding with the ACh. On the other hand, once the action potential is generated in an area wiht high AChRs density, the signal propagates along the sarcolemma, determining the release of calcium from the intracytoplasmic reticulum and, consequently, muscle contraction. The action of acetylcholine is terminated by the enzyme acetylcholinesterase that is located close to the AChR and hydrolyses ACh into its two basic components (choline and acetyl-CoA).

1.5.3) Negative regulation of AChR clustering

It is worth noting that the continuous muscle stimulation by the release of acetylcholine from the nerve is the main negative regulator of AChR clustering. Prolonged Ca^{++} influx, due to sustained ACh stimulation, activates calpain, a protease constitutively inhibited by rapsyn. Once activated, calpain induces AChR cluster dispersal through Cdk5 activation (Lin et al, 2005; Chen et al, 2007) Muscle contraction also leads to a suppression of AChR expression (Tang et al, 2004) and promotes the dispersal of AChR clusters (Lin et al, 2005; Misgeld et al, 2005). This represents a protective mechanism to reduce the risk of a tetanic contraction caused by an overstimulation of the muscle. Moreover, negative regulators and controllers of AChR play a fundamental role avoiding an uncontrolled and scattered localisation of AChRs on the muscular sarcolemma and addressing the clusters next to the nerve terminal where the functional junction should properly develop. In this scenario, one of the most important regulators the pathway is SRC homology 2 domain containing phosphotyrosine phosphatase 2 (SHP2). This phosphatase is activated by MuSK through the intermediate action of Src and SIRPα1 proteins and, in a negative feedback loop, it reduces MuSK phosphorylation. Therefore, SHP2 is able to induce AChRs dispersal in extrasynaptic sites, in particular during the early stages of the junction development (Qian et al, 2008).

1.6) Pathophysiology of myasthenia gravis

For several reasons, myasthenia gravis is considered a paradigm of antibody-mediated diseases. The pathogenic mechanisms underlying the symptoms have

been studied intensely over the last 50 years and have provided a wide understanding of the role of the different IgG subclasses and how they cause impairment of the neuromuscular transmission. In particular, important differences have emerged in the pathogenesis of AChR- and MuSK-MG, the two most frequent and best characterised forms of the disease, and they will be described in detail in the following paragraphs.

1.6.1) AChR-MG

Role of antibodies

Myasthenia gravis is associated in more than 80% of the cases with antibodies directed against the acetylcholine receptor and there is much evidence supporting a pathogenic cause of the damage and destruction of the postsynaptic muscle membrane. AChR antibodies target an epitope formed around aa 67-76 on each α subunit of the AChR, which are termed the "main immunogenic regions" (MIR). The antibodies are mainly of the IgG1 and IgG3 subclasses and, therefore, they activate the classic complement cascade following their binding to the AChRs (Aharonov et al., 1975; Lennon and Lambert, 1981; Vincent, 2002). The final effect of the complement activation causes a rapid calcium influx into the muscle cytoplasm and the consequent destruction of the adjacent membrane together with loss of the AChRs and voltage-gate sodium channels which are concentrated at the bottom of secondary folds of the sarcolemma (Tüzün et al, 2013; Ruff and Lennon, 1998). These latter events determine the reduction in acetylcholine response and also the increase of the threshold necessary to trigger the action potential. Another mechanism of action of the AChR-Abs is related to their ability to bind two different AChR molecules, mainly through the two main immunogenic regions. This divalent binding causes the internalisation of the receptors increasing their turnover and lysosomal degradation inside the muscle cell (Heinemann et al, 1977; Drachman et al, 1978). Finally, a third and apparently less important pathogenic effect of the antibodies, described in a minority of patients' sera, is the direct block of AChR channel function (Burges et al, 1990).

There are two main adaptive mechanisms actuated by the nerve and the muscle to compensate the effects of antibody mediated damage to the junction. First, in the presynaptic terminal, the number of acetylcholine vesicles rise in order to

reinforce the amount of neurotransmitter realised into the synaptic cleft. Furthermore, on the other side of the junction, the muscle increases the transcription of AChR subunits genes trying to replace the receptors that have been lost (Weidoff et al, 1981; Plomp et al, 1995. The efficacy of these compensatory mechanisms could have a significant impact in the variability and distribution of the symptoms.

Role of the thymus

Although the pathogenic effects of the antibodies on the neuromuscular junction are quite well understood, the very first stages of the aetiology of the disease concerning the loss of tolerance for the self antigen are still a matter of speculations. In AChR-Ab myasthenia, pathological changes on the thymus play a significant role in the future development of the disease but the association with thymic pathology is not found with other subtypes of myasthenia, especially in the MuSK-MG.

Some evidence regarding how the self-tolerance for the AChR is lost come from a study on the tymic expression of the gene that encodes for the AChR α subunit, *CHRNA1*. A polymorphism of the *CHRNA1* promoter been associated with early onset of myasthenia in French and UK populations (Giraud et al, 2007). This variant of the *CHRNA1* promoter prevents binding of interferon regulatory factor 8 (IRF8) and reduces the promoter activity in thymic epithelial cells. Therefore, IRF8, together with the *A*uto*I*mmune *RE*gulator (AIRE), modulates the expression of the AChR α subunit and regulates a subtle balance (plays a tug of war) between self-tollerance and autoimmunity.

In early-onset myasthenia, the thymus usually presents lymphofollicular hyperplasia with an increased number of germinal centres and lymphoid follicles. MHC-class II expressing thymic epithelial cells present the unfolded AChR subunits and activate auto-reactive $CD4^+$ T cells (Marx et al, 2013). The theory is that T cells sustain the formation of early AChR antibodies that are able to recognise and attack the properly folded AChRs expressed on the membrane of the myoid cells of the thymus. The consequent inflammation, complement activation and release of AChR-Ab/immune complexes cause the activation of other professional antigen presenting cells and initiate an activation loop of $CD4^+$ T cells and the expansion of auto-reactive B cells. Finally, the maturation of

B cell receptors leads to the production of high-affinity AChR-Abs and eventually result in spreading of the autoimmune process to peripheral lymph nodes (Willcox et al, 2008; Thiruppathi et al, 2012). However, this is still largely speculative, and whether the autoimmune reaction in the thymus is the primary event or a secondary expansion is not yet clear.

In thymoma related myasthenia, the pathogenic thymic tissue has many features that could impair self tolerance. The neoplastic epithelial cells express a variety of striatal antigen epitopes, including sequences of the AChR subunits and titin. The theory here is that concomitant reduced expression of both AIRE immune regulator and MHC-class II (Strobel et al, 2008) interfere with the correct maturation of regulatory T cells resulting in development of naïve and pre-primed autoreactive T cells in the peripheral blood that further activate autoimmune B cells (Hoffacker et al, 2000).

1.6.2) MuSK-MG

As mentioned above, MuSK-MG differs in several ways from the more common AChR-MG. MuSK-Abs are mainly of the IgG4 subclass (McConville et al, 2004) and, consequently, they do not activate the complement cascade like the IgG1-3 subclasses. Moreover, IgG4 are functionally monovalent as they exchange their antigen binding fragment (Fab) with other IgG4 antibody Fabs, independently of antigen specificity (Koneczny et al, 2016). For these reasons, the main pathogenic effect of MuSK-Abs is thought to be interference with the physiological function of MuSK rather than complement-mediated damage or internalisation of the protein.

Evidence of the pathogenicity of MuSK-Abs come from different animal models created by both passive and active immunization. All these models showed clinical myasthenic features and/or impaired neuromuscular transmission, with reductions in endplate AChR and in EPP amplitudes (Shigemoto et al, 2006; Cole et al, 2010, Klooster et al, 2012; Viegas et al, 2012). *In vitro* experiments on C2C12 myotubes provided further insights on the effects and role of MuSK-Abs showing their ability to inhibit MuSK phosphorylation and disperse AChR clustering (Koneczny et al, 2013; Huijbers et al, 2013). The first Musk Ig-like domain, located in its extracellular part, is the main epitope recognised by the antibodies. This particular segment mediates the interaction between LRP4 and

MuSK and, therefore, the binding of the antibodies prevents agrin-induced LRP4-MuSK dimerization (Huijbers et al, 2013). MuSK is not therefore activated and, consequently, the whole pathway that leads to AChR clustering is inhibited at the beginning. The effect of Ach which is to disperse the clusters, then dominates with impairment of neuromuscular signalling.

The role of the small proportion of IgG1-3 is still controversial. Like MuSK IgG4, IgG1-3 antibodies have also been reported to inhibit agrin-induced AChR clustering in C2C12 myotubes indicating that all four subclasses have pathogenic potential (Koneczny et al, 2013). Moreover, a mouse model knockout for murine IgG1 (equivalent to human IgG4) developed a full myasthenic symptomatology once immunised against MuSK, and the immune response was sustained by the murine equivalent of human IgG1-3 subclasses (Küçükerden et al, 2016). Finally, all MuSK IgG subclasses were able to disperse the clusters in Dok7 overexpressing myotubes, that form spontaneous AChR clusters independently of agrin (Koneczny et al, 2013). This suggests that MuSK-Abs have different mechanisms of action and their pathogenic effects are not confined to the block of LRP4-MuSK interaction.

It is worth noting that the *in vivo* models of MuSK myasthenia lack the presynaptic adaptive increase of ACh release observed in the AChR-Ab models (Mori et al, 2012; Patel et al, 2014; Viegas et al, 2012). An effective explanation of this observation has not been proposed yet. However, it is likely that MuSK-Abs are able to disrupt retrograde signalling that compensates for the loss of AChRs in the AChR-Ab disease. The absence of this adaptive mechanism could partially explain the higher severity and resistance to treatment observed in MuSK patients.

1.6.3) LRP4-MG

AChR and MuSK related myasthenia are the only two subtypes of the disease for which the pathogenic role of antibodies has been proven. Nevertheless, LRP4-Abs are mainly of the IgG1 and IgG2 subclasses and could have pathogenic potential. They bind complement and, moreover, they could interfere with LRP4-MuSK interaction similarly to the way already described for MuSK-Abs. Both *in vitro* and *in vivo* experiments (Zhang et al, 2012; Pevzner et al, 2012; Shen et al, 2013) have provided some important clues for their pathogenic effects but the

high variability in the incidence of LRP4 antibodies in different studies, often using less reliable techniques (eg. ELISA) and the concomitant detection of MuSK-Abs in a significant proportion of cases suggest that further studies are needed in order to determine the true clinical relevance of these antibodies.

1.7) Diagnosis

The diagnosis of myasthenia is based on clinical symptomatology, electromyographic recording and antibody characterisation. Clinical suspicion arises when the patient describes fluctuant weakness, without concomitant sensory impairment, that improves with rest and that affects skeletal muscles, particularly the ocular and those of the proximal limbs.

Further proof is usually provided by electromyography (EMG) with repetitive stimulation of the peripheral nerve. In myasthenic patients, there is a typical decrement of about 10% in the amplitude of the muscle action potential while stimulating the nerve at 2–5 Hz. The sensitivity of this test reaches its maximum if performed in generalised forms on proximal or facial districts (up to 90% of sensitivity) but it drops dramatically in the pure ocular forms (30-60%) and when tested on distal muscles such as the abductor digiti quinti (about 60%) (Zambelis et al, 2011). To increase the sensitivity and specificity of the test, it is possible to perform repetitive stimulation on a single muscle fibre (Single Fiber ElectroMyoGram - SFEMG) although it requires a high skilled electromyographer together with a collaborative patient and it is available only in specialised centres. SFEMG analyses the variation of inter-potential interval (jitter) between different muscular fibres. A prolonged jitter value (55 μs for a 55 μs for an individual value and 36 μs for a mean value, although the threshold varies among different muscles at different ages and have been defined in a collaborative multicentre study by Bromberg and Scott 1994) is considered abnormal and diagnostic for impairment of neuromuscular transmission. A properly performed SFEMG on a proximal muscle reached a very high sensitivity (up to 99%) in the detection of myasthenia gravis (Sarrigiannis et al, 2006; Sanders et al, 1996). Despite its sensitivity, SFEMG has a lower specificity as abnormal jitter values can be found in other diseases such as myopathies and neuropathic disorders (Sarrigiannis et al, 2006). Therefore, its results should be interpreted carefully considering the whole clinical picture of the patient, and the differential diagnoses considered.

Laboratory tests have become progressively more and more important over the years and, nowadays, antibody detection and characterisation represent a necessary step during the diagnostic process. Different antibodies sustain the diagnosis of specific forms of the disease and their pathogenic mechanisms influence which therapeutic strategy is the most appropriate for the correct treatment of the patient.

The radio immunoprecipitation assays (RIA) represent the most available and specific tests for detection of AChR and MuSK-Abs. In AChR generalised myasthenia, RIA sensitivity is above 85% and reaches almost 100% in patients with thymoma while it is positive in only 50-60% of ocular forms (Oger et al, 1987). On the other hand, RIA specificity approaches 100%, regardless of distribution of the deficit and, therefore, a positive test is sufficient to confirm the diagnosis of AChR-MG. The radioimmuno assay was first introduced by Lindstrom in 1973. The acetylcholine receptor is mixed with ^{125}I-α bungarotoxin (a radioactive-labelled snake toxin that binds selectively to the nicotine AChR) and after incubation with the patient serum, a second antibody is added to precipitate the ^{125}I-α bungarotoxin-AChR-Ab complex. The radioactive counts are measured and results are compared to healthy control sera. A similar assay that uses the same principles of AChR RIA, is available for the detection of MuSK-Abs, where the whole extracellular domain of MuSK is labelled with ^{125}I and used as radioactive antigen (Matthews et al, 2004). The specificity of MuSK RIA reaches 100% but its sensitivity is hard to estimate as the proportion of MuSK patients varies among the different populations studied. Despite the sensitivities of these two assays, there are always seronegative patients (see above) and the introduction of cell-based assay (CBA) in the last decade has increased the sensitivity of both AChR and MuSK-Ab detection. In the CBAs, human embryonic kidney-293 (HEK) cells are transfected with the DNA of the gene to express the protein on the cell surface together with a fluorescent tag. For the AChR assay, all five of the genes of the AChR subunits (adult type) are transfected together with rapsyn in order to express a full clustered AChR and mirror a more physiological condition compared to the RIA. The AChR CBA is able to identify up to 66% of patients resulted previously negative in the conventional RIA, including 50% of the ocular forms and is particularly useful in differentiating SNMG from genetic forms of myasthenia (Jacob et al, 2012;

Rodriguez Cruz et al, 2015). Also in the case of MuSK, a CBA has increased by a small amount detection of antibodies in a further 8% of previously seronegative patients. The MuSK patients who were positive only in the CBA, presented a milder phenotype and less effective clustering inhibition in *in vitro* experiments compared to the patients positive in the RIA (Huda et al, 2017).

In respect of LRP4 antibodies, CBA and ELISA are the main tests used for their detection (Zhang et al, 2012; Pevzner et al, 2012; Zisimopoulou et al, 2014) but their comparability, sensitivity and specificity have not been determined yet. A commercial and reliable assay to detect LRP4 antibodies is therefore needed in order to better understand the real incidence and significance of LRP4 antibodies.

1.8) Therapy

Among neurological and neuromuscular diseases, myasthenia gravis is one of the few that can be successfully treated providing a complete and stable remission in a significant proportion of patients; in paralleladvances in therapy have markedly reduced both mortality and morbidity. Due to our growing understanding of the pathogenic mechanisms that sustain the disease, a variety of treatments has been developed during the last decades spreading from symptomatic drugs, that improve neuromuscular transmission, to specific immunomodulatory therapies that inhibit the production of antibodies.

1.8.1) Acetylcholinesterase inhibitors

Acetylcholinesterase inhibitors represent the first known treatment for myasthenia. Their efficacy was discovered thanks to the intuition of a Scottish clinical fellow, Mary Walker, in 1935. Recognising that myasthenic symptoms were similar to those caused by curare poisoning, Dr. Walker administered an intravenous dose of physostigmine to a patient with generalised myasthenia producing a partial and temporary improvement of her symptomatology (Pearce, 2005). The discovery of Mary Walker not only provided the first safe therapy for myasthenic patients but also suggested, for the first time, that the disease was caused by an impairment of the neuromuscular junction. Oral acetylcholinesterase inhibitors (pyridostigmine) are still broadly used as a first line symptomatic treatment in AChR-Ab myasthenia. Acting inside the synaptic cleft, they reduce the enzymatic cleavage of ACh molecules, increasing the total amount of the

neurotransmitter and prolonging the time during which ACh can stimulate its receptor. Considering its half-life, oral pyridostigmine should be administered about every 4 hours. Generally, most common side effects appear during the first weeks of treatment and are consistent with muscle cramps and muscarinic stimulation of autonomic nervous system. Long-term treatment is generally safe and addiction or cumulative side effects have not been reported. Acetylcholinesterase inhibitors are usually less effective and tolerated in MuSK myasthenia (Evoli et al, 2003; Guptill et al, 2011). The reason underneath this phenomenon is not known yet but an explanation could be related to the inhibition of the whole AChR clustering pathway by MuSK-Abs. This hypothesis is supported by the evidence that a passive immunised animal model of MuSK myasthenia, treated with pyridostigmine, showed increased endplate AChR loss, probably due to increased dispersal of AChRs by the prolonged action of acetycholine (Morsch et al, 2013).

1.8.2) Corticosteroids

In most cases, acetylcholinesterase inhibitors are not able to control completely the symptoms and, therefore, steroids (prednisone and prednisolone in particular) are introduced as first-line immunosuppressant drug. Corticosteroids affect the immune system in several different ways. They inhibit inflammation suppressing and modulating the expression and release of TNF-α and IL-1, they reduce leucocyte proliferation inhibiting the transcriptional factor NF-KB and some evidence suggest that they can impair T cell maturation in the thymus (reviewed by Coutinho and Chapman, 2011). Steroids are usually efficient in controlling symptoms and preventing relapse of the disease and their effect is usually evident within 3 weeks after the beginning of treatment. However, an initial and temporary deterioration of muscle strength can occur during the first days especially when the treatment is started at high dose without a gradual increase (Skeie et al, 2010; Benatar et al, 2012). Some studies have also suggested that steroid treatment can reduce the risk of generalisation in pure ocular forms (Kerty et al, 2013; Benatar et al, 2012). The major issue of long-term administration of steroids concerns the occurrence of serious side effects such as increased blood pressure, diabetes, increase in weight, osteoporosis and muscular atrophy. For these reasons, once control of the symptoms is achieved, steroids should be

decreased gradually in order to achieve the lowest dose able to maintain pharmacological remission.

1.8.3) Immunosuppressive drugs

Immunosuppressive drugs are introduced with the purpose of "sparing" steroids and prevent the need for long-term high doses. Azathioprine is usually the first choice in a plethora of other immunosuppressant possibilities (Bromberg et al, 1997; Palace et al, 1998) and its mechanism of action leans on the inhibition of purine synthesis and the consequent reduction in T and B lymphocytes replication. Azathioprine requires several months (up to more than one year) before showing its effect and, in the meanwhile, the dose of steroids can only be cautiously decreased (Palace et al, 1998). The most important side effect of the drug involves the bone marrow inhibitionwith the risk of medullary aplasia, together with toxicity of the liver, where azathioprine is metabolized by the enzyme thiopurine S-methyltransferase. Some isoforms of this enzyme can modify significantly its activity, therefore their detection in patients' samples should be done before starting the treatment.

Second line immunosuppressants include cyclosporine and mycophenolate mofetil. Both of them are efficient in the treatment of myasthenia gravis in clinical trials (Tindall et al, 1993; Meriggioli et al, 2003) but they are mosts appropriate if azathioprine can not be tolerated or fails to achieve steroid sparing. They present major and more severe side effects compared to azathioprine including nephrotoxicity, increased risk of infections and tumours. Methotrexate is also commonly used in myasthenia despite the fact that clinical trials have never been performed to justify its use. Nevertheless, justification for its application in myasthenia comes from its effectivness in other autoimmune diseases.

For those severe myasthenic patients that do not respond to any other treatments, there is an increasing number of reports regarding the potential benefits of rituximab, a monoclonal chimeric IgG1 that depletes B lymphocytes through specific binding to the CD20 transmembrane antigen (Benveniste and Hilton-Jones D, 2010; Maddison et al, 2011). Despite the fact that controlled studies have not been done yet, early evidence showed that about two thirds of patients with insufficient response to other immunosuppressive treatments had a significant improvement following rituximab administration. This seems to be

particularly true for MuSK myasthenia (Keung et al, 2013; Yi et al, 2013). However, only selected patients should undertake rituximab treatment as it implies several risks, in particular the development of JC-virus-related progressive multifocal leukoencephalopathy as reported during the treatment of other autoimmune disorders (Tan and Koralnik, 2010) and it is expensive.

1.8.4) Thymectomy

In myasthenic subtypes associated with thymic pathologies (early-onset myasthenia with thymic hyperplasia and in case of thymomas), there is a strong indication to proceed with the removal of the gland. Although thymectomy has been practiced since 1941 in myasthenic patients (Blalock et al, 1941), only a recent randomized trial study has finally provided the evidence that the procedure gives substantial clinical benefits compared to the use of steroids alone (Wolfe et al, 2016). In early-onset myasthenia (<50 years old), thymectomy should be performed soon after the diagnosis as it has its highest effectiveness within 5 years from onset (Gronseth and Barohn, 2000). All thymic tissue should be removed and less invasive video- and roboti-assisted thoracoscopic approaches are quickly overtaking the classical sternotomy (Ye at al, 2013).

Obviously, in case of malignancy, thymectomy represents a necessary therapeutic procedure in order to avoid the spreading of the neoplasia and local thoracic compression. With respect to myasthenic symptoms, the removal of thymoma usually does not correspond to a significant improvement of muscle weakness as the autoimmune process has already triggered and sustained by peripheral cells (Hoffacker et al, 2000; Buckley et al, 2001).

Thymectomy is not indicated in MuSK- and LRP4-myasthenia nor in late-onset forms as there is little evidence of thymic involvement and no therapeutic effect has been reported.

1.8.5) Plasmapheresis and intravenous immunoglobulins

In severe relapses of myasthenia and myasthenic crises that require a rapid and effective treatment, both plasmapheresis and administration of intravenous immunoglobulins (IVIG) have shown to provide quick and reliable action. The level of their effectiveness is comparable (Ronager et al, 2001) and their effects usually last about 4-6 weeks.

Plasmapheresis consists in the removal of pathogenic autoantibodies and other pathogenic factors, such as complement proteins, from the blood stream through the exchange of 20–50 mL/kg of plasma every alternate day. The whole procedure is repeated five times, but has been performed chronically in rare cases (Gajdos et al, 2002). Adverse effects include risk of infection, hypocalcemia, hypotension, and thrombocytopenia.

IVIG are less invasive and better tolerated than plasmapheresis and present slightly fewer side effects (Ronager et al, 2001; Zinman et al, 2007). The procedure consists in the injection of 2g/kg/day of concentrated immunoglobulins, mainly IgG, for 5 consecutive days. The mechanism of action is not fully understood but implies cytokine and complement inhibition, competition with autoantibodies, interference with Fc receptor binding or antigen recognition by sensitized T cells. Most common side effects are flu-like symptoms while anaphylaxis reaction can happen in patients with congenital deficiency of IgA (Qureshi et al, 1999). Therefore, IgA level should be determined before beginning IVIG administration.

1.8.6) A new potential therapeutic target: SHP2

As described above, there are several efficient treatments for myasthenia gravis and most patients can now live their lives without significant impairment. Nowadays, several clinicians pointed out that the adjective "*gravis*" should not be used anymore to describe myasthenia as its mortality rate has dropped dramatically over the last decades. Nevertheless, none of the drugs available at the moment are specific as they involve the immune system as a whole. This leads to a variety of side effects, especially when the severity of symptoms requires long lasting immunosuppressive therapy. In this scenario, a treatment able to target and counteract specifically the pathogenic mechanisms of the disease would be important in order to achieve a better and stable control of the symptoms and to decrease the risk of side effects.

Targeting the intracellular regulators of the acetylcholine receptor pathway represents one of the possible therapeutic strategies that could be considered. In particular, SRC homology 2 domain containing phosphotyrosine phosphatase 2 (SHP2) acts as a negative regulator that reduces MuSK phosphorylation and inhibits the AChR clustering pathway (Qian et al, 2008). SHP2 is a nonreceptor

protein tyrosine phosphatase that consists of two SH2 domains, a catalytic protein tyrosine phosphatase (PTP) domain, a c-terminal tail with tyrosyl phosphorylation sites (Y542 and Y580), and a proline-rich motif. SHP2 is basally inactive as the n-terminal SH2 region inhibits the catalytic PTP domain, but upon stimulation by tyrosine-phosphorylated docking proteins, SH2 undergoes a conformational change to facilitate phosphatase activation (Neel et al, 2003; Alonso et al, 2004; Cunnick et al, 2001).

Apart from its specific role AChR clustering pathway, SHP2 also mediates and enhances growth cell signalling in different tissues. SHP2 is involved in activation of Erk1/2 MAP kinase by EGF (Deb et al, 1998), and gain of function mutations of its gene, *PTPN11*, are associated with Noonan's syndrome, juvenile myelomonocytic leukemia, and several types of human malignancies (Bentires-Alj et al, 2004; Tartaglia and Gelb, 2005). For these reasons, SHP2 inhibition has been studied with the aim to understand better tumorigenesis and to develop new antineoplastic drugs (Schneeberger et al, 2015; Grosskopf et al, 2015; Bunda et al, 2015).

Of particular interest is NSC-87877, a SHP 1/2 inhibitor that binds to the catalytic cleft of SHP2 through hydrogen bonds inhibiting its phosphatase activity (Figure 3A, B) (Chen et al, 2006). For the aim of our study, it is important to highlight that the inhibition of SHP2 by NSC-87877 has already been shown to increase AChR clustering in C2C12 mouse myotubes independent of agrin stimulation (Zhao et al 2007). This is an important first evidence of the potential role of SHP2 as a specific target in the treatment of myasthenia, in particular the form associated with MuSK-Abs.

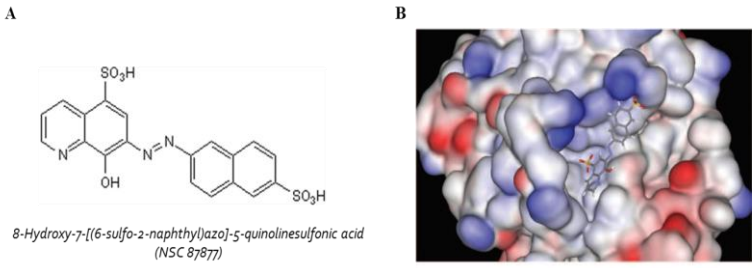

Figure 3. Structure of NSC-87877 and its binding site on SHP2. In A: chemical structure of NSC-87877. In B: Molecular model of NSC-87877 binding to the SHP2 PTP domain. Positively charged areas are coloured in blue, and negatively charged areas coloured in red. For NSC-87877, carbon atoms are coloured in grey, oxygen in red, nitrogen in blue, hydrogen in white, and sulphur in yellow (from Chen et al, *Discovery of a novel SHP2 protein tyrosine phosphatase inhibitor*, Mol Pharmacol, 2006)

Aims of the study

Targeting the intracellular regulators of the acetylcholine receptor (AChR) pathway represents a novel therapeutic strategy in myasthenia gravis. The development of a specific treatment would be important in order to achieve a better and stable control of the symptoms and to decrease the risk of side effects. SH2 domain-containing phosphatase (SHP2) represents a potential target because of its role as a key regulator of the AChR clustering pathway. Through a negative-feedback loop, SHP2 reduces the phosphorylation of Muscle Specific Kinase (MuSK), and thus controls MuSK activation by neural agrin. Its selective inhibition by the drug NSC-87877 has been shown to increase AChR clustering in C2C12 myotubes in either the presence or absence of agrin (Zhao et al 2007). This work started by confirming these preliminary observations and aimed to evaluate, in *in vitro* condition, whether the inhibition of SHP2 by NSC-87877 is able to counteract the pathogenic effects of MuSK-Abs. Therefore, this study tried to answer the following questions:

- Is NSC-87877 able to enhance MuSK phosphorylation level and AChR clustering independently by agrin and which dose causes the highest increase?
- What is the time-course of MuSK phosphorylation after agrin stimulation *in vitro*, and how would it differ after exposure to NSC-87877?
- Is NSC-87877 able to increase MuSK phosphorylation and AChR clustering in the presence of MuSK-Abs?
- Is there any difference in the pathogenic effects between MuSK IgG4 and MuSK IgG1-3 subclasses and, if so, is NSC-87877 effective with all the different IgG subclasses?

Assessing the first two questions allowed us to understand the kinetics of NSC-87877 and its action on the AChR clustering pathway and to set the basic parameters to use in the final experiments aimed to test the efficacy of the drug in the presence of MuSK-Abs.

Chapter 2
Materials and Methods

2.1) MuSK-MG plasma samples

Plasma samples from three different patients affected by MuSK-MG were used for all the following experiments. A diagnosis of MuSK-myashtenia was confirmed on the basis of characteristic clinical features, detection of MuSK-Abs by radioimmunoassay (RIA) and beneficial response to immunotherapy.

2.2) Tissue culture

Human embrionic kidney 293 (HEK 293) cells and C2C12 mouse myoblasts were purchased from ATCC. HEK 293 cells were maintained in 5% CO_2 at 37ºC in Dulbecco-modified essential medium (DMEM) (Sigma-Aldrich) supplemented with 10% of Foetal Calf Serum (FCS - TCS Cellworks Ltd) together with 100 units/ml each of penicillin G and streptomycin (PS - Invitrogen). C2C12 myoblasts were grown in growth medium (DMEM supplemented with 15% FCS and 1% PS) and differentiated for 5-6 days in fusion medium (DMEM containing 2% FCS – 2% Horse Serum and PS, DM) at 37°C in an atmosphere of 8% CO_2.

2.3) Preparation of agrin plasmid and transfection

To generate soluble agrin, cDNA encoding the full-length human neural agrin was cloned into pcDNA3.1hygro(+). The GFP-tag was also inserted at the C-terminus of the agrin. The recombinant protein contains its own signal peptide, which allows agrin to be secreted as a soluble form. HEK 293 cells were seeded at 3.5 x 10^6 cells per T125 tissue culture flask and then transfected using polyethyleneimine (PEI) with 18µg of full-length agrin. Following 48 hours of transfection, conditioned media were harvested.

2.4) Agrin titration

C2C12 myoblasts were seeded at 1.5 x 10^5 per well in 6-well plates and were allowed to fuse to form myotubes. C2C12 myotubes were incubated with seriate dilutions of agrin (1:50, 1:100, 1:200, 1:400, 1:800, 1:1600) at 37 ºC for 16 hours. C2C12 myotubes exposed to DMEM only were used as negative control. The following day, the cells were incubated with Alexa Flour 594-conjugated α-

bungaratoxin (Invitrogen) diluted at 1:1000 in fusion medium for 1 hour at 37ºC. Myotubes were washed 3 times with 500 µl fusion medium, fixed with 3% formaldehyde, and stored in PBS at 4ºC. Images (20 random fields at 20x objective) were captured using Olympus IX71 fluorescence microscope with Simple PCI (Digital Pixel). The number of AChR clusters was counted and analysed using a macro for the ImageJ software.

2.5) IgG and IgG subclasses purification

According to the amount of plasma available, samples from patients 1 and 2 were used to purify total IgG, IgG4 and IgG1-3 subclasses while samples from patient 3 were sufficient to perform only the purification of the IgG subclasses.

For the purification of total IgG, 10 ml of plasma were filtered using 0.2 µm syringe filters, diluted 1:2 in PBS and incubated overnight with 2.5 ml of Protein G Sepharose Fast-Slow (Sigma) at 4°C with gentle shaking. The bead slurry was packed into a column, washed 3 times with 5 ml PBS, and bound IgG were eluted with 0.1 M glycine, pH 2.3. 20 fractions of 1 ml were collected into eppendorf tubes containing 150 µl Tris-HCl pH 8.0 to neutralise the pH, and analysed for protein content by measuring the OD280 with nanodrop. The fractions with the highest OD280 were pooled and dialysed overnight against 200 volumes of DMEM.

For the IgG subclass purification, IgG4 affinity matrix (CaptureSelect™ IgG4 Hu Affinity Matrix – Thermofisher) was used in a similar way as protein G sepharose. 10 ml of plasma were filtered using 0.2 µm syringe filters and diluted 1:2 with PBS, then incubated for 1h at 4°C with 1 ml of IgG4 affinity matrix and packed into a column. After washing 3 times with 5 ml PBS, IgG4 were eluted with 0.1 M glycine pH 2.3. 20 fractions of 1 ml were collected into eppendorf tubes containing 150 µl Tris-HCl pH 8 to neutralize the pH. The flow-through containing IgG1-3 was loaded a second time onto the IgG4 affinity matrix to ensure complete depletion of IgG4. The second flow-through was then incubated overnight with 2.5 ml protein G sepharose and eluted as previously described for total IgG purification. The fractions with the highest OD280 of IgG 4 and IgG1-3 were pooled and dialysed overnight against 200 volumes of DMEM. The fractions with a lower OD280 were pooled and concentrated using Centriprep® 30K

centrifugal filter units (Millipore) in order to reach a similar concentration of the other fractions.

It is worth noting that protein G sepharose has a binding capacity for human IgG of 17 mg/ml while average IgG concentration in the plasma is about 8-18 mg/ml. Therefore, using 10 ml of plasma and 1 ml of matrix, it is possible to obtain only about 1/10 of the total amount of IgG of the original sample. Conversely, IgG4 matrix has a binding capacity of 6 mg/ml. The normal concentration of IgG4 in the plasma is usually between 6-10% of the total IgG (about 0.8-1.8 mg/ml). Therefore, from 10 ml of plasma using 1 ml of matrix, about 1/2- 1/3 of the original IgG4 were purified.

Prior to use the purified samples in the following experiments, the samples were sterile-filtered with Ultrafree®-CL centrifugal devices (Millipore) and then heated at 55ºC for 30 minutes for the inactivation of any residual complement proteins.

2.6) Cell-based assay

In order to verify the effectiveness of IgG subclasses purification, purified samples were tested on a cell-based assay with HEK 293 cells expressing MuSK on their surface. HEK 293 cells were seeded at 1.5 x 10^4 per well in 24-wells plates. The wells were pre-treated with PBS 0.01% poly-L-lysine (PLL) in order to enhance the attachment of the cells to the surface. The following day, cells were transfected overnight with a solution of 0.6 µg pcDNA 3.1 hygro MuSK mCherry, 0.3 µg polyethylenimine (PEI), 0.4 µg 20% glucose, 0.15 µl water per well. 24 hours later, successful transfection was confirmed by visualising mCherry expression using an Olympus IX71 fluorescence microscope. MuSK transfected HEK cells were then incubated with serum, total IgG, IgG4 and IgG1-3 samples at 1:20 dilution for 1 hour at room temperature. Cells were then washed 3 times with 500 µl DMEM and then probed with anti-human IgG, anti-human IgG4, -IgG1, -IgG2, -IgG3 monoclonal mouse antibodies (Sigma) at 1:50 dilution for 1 hour at room temperature. After washing 3 times 500 µl DMEM, cells were fixed with 3% formaldehyde for 20 minutes and then washed again 3 times with 500 µl PBS. Finally, cells were incubated with Alexa Fluor 488 goat anti-mouse IgG (Invitrogen) at 1:200 dilution for 1 hour at room temperature in the dark. Cells were washed 3 times with 500 µl PBS and stored in PBS at 4ºC. Images

were captured using Olympus IX71 fluorescence microscope with Simple PCI (Digital Pixel).

2.7) Radioimmunoassay

MuSK-Ab concentrations were determined by radioimmunoassay (RIA) as previously described (McConville et al, 2004). Plasma samples, purified IgG or IgG subclasses were serially diluted 5-fold in PTX (0.02M PBS, 0.1% Triton X) to a total volume of 50 µl and incubated with 50 µl of ^{125}I labelled MuSK overnight at 4°C. 50 µl anti-human IgG and 5µl of healthy control serum were added and incubated at room temperature until precipitation was visible (approximately 60 minutes). After addition of 500 µl PTX, the samples were centrifuged 5 min at 10000 rpm at room temperature, washed 3 times with 500 µl PTX and then cpm were measured with a Wallac Wizard counter. MuSK-Ab concentrations were calculated using the following equation:

$$x\ nM = \frac{(cpm\ sample - cpm\ control) \times decay\ factor}{(Vol.\ sample\ (\mu l) \times specific\ activity)\ (Ci/mmol) \times counter\ efficiency \times 2.22}$$

assuming a counter efficiency of 0.815.

2.8) Effects of NSC-87877 on MuSK phosphorylation

C2C12 myoblasts were seeded at 1.5 x 10^5 per well in 6-well plates and were allowed to form myotubes after 5-6 days in fusion medium. Myotubes were then starved for 3 hours with DMEM-1% PS to reduce basal phosphorylation levels. Cells were incubated with increasing concentration of NSC-87877 (Tocris®) (1 µM, 10 µM, 100 µM, 200 µM) for 40 minutes at 37°C while myotubes exposed to a non-saturating agrin dilution (1:800) and DMEM were used as positive and negative controls respectively.

The time-course of MuSK phosphorylation was studied incubating the myotubes with NSC-87877 100 µM at different time intervals (15, 40, 90, 180 and 360 minutes) in the presence and absence of agrin (1:800).

Finally, in order to access the effects of NSC-87877 on MuSK phosphorylation in the presence of MuSK-Abs, 0.5 nM purified MuSK total IgG, IgG4 and IgG1-3

were incubated with agrin (1:800) in the presence and absence of NSC-87877 100 μM for 40 minutes at 37°C.

2.9) Immunoprecipitaion of MuSK and western blot analysis

To detect and quantify MuSK phosphorylation levels, after incubation with the different compounds, myotubes were extracted in cold lysis buffer (10 mM Tris-HCl, 1 mM EDTA, 100 mM NaCl, 1% Triton X-100, 1x protease inhibitor cocktail, 1x phosphatase inhibitor cocktail) followed by centrifugation. To precipitate endogenous MuSK, the whole cell lysate was incubated with an anti-MuSK polyclonal antibody (AF562, R&D) at 4 ºC overnight. Bound antibody was captured with Dynabeads® protein G (Invitrogen). For the cells that were incubated with patient purified IgG or IgG subclasses, cell lysates were directly incubated with Dynabeads to immunoprecipitate MuSK with the antibodies from the patients. Bead-precipitated proteins were eluted into SDS sample buffer, subjected to SDS-PAGE and incubated with monoclonal mouse anti-phosphotyrosine antibody (4G10, Upstate Biotechnology). The membrane was then harsh stripped (20 mL SDS 10%, 12.5 mL Tris HCl pH 6.8 0.5 M, 67.5 mL pure water, 0.8 ml β-mercaptoethanol) and reprobed for MuSK by incubating with anti-MuSK polyclonal antibody (AF562, R&D). Densitometry of bands was analysed using ImageJ software and the level of MuSK phosphorylation normalised to levels of immunoprecipitated MuSK.

2.10) AChR cluster assay

C2C12 myoblasts were seeded at a density of 1.5 x 10^5 per well into 6-wells plates and differentiated as described above. First, the myotubes were incubated for 12 hours with increasing concentration of NSC-87877 (1 μM, 10 μM, 100 μM, 200 μM) in order to titrate its effect on AChR clustering. Secondly, the ability of NSC-87877 to reverse the effects of MuSK-Abs was tested. The cells were exposed to 0.5 nM purified MuSK total IgG, IgG4 and IgG1-3 for 30 minutes and then incubated overnight together with agrin (1:800) and in the presence and absence of NSC-87877 100 μM. the following day, AChR clusters were labeled using Alexa Flour 594-conjugated α-bungaratoxin (Invitrogen) diluted 1:1000 in differentiation media for 60 minutes at 37°C. Myotubes were then washed 3 times in differentiation media, fixed in 3% formaldehyde for 20 minutes, and

washed and stored in PBS at 4°C. Twenty fields containing myotubes were selected with bright field and red fluorescent images were captured using an Olympus IX71 fluorescence microscope and Simple PCI (Digital Pixel) software. Images were analyzed for AChR cluster number using Image J software.

2.11) Statistical analysis

All data were analysed using GraphPad Prism 7. Data from at least 3 experiments were pooled and analysed with one-way ANOVA test for multiple comparison. Error bars represent the standard deviation from the mean.

Chapter 3
Results

3.1) Developing the materials

3.1.1) MuSK-MG samples

The experiments used plasma samples from 3 patients with typical clinical myasthenic features who were positive for MuSK-Abs in the radioimmunoassay and negative for AChR and LRP4 antibodies. All the patients were female with an early onset of the disease (< 40 years). Patient 1, at the moment of the sampling, had a severe form of myasthenia (class IIIB) with mainly facial and bulbar involvement. During the course of the disease, she underwent several immunosuppressive treatments (including steroids, azathioprine, and cyclosporine) and plasmapheresis. She finally achieved full pharmacological remission with rituximab. Patient 2 had a bulbar onset (class IIIB) with proximal involvement of the limbs. Conversely to other cases, she responded well to the therapy and achieved pharmacological remission with azathioprine and prednisolone. Patient 3 was sampled during a myasthenic crisis (class IVB) with respiratory failure. Over the years, she has been treated with steroids, azathioprine, methotrexate and several administrations of IVIG and plasmapheresis. Although the different therapies allowed a remarkable improvement in her symptoms, she has never achieved a complete remission.

3.1.2) Agrin titration

Agrin is a fundamental component of all our experiments as it provides the physiological stimulation for the MuSK pathway. Therefore, agrin was used as a positive control to which to compare the effects of SHP2 inhibition and MuSK-Abs. Agrin was produced by transfecting HEK 293 cells with a cDNA plasmid containing the full-length human neural protein together with a fluorescent tag (used to check the efficacy of cell transfection). Once harvested from the cell medium, agrin was tested at different dilutions on C2C12 myotubes in order to titrate its effects on AChR clustering. Myotubes were exposed to agrin for 12 hours at 37ºC, then fixed in formaldehyde and finally labelled with fluorescent α-bungarotoxin, a snake toxin that binds specifically to the acethylcholine receptors. Myotubes exposed to DMEM were used as negative controls. As expected, we

observed a direct correlation between agrin concentration and the number of AChR clusters (Figure 4). At each dilution, agrin significantly increased AChR clustering compared to DMEM ($p<0.0001$ for 1:50, 1:100, 1:200, 1:400, 1:800 and $p<0.001$ for 1:1600). We chose the 1:800 non-saturating agrin concentration for the following experiments in order to see the maximum effect of NSC-87877 and MuSK-Abs on AChR clustering and MuSK phosphorylation.

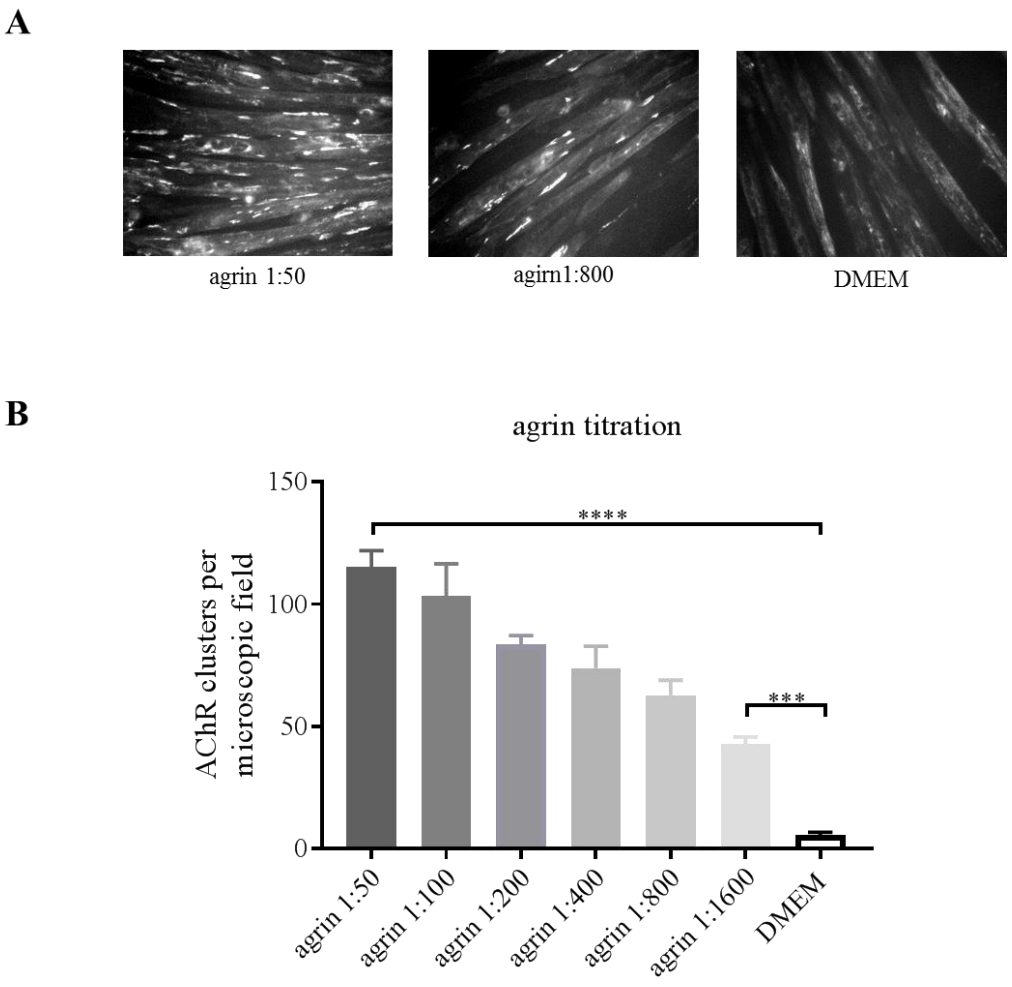

Figure 4. Effect of agrin on AChR clustering (titration curve). In A: AChR clusters labelled with α-bungarotoxin on C2C12 myotubes after incubation with agrin (1:50), agrin (1:800) and DMEM. (Olympus IX71 fluorescence microscope - 20x magnifications). In B: bar chart representing the average number of AChR clusters per microscopic field for different agrin dilutions. Each dilution of agrin significantly increased AChR clustering compared to DMEM ($p<0.0001$ for 1:50, 1:100, 1:200, 1:400, 1:800 and $p<0.001$ for 1:1600; one-way ANOVA; n=3)

3.1.3) Purification of total IgG and IgG subclasses

Total IgG and IgG subclasses (IgG4 and IgG1-3) were purified from the plasma samples of three different MuSK-MG patients. The amount of plasma from patients 1 and 2 was sufficient to purify both total IgG and IgG subclasses, while sample from patient 3 was enough for the purification of IgG subclasses only.

IgG purification consists in an affinity matrix chromatography with protein G sepharose for the total IgG while a IgG4 matrix was used to bind specifically the IgG4 subclass and divide it from IgG1-3. A glycine acid solution (pH 2.3) was used to eluate IgG from the matrix. The first 5-6 fractions usually contain the highest amount of IgG whilst the concentration gradually decreases in the following fractions. In order to not waste precious IgG, the late elutions were pooled and further concentrated. In Figure 5 the elution profiles of the purification of MuSK plasma samples, divided according to the IgG subclasses, are shown.

The final results and the efficacy of IgG purification are represented in Table 1. All the volumes from the different stages of purification are indicated (initial plasma amount, dilution with PBS, flow-through total IgG and IgG4 matrix) together with the relative protein concentrations measured with the nanodrop. After purification, the samples were pooled, dialysed against DMEM to provide a physiological solution for the experiments, sterile-filtered and heated in order to eliminate all residual complement fractions and eventual contamination. All these latter procedures could explain the partial loss of volume and concentration measured in the final purified samples.

.

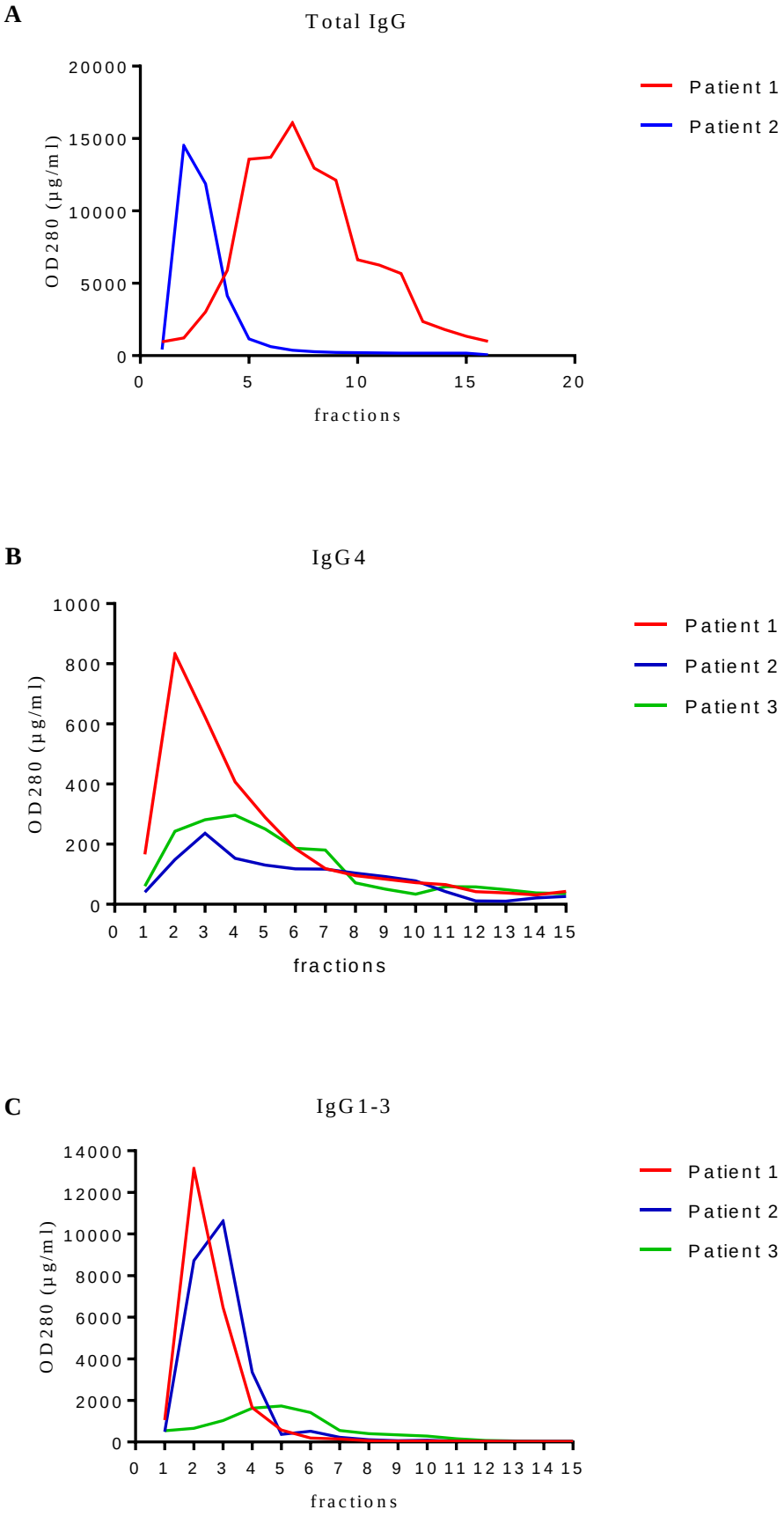

Figure 5. Elution profiles of purified fractions of total IgG (A), IgG4 (B) and IgG1-3 (C) from the three MuSK-MG patients (in red, blue and green respectively). Elution fractions are indicated on the X axis; protein concentrations are indicated on the Y axis.

Patient	Sample	Volume (ml)	OD280 (µg/ml)
1	Plasma	10	29860
	Plasma + PBS (1:1)	20	14711
	Flow-through IgG matrix	17.5	7842
	Total IgG	5	6827
	Flow-through IgG4 matrix	17.5	11378
	IgG4	6.5	294
	IgG1-3	5	6855
2	Plasma	10	32781
	Plasma + PBS (1:1)	20	15356
	Flow-through IgG matrix	18	8245
	Total IgG	7	4764
	Flow-through IgG4 matrix	17.5	7629
	IgG4	7	121
	IgG1-3	5	7767
3	Plasma	7.5	63617
	Plasma + PBS (1:1)	15	36520
	Flow-through IgG4 matrix	15	15441
	IgG4	6	643
	IgG1-3	7	3723

Table 1. IgG purification from MuSK-MG patient's samples: volumes and corresponding protein concentrations (OD280) collected during the different stages of IgG purification for each MuSK-MG patient.

3.1.4) Cell-based assay to access efficiency of MuSK subclasses purification

Once the purification of IgG4 and IgG1-3 was completed, it was important to determine the efficiency of the entire process and to test whether the samples were completely depleted from the complementary IgG subclasses. A MuSK cell-based assay was then performed on HEK 293 cells. The cells were transfected with a MuSK construct together with a fluorescent tag (mCherry) that gives a red coloration on the membrane were MuSK is expressed proving the efficacy of transfection. The cells were incubated with the samples containing IgG4 or IgG1-3 in 1:20 dilution and then probed with specific secondary mouse antibodies directed against the different IgG subclasses. Finally, the samples were exposed to a tertiary green fluorescent antibody directed against mouseIgG. IgG1-3 samples resulted completely depleted from MuSK IgG4 (Figure 6). On the other hand, the IgG4 fraction still showed some positivity for MuSK IgG1-3 indicating that the IgG4 matrix is not completely selective (Figure 7). This should be taken into account in the interpretation of the results of the following experiments.

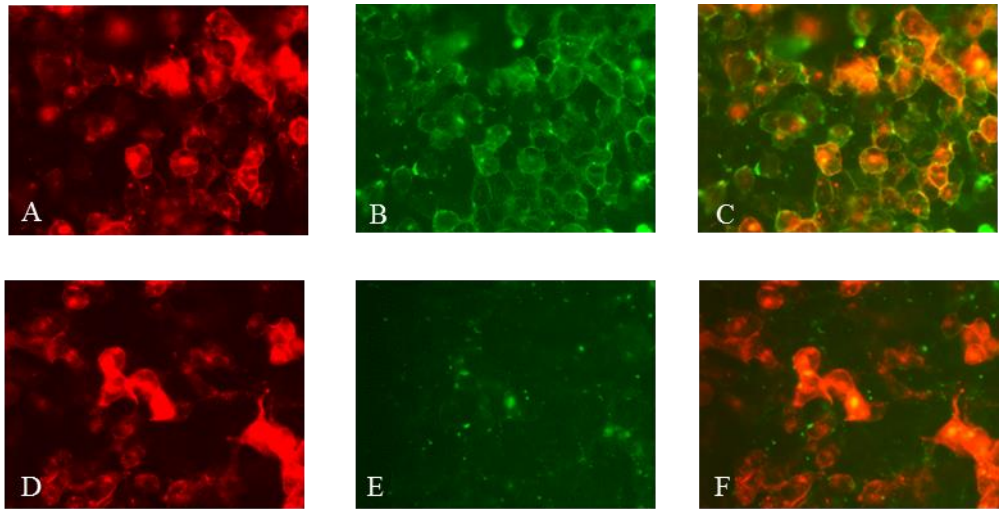

Figure 6. Cell-based assay of MuSK IgG1-3 antibody subclasses. HEK 293 cells were transfected with MuSK-mCherry (in red; A, D). Cells were exposed to MuSK IgG1-3 antibody purified from the three MuSK-MG patients and incubated with mouse anti-IgG1-3 (B) and anti-IgG4 (E) antibodies, and with a tertiary anti-mouse IgG antibody (Alexa Fluor 488 - in green). In C: merge picture showing a strong positivity for the presence of MuSK IgG1-3. In F: only not-specific binding is detectable when IgG1-3 were probed with anti-IgG4 antibody, confirming the effectiveness of IgG1-3 purification (Olympus IX71 fluorescence microscope - 40x magnifications).

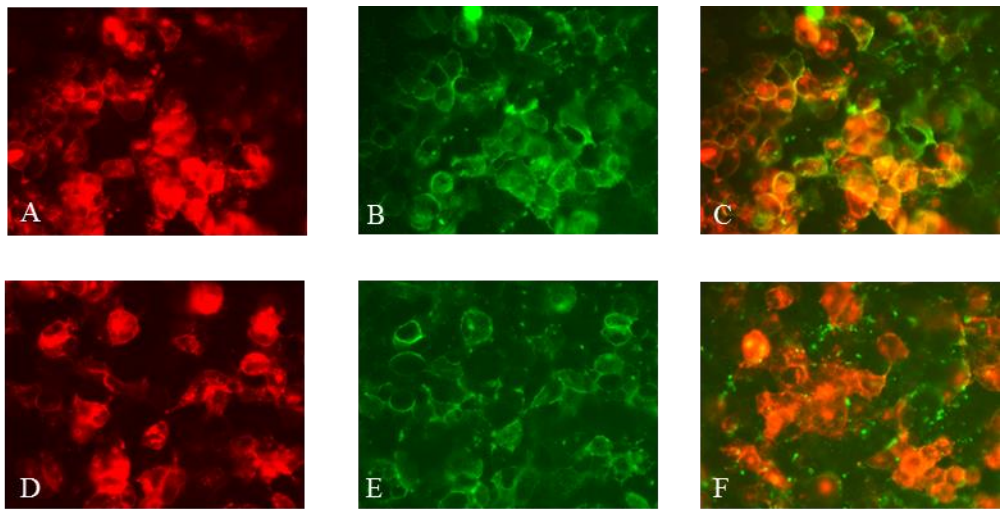

Figure 7. Cell-based assay of MuSK IgG4 antibody subclasses. HEK 293 cells were transfected with MuSK-mCherry (in red; A, D). Cells were exposed to MuSK IgG4 antibody purified from the three MuSK-MG patients and incubated with mouse anti-IgG4 (B) and anti-IgG1-3 (E) antibodies, and with a tertiary anti-mouse IgG antibody (Alexa Fluor 488 - in green). In C: merge picture showing a strong positivity for the presence of MuSK IgG4. In F: IgG4 fraction still showed some positivity for MuSK IgG1-3 indicating that the IgG4 matrix is not completely selective (Olympus IX71 fluorescence microscope - 40x magnifications).

3.1.5) Radioimmunoassay

Estimation of the titre of the MuSK-Ab fractions was obtained through radioimmunoassay (RIA) of different dilutions (from 1:10 up to 1:1280) of the samples from each patient, in order to determine and to standardise the amount of antibodies to use for the experiments. The purified IgG, IgG4 and IgG1-3 were incubated overnight with PTX buffer and 50 µl of MuSK labelled with ^{125}I. 50 µl of anti-human IgG and 5 µl of plasma from a healthy control were then added to the solution to enhance immunoprecipitation. Antibody titration was performed also on the original plasma to evaluate the amount of antibodies lost during the purification process. The titre of MuSK-Abs was calculated according to the equation (see previous chapter "*materials and methods*") using the dilution of the sample and the correspondent radioactive count. The reading of the negative control was deducted from the final count. Figure 8 shows the titration of MuSK-Abs for each patient studied. The number of cpm reach a plateau with lower dilutions of the samples and this corresponds to the saturation level of the assay. The dilution at about half of the maximum cpm was considered the most appropriate point at which to estimate antibody titre.

The titre of MuSK-Abs and the efficiency of IgG purification varied considerably among the patients. For example, patient 3 had a very high concentration of MuSK-Abs in the plasma and the counts decreased slowly as the dilutions increased. On the other hand, in patient 2, cpm dropped sharply after 1:160 dilution indicating a significant lower titre of MuSK-Abs compared to the other patients. It is worth noting that patient 2 had the most efficient purification among the patients, in particular for the IgG4 subclass with a very low decrease in antibody titre. This could be related to the lower amount of antibodies in the original plasma. For the other two patients, IgG purification seemed to be much less efficient considering the loss of more than 10 folds of the initial antibody titre. Table 2 shows the summary of MuSK IgG purification of the three patients including the starting and final volumes, protein concentrations, and antibody titres. In Tables 3 and 4 all the samples' dilutions with the corresponding cpm and estimation of MuSK-Abs amount (mmol) and titres (nM/ml) are shown. As expected, in all patients the titre of MuSK IgG4 was significantly high compared to IgG1-3, confirming that IgG4 is the most represented subclass in MuSK myasthenia.

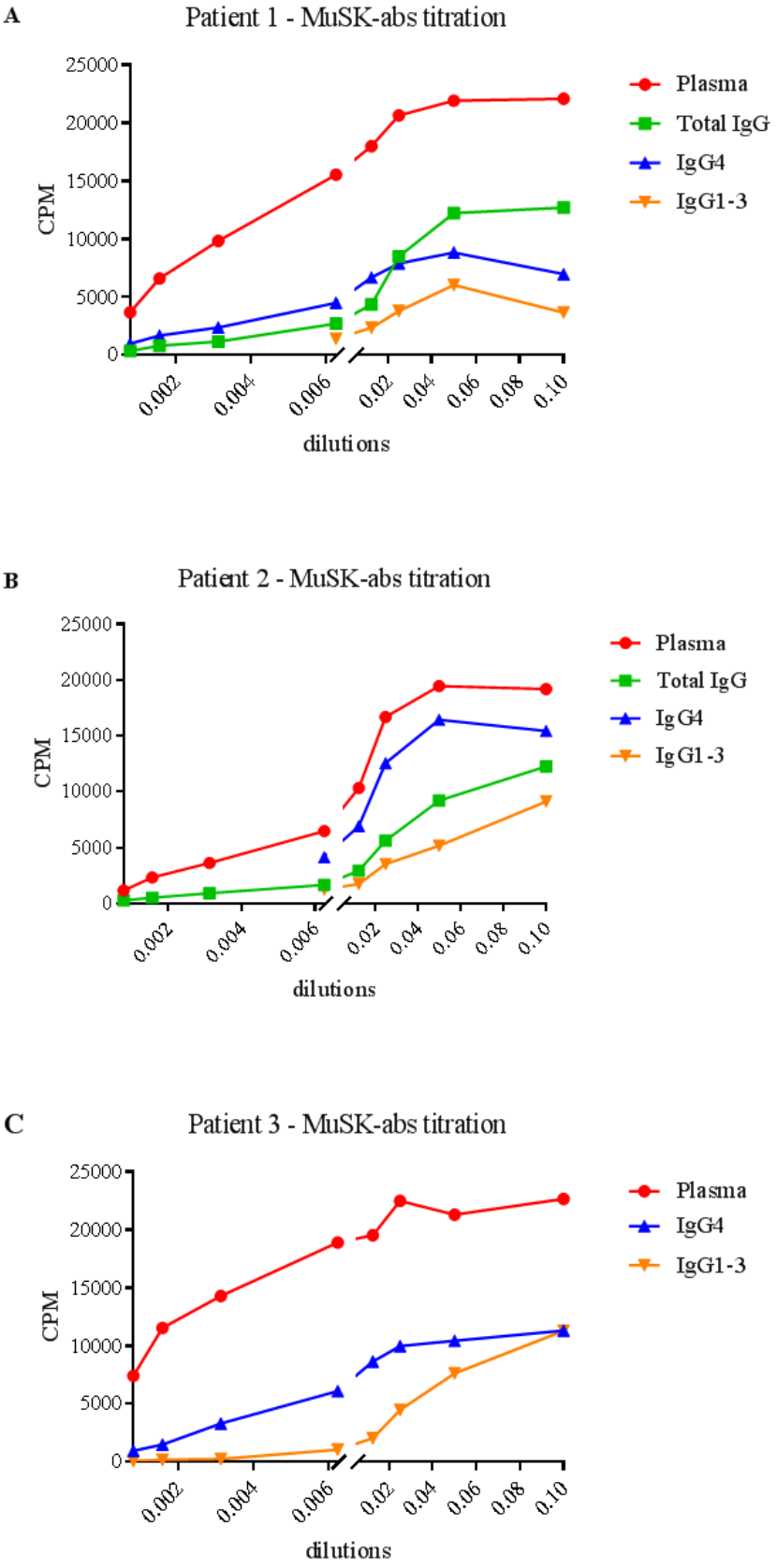

Figure 8. Titration of MuSK antibodies on plasma (red), total IgG (green), IgG4 (blue) and IgG1-3 (orange) samples from the three patients (A, B and C). Sample dilutions are indicated on the X axis; cpm (counts per minute) are indicated on the Y axis.

	Patient 1			Patient 2			Patient 3		
	Vol (ml)	OD280 [µg/ml]	Titre (nmol/ml)	Vol (ml)	OD280 [µg/ml]	Titre (nmol/ml)	Vol (ml)	OD280 [µg/ml]	Titre (nmol/ml)
Plasma	10	29860	11.82	10	32781	3.9	7.5	63617	27.7
Tot IgG	5	6827	1.31	7	4764	0.84	-	-	-
IgG1-3	5	6855	0.71	5	7767	0.53	7	3723	0.6
IgG4	6.5	294	2.86	7	121	3.12	6	643	3.66

Table 2. Initial and final volumes with corresponding protein concentrations and estimated antibody titres of purified total IgG and IgG antibody subclasses for each MuSK-MG patient.

Patient	sample	dilution	cpm	mmol	Titre (nmol/ml)
1	Plasma	1/10	22092	4.14×10^{-12}	0.83
		1/20	21924	4.11×10^{-12}	1.65
		1/40	20666	3.87×10^{-12}	3.1
		1/80	18010	3.38×10^{-12}	5.4
		1/160	15560	2.92×10^{-12}	9.3
		1/320	9843	1.84×10^{-12}	11.82
		1/640	6624	1.24×10^{-12}	15.91
		1/1280	3696	6.93×10^{-11}	17.76
	Tot IgG	1/10	12713	2.38×10^{-12}	0.47
		1/20	12243	2.29×10^{-12}	0.92
		1/40	8501	1.59×10^{-12}	1.27
		1/80	4365	8.19×10^{-11}	1.31
		1/160	2723	5.11×10^{-11}	1.635
		1/320	1183	2.22×10^{-11}	1.421
		1/640	818	1.53×10^{-11}	1.965
		1/1280	371	6.92×10^{-10}	1.78
	IgG4	1/10	6987	1.31×10^{-12}	0.26
		1/20	8844	1.65×10^{-12}	0.66
		1/40	7901	1.48×10^{-12}	1.18
		1/80	6688	1.25×10^{-12}	2
		1/160	4506	8.45×10^{-11}	2.71
		1/320	2385	4.47×10^{-11}	2.86
		1/640	1692	3.17×10^{-11}	4.06
		1/1280	999	1.87×10^{-11}	4.8
	IgG1-3	1/10	3686.2	6.91×10^{-11}	0.14
		1/20	6060.5	1.13×10^{-11}	0.54
		1/40	3792.1	7.11×10^{-11}	0.56
		1/80	2372.3	4.45×10^{-11}	0.71
		1/160	1432.3	2.68×10^{-11}	0.85

Table 3. Titration of MuSK antibody from plasma, purified total IgG, IgG4 and IgG1-3 of patient #1. The dilution at about half of the maximum cpm was considered the most appropriate point at which to estimate antibody titre (highlighted in red).

Patient	sample	dilution	cpm	mmol	titre (nmol/ml)
2	Plasma	1/10	19201	3.60×10^{-12}	0.72
		1/20	19465	3.65×10^{-12}	1.46
		1/40	16691	3.13×10^{-12}	2.5
		1/80	10347	1.94×10^{-12}	3.1
		1/160	6499	1.21×10^{-12}	3.9
		1/320	3643	6.83×10^{-11}	4.37
		1/640	2339	4.39×10^{-11}	5.61
		1/1280	1183	2.22×10^{-11}	5.72
	Tot IgG	1/10	12271	2.30×10^{-12}	0.46
		1/20	9209	1.72×10^{-12}	0.68
		1/40	5625	1.05×10^{-12}	0.84
		1/80	2943	5.52×10^{-11}	0.88
		1/160	1672	3.13×10^{-11}	1
		1/320	920	1.72×10^{-11}	1.1
		1/640	536	1.00×10^{-11}	1.28
		1/1280	288	5.40×10^{-10}	1.38
	IgG4	1/10	15456	6.01×10^{-12}	0.58
		1/20	16444	3.08×10^{-12}	1.24
		1/40	12572	2.35×10^{-12}	1.88
		1/80	6933	1.30×10^{-12}	2.26
		1/160	4161	7.81×10^{-11}	3.12
	IgG1-3	1/10	9138	1.71×10^{-12}	0.34
		1/20	5183	9.72×10^{-11}	0.389
		1/40	3531	6.62×10^{-11}	0.53
		1/80	1760	3.30×10^{-11}	0.66
		1/160	1252	2.34×10^{-11}	0.94
////////////////	////////////////	////////////////	////////////////	////////////////////	//////////////////////
3	Plasma	1/10	22658	4.25×10^{-12}	0.8
		1/20	21298	3.99×10^{-12}	1.6
		1/40	22496	4.22×10^{-12}	3.37
		1/80	19531	3.66×10^{-12}	5.8
		1/160	18906	3.54×10^{-12}	11.3
		1/320	14306	2.68×10^{-12}	17.18
		1/640	11552	2.16×10^{-12}	27.7
		1/1280	7432	1.39×10^{-12}	35.71
	IgG4	1/10	11333	2.12×10^{-12}	0.42
		1/20	10440	1.95×10^{-12}	0.78
		1/40	9990	1.87×10^{-12}	1.48
		1/80	8646	1.62×10^{-12}	2.59
		1/160	6105	1.14×10^{-12}	3.66
		1/320	3318	6.22×10^{-12}	3.98
		1/640	1520	2.85×10^{-12}	3.65
		1/1280	971	1.82×10^{-12}	4.6
	IgG1-3	1/10	11299	2.12×10^{-12}	0.42
		1/20	7639	1.43×10^{-12}	0.57
		1/40	4485	8.41×10^{-11}	0.67
		1/80	2049	3.84×10^{-11}	0.61
		1/160	1082	2.03×10^{-11}	0.64
		1/320	253	4.74×10^{-10}	0.47
		1/640	202	3.79×10^{-10}	0.48
		1/1280	98	1.83×10^{-10}	0.47

Table 4. Titration of MuSK antibody from plasma, purified total IgG, IgG4 and IgG1-3 of patient #1 and #2. The dilution at about half of the maximum cpm was considered the most appropriate point at which to estimate antibody titre (highlighted in red).

3.2) Experimental results

3.2.1) SHP2 inhibition induced agrin-independent AChR clustering

SHP2 inhibition by NSC-87877 has already been proven to induce AChR clustering on C2C12 myotubes independently by agrin (Zhao et al, 2007). For our experiments it was important to confirm these results and to titrate the effects of the drug on both AChR clustering and MuSK phosphorylation in order to identify the most efficient dose and incubation period to use in the experiments with MuSK-Abs. We studied first the effect of SHP2 inhibition on AChR clustering. Increasing concentrations of NSC-87877 were applied for 12 hours on C2C12 myotubes and then the cells were fixed in formaldehyde and the AChR clusters labelled with α-bungarotoxin. The inhibition of SHP2 resulted in a dose-dependent increase of AChR clustering (Figure 9) compared to medium alone. NSC-87877 had the maximal effect at around 100 µM ($p<0.01$ compared to DMEM) which was similar to that achieved by a non-saturating concentration of agrin (1:800). Higher concentrations of the drug did not correspond to a further increase in AChR clustering, indicating a saturation of the process. On the other hand, when myotubes were exposed to NSC-87877 100 µM together with agrin (1:800), the combined effect of the two compounds led to an increase in the number of clusters ($p<0.001$ against DMEM) compared to that observed after incubation with agrin or SHP2 inhibitor alone (Figure 10A, B).

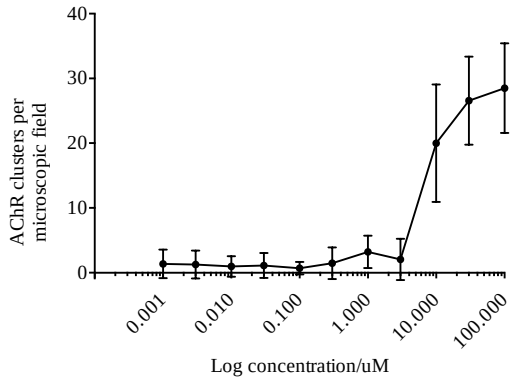

Figure 9. Dose-effect titration curve of NSC-87877 on AChR clustering performed on C2C12 myotubes. The maximal effect was reached at a dose of 100 µM. On the X axis: increasing concentration of NSC-87877. On the Y axis: average number of AChR clusters per microscopic field.

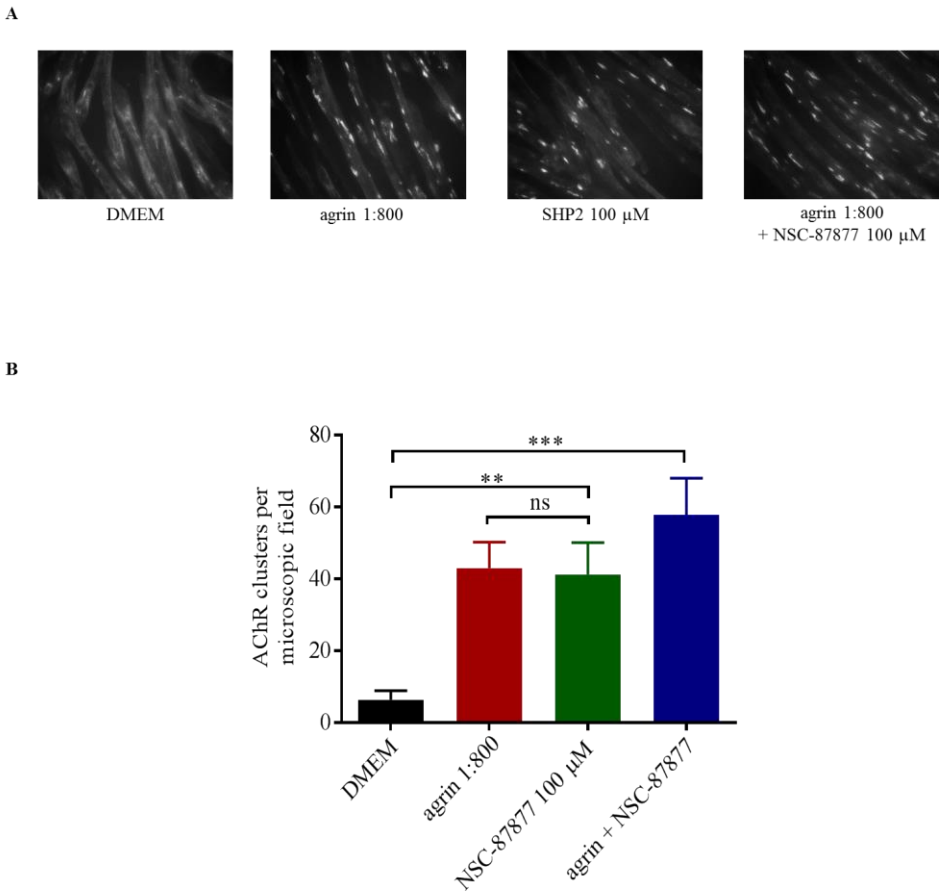

Figure 10. Effects of NSC-87877 (100 µM) on AChR clustering, in the presence and absence of agrin. In A: AChR clusters after incubation with DMEM, agrin (1:800), NSC-87877 (100 µM), and agrin plus NSC-87877 on C2C12 myotubes (Olympus IX71 fluorescence microscope - 20x magnifications). In B: bar chart showing a significant increase of AChR clusters after incubation with NSC-87877 (100 µM) and with NSC-87877 (100 µM) combined with agrin (1:800) compared to DMEM only ($p<0.01$ and $p<0.001$ respectively; one-way ANOVA; n=3). No significant difference was observed between NSC-87877 and agrin alone.

3.2.2) NSC-87877 increases MuSK phosphorylation

To show that the SHP2 inhibitor was acting through MuSK phosphorylation, increasing concentrations of NSC-87877 (1 µM, 10 µM, 100 µM, 200 µM) were applied to C2C12 myotubes for 40 minutes. After incubation, myotubes were lysed in cold lysis buffer to preserve protein phosphorylation and MuSK was immunoprecipitated with Protein G magnetic beads pre-incubated with a commercial anti-MuSK-Ab. MuSK phosphorylation was determined by western blotting, probing the precipitate with a monoclonal antibody specific for phosphotyrosine. Phosphorylation level was normalised to MuSK expression, detected with a commercial anti-MuSK-Ab on the same blot. Agrin (1:800) was used as a positive control and results were compared with DMEM only.

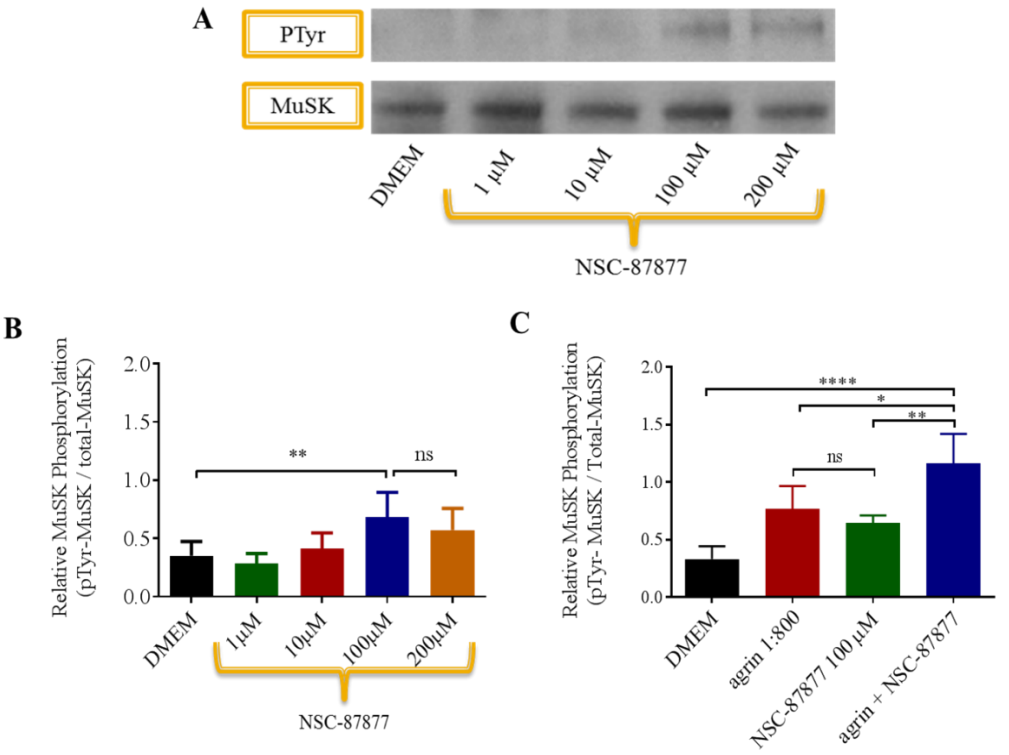

Figure 11. Effects of NSC-87877 on MuSK phosphorylation. In A: example of western blot showing, in the first row, the level of phospho-tyrosine MuSK and, in the second row, the corresponding MuSK expression. Normalised densitometry values of phosphorylated MuSK, obtained by pooling the results of at least 3 different experiments, are represented in the bar charts (B and C). In B: dose-dependent increase of MuSK phosphorylation after incubation with NSC-87877 with maximal effect at 100 µM ($p<0.01$; one-way ANOVA; n=6). In C: effects of NSC-87877 (100 µM) in the presence and absence of agrin (1:800). The combined effect of NSC-87877 (100 µM) and agrin (1:800) caused a significant increase of MuSK phosphorylation compared to DMEM ($p<0.0001$), agrin ($p<0.01$) and NSC-87877 (0<001) alone (one-way ANOVA: n=3).

Consistently with the results observed on AChR clustering, a significant increase of MuSK phosphorylation ($p<0.01$) was observed after incubation with NSC-87877 at 100 µM and 200 µM in the absence of agrin (Figure 11A, B). There was no significant difference between the level of MuSK phosphorylation induced by the SHP2 inhibitor at 100 µM or agrin (1:800), but the combined exposure to both NSC-87877 and agrin caused an increase in MuSK phosphorylation significantly higher compared to each one of the two compounds alone ($p<0.05$ against agrin; $p<0.01$ against NSC-87877; $p<0.0001$ against DMEM) (Figure 11C). Thus, SHP2 inhibition increased MuSK phosphorylation both alone and in the presence of agrin as shown for AChR clustering.

3.2.3) MuSK phosphorylation time-course

Once it was clear that NSC-87877 was able to induce its maximum effect on both AChR clustering and MuSK phosphorylation at a dose of 100 µM, we studied the variation of MuSK phosphorylation over time in order to identify the best temporal interval to perform the experiments with MuSK-Abs.

C2C12 myotubes were exposed over 15 minutes to 6 hours to NSC-87877 100 µM, in presence and absence of agrin (1:800). Myotubes were lysed and MuSK immunoprecipitated at the end of each time interval (15, 40, 90, 180 and 360 minutes). MuSK phosphorylation levels were analyzed by western blotting as describe previously (Figure 12A). The maximum effect was consistently observed between 40 and 90 minutes (Figure 12B, in green) which was similar to the results of agrin alone (red) or both agrin and NSC-87877 (blue). The combined action of agrin and NSC-87877 did not make the MuSK phosphorylation process faster despite the overall increase in phosphorylation level. The submaximal incubation time of 40 minutes was chosen for the following experiments in order to allow the detection of subtle changes in MuSK phosphorylation caused by MuSK-Abs.

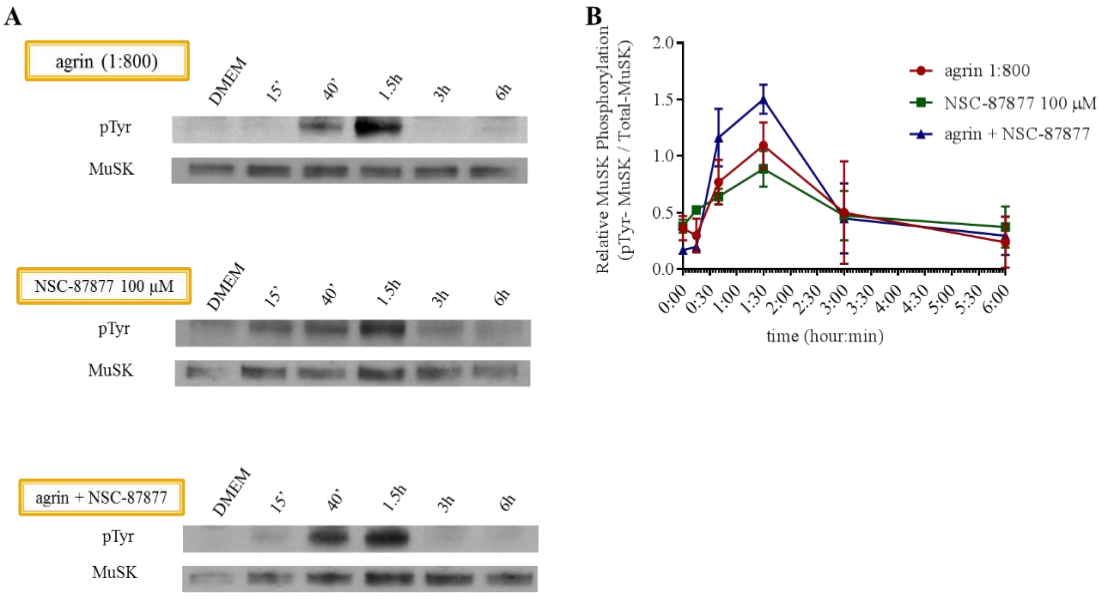

Figure 12. MuSK phosphorylation time-course. In A: western blot examples showing phospho-tyrosine bands and corresponding MuSK expression after incubation with agrin (1:800), in the presence and absence of NSC-87877 (100 µM) at different time intervals (from 15 minutes to 6 hours). In B: variations over time of MuSK phosphorylation (normalised densitometry analysis from 3 different experiments) after exposure to agrin (1:800) (red), NSC-87877 (100 µM) (green) and agrin (1:800) combined with NSC-87877 (100 µM) (blue). All the different compounds showed a similar time-course reaching the maximum effect between 40 and 90 minutes and decreasing progressively after 180 and 360 minutes. The incubation with agrin and NSC-87877 did not induce a faster phosphorylation of MuSK phosphorylation despite an overall increase in phosphorylation levels.

3.2.4) SHP2 inhibition counteracts the effects of MuSK-Abs on both MuSK phosphorylation and AChR clustering

The main question was to ask whether SHP2 inhibition was able to increase MuSK phosphorylation and AChR clustering in the presence of MuSK-Abs and, therefore, to counteract their pathological effects. C2C12 myotubes were incubated with 0.5 nM of purified total MuSK-IgG, IgG1-3 and IgG4 form patients 1 and 2 together with agrin (1:800), in the presence and absence of NSC-87877 100 µM. After 40 minutes of exposure, the cells were lysed and incubated with protein G magnetic beads in order to immunoprecipate MuSK using directly the antibodies from the patients. Levels of MuSK phosphorylation were analysed by western blotting as previously described.

We observed that MuSK-IgG and IgG4 were able to prevent MuSK phosphorylation in the presence of agrin, consistently with that reported by Huijbers in 2013. Consequently, the level of MuSK phosphorylation was not significantly increased in the samples exposed to total IgG and IgG4 compared to DMEM. In both cases, the addition of NSC-87877 caused a dramatic increase in MuSK phosphorylation overwhelming the inhibitory effects of MuSK-Abs ($p<0.0001$) (Figure 13A, B). On the other hand, MuSK phosphorylation was not affected by IgG1-3 and, even more interestingly, the SHP inhibition did not show any effect on MuSK phosphorylation when incubated with IgG1-3 MuSK-Abs. In Table 5 are shown the densitometry results of each experiments divided accordingly to the patients' sample used.

To further confirm the pathogenic effects of the antibodies and the potential therapeutic properties of SHP2 inhibition observed in the MuSK phosphorylation experiments, an AChR clustering assay was performed incubating the myotubes with total IgG purified from patient 1 and the different IgG subclasses purified from patient 3. The myotubes were exposed to 0.5 nM of each IgG subclass (the same amount used for the phosphorylation assay) for 30 minutes. Then, agrin (1:800) and NSC-87877 100 µM were added to the medium. As described above, the cells were incubated overnight with the different compounds and then fixed in formaldehyde and labelled with fluorescent α-bungarotoxin.

Total IgG, IgG1-3 and IgG4 all prevented the formation of AChR clusters despite the presence of agrin with a significant reduction of cluster numbers in the myotubes incubated with MuSK-Abs compared to agrin alone ($p<0.0001$). This

confirms the previous observation from Koneczny and colleagues in 2013 that all MuSK IgG subclasses have pathological effect including IgG1-3. Finally, and in contrast to the lack of effect on phosphorylation, SHP2 inhibition by NSC-87877 increased AChR clustering in all the samples ($p<0.01$ compared to total IgG, $p<0.05$ to IgG1-3, $p<0.001$ to IgG4) further demonstrating its protective effect (Figure 14A, B).

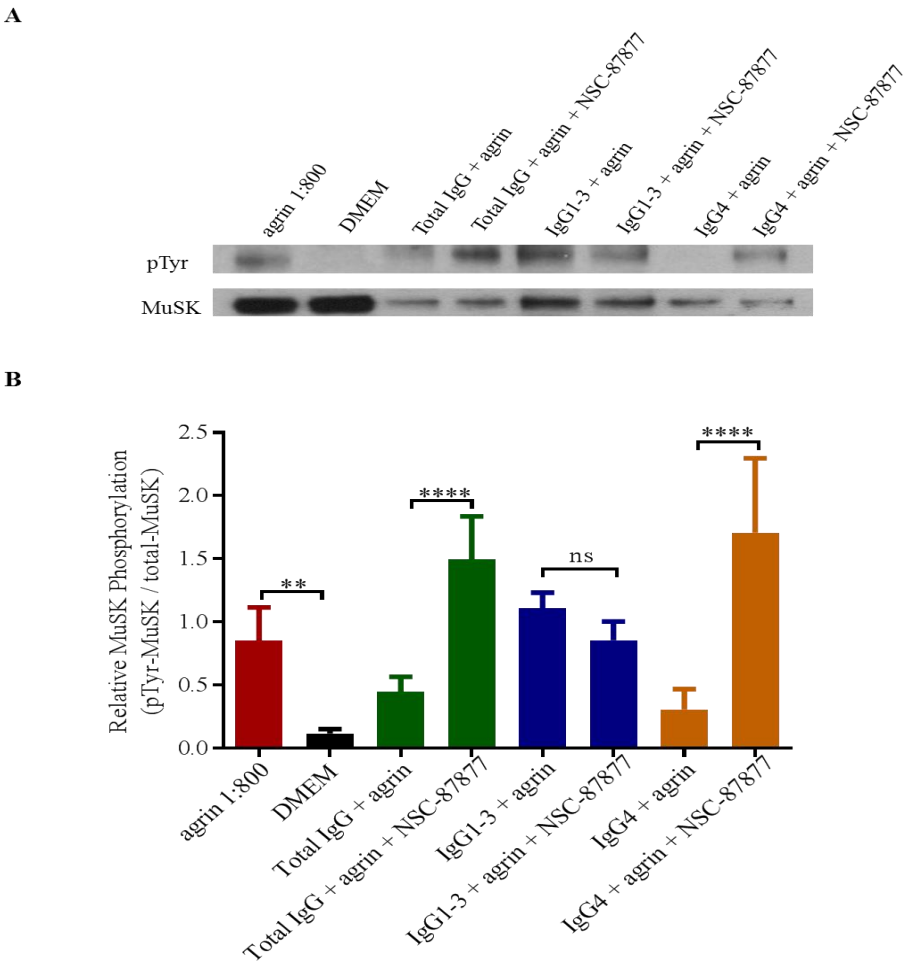

Figure 13. Effects of the different MuSK IgG antibody subclasses and NSC-87877 on MuSK phosphorylation. In A: western blot example showing, in the first row, the level of phospho-tyrosine MuSK and, in the second row, the corresponding MuSK expression after incubation with 0.5 nM of MuSK total IgG, IgG1-3, and IgG4, with agrin (1:800) and in the presence and absence of NSC-87877 (100 µM). In B: bar chart representing normalised densitometry values of phosphorylated MuSK, obtained by pooling the results of at least 3 different experiments. In the samples incubated with MuSK total IgG and IgG4, MuSK phosphorylation did not increase significantly compared to DMEM. However, once the myotubes were exposed to NSC-87877 (100 µM), SHP2 inhibition induced a significant increase of MuSK phosphorylation despite the presence of MuSK antibodies ($p<0.0001$; one-way ANOVA; $n\geq3$). IgG1-3 did not prevent MuSK phosphorylation in the presence of agrin stimulation and NSC-87877 did not show any effect (one-way ANOVA; n=3).

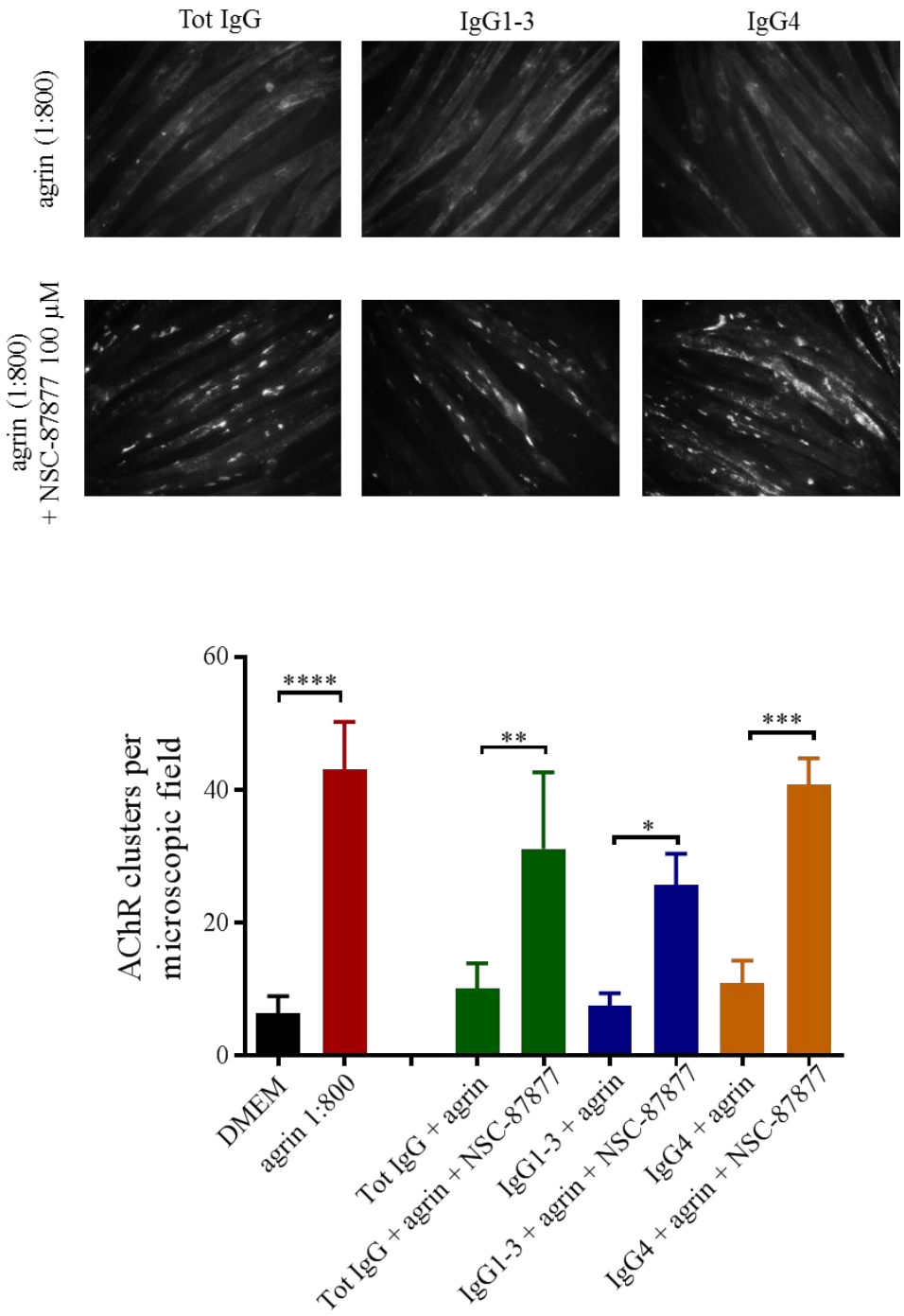

Figure 14. Effects of the different MuSK IgG antibody subclasses and NSC-87877 on AChR clustering. In A: AChR clusters after overnight incubation with MuSK total IgG, IgG1-3, and IgG4, with agrin (1:800) and in the presence and absence of NSC-87877 (100 µM) on C2C12 myotubes (Olympus IX71 fluorescence microscope - 20x magnifications). In B: bar chart representing AChR cluster counts per microscopic field, obtained by pooling the results of 3 different experiments. MuSK total IgG, IgG1-3 and IgG4 inhibited the formation of AChR clusters in the presence of agrin. However, once the myotubes were exposed to NSC-87877 (100 µM), SHP2 inhibition induced a significant increase in AChR clustering despite the presence of MuSK antibodies ($p<0.01$ compared to total IgG, $p<0.05$ to IgG1-3, $p<0.001$ to IgG4; one-way ANOVA; n=3).

Patient	Total IgG + agrin	Total IgG + agrin + NSC-87877	IgG1-3 + agrin	IgG1-3 + agrin + NSC-87877	IgG4 + agrin	IgG4 + agrin + NSC-87877
1	0.38	1.87	-	-	0.12	1.7
	0.39	1.68	1.01	1.02	0.25	2.35
	0.65	1.44	1.07	0.75	0.6	1.31
2	0.46	0.96	1.24	0.79	0.28	1.3
	0.35	1.5	-	-	0.35	2.5
	-	-	-	-	0.25	1.08

Table 5. Normalised level of MuSK phosphorylation in western blot analysis after incubation with MuSK total IgG, IgG1-3 and IgG4 from patient #1 and #2 in the presence and absence of NSC-87877 (100 µM). The results represent the ratio between the densitometry values of phospho-tyrosine-MuSK and MuSK expression of each experiment conducted on the two different MuSK-MG patients.

Chapter 4
Discussion

Within the different forms of myasthenia gravis, the one associated with MuSK-Abs often represents a difficult clinical challenge for its correct management and treatment. MuSK patients are generally more severe compared to those affected by AChR-myasthenia as they present more frequently bulbar involvement and with a higher incidence of life-threatening respiratory crises. Moreover, they often do not respond well to symptomatic therapy with cholinesterase inhibitors while high dose of steroids and other immunosuppressant drugs are required for long-term treatment. Therefore, the development of a therapy that acts specifically on the pathological mechanisms of the disease would be important in order to achieve a better and stable control of the symptoms and to decrease the risk of side effects.

Targeting the intracellular regulators of the AChR clustering pathway represents a novel and specific therapeutic strategy in myasthenic syndromes with either autoimmune or genetic pathogenesis. There are several proteins in the pathway downstream of MuSK that could be potential pharmacological targets including Abl tyrosine kinases and GTPases of the Rho family. However, increasing the activity of these regulators in order to enhance AChR clustering could lead to the development of tumours as many of them play an important role in favouring cell-growth signalling. On the other hand, SH2 domain-containing phosphatase (SHP2) seems to be a safer target. In physiological conditions, through a negative-feedback loop, SHP2 reduces the phosphorylation of MuSK, helping to control the formation of AChR clusters at the neuromuscular synapses. SHP2 also activates cell replication through different pathways such as Ras/Erk, PI3K, AKT, and JAK-STAT. For these reasons, inhibition of SHP2 would have the combined positive effect to increase AChR clustering/density and, at the same time, to reduce the risk of tumorigenesis. In fact, pharmacological inhibition of SHP2 has already demonstrated efficacy in the treatment of mouse tumour xenograft models and a glioma mouse model (Bunda et al, 2015).

With respect to MuSK myasthenia, MuSK-Abs, that are mainly of the IgG4 subclass, inhibit MuSK activation by blocking its interaction with LRP4. This leads to a reduced MuSK phosphorylation and to the inhibition of downstream

signalling which is essential for maintaining the high density of acetylcholine receptors at the neuromuscular junction. The selective inhibition of SHP2 by the drug NSC-87877 has been previously shown to increase AChR clustering in C2C12 myotubes in either the presence or absence of agrin (Zhao et al 2007). Therefore, SHP2 inhibition would be able to activate MuSK, independently by agrin, removing the negative restraint of its physiological regulator and to overcome the effects of MuSK-Abs.

In the first part of our study, we analysed the effect of NSC-87877 on MuSK phosphorylation and AChR clustering in order to determine which concentrations and incubation times were the most appropriate to use in the experiments with MuSK-Abs. We consistently observed that NSC-87877 showed a dose-dependent increase of both MuSK phosphorylation and AChR clustering reaching the maximal effect at a concentration of 100 µM. A further increase of the dose did not correspond to any additional responses suggesting that a saturation of the effect was reached. Furthermore, once we looked at the phosphorylation time-course, we observed that both NSC-87877 and agrin determined a similar MuSK phosphorylation pattern activating MuSK early after the beginning of stimulation (between 15 and 40 minutes), reaching the peak level after 90 minutes and then decreasing progressively to the basal condition during the following 6 hours. It is worth noting that NSC-87877 and agrin, when incubated together on the myotubes, induced a combined and more powerful effect on both MuSK phosphorylation and AChR clustering. This is not surprising considering that agrin and SHP2 inhibition stimulate MuSK in two different and complementary ways to create a cooperative effect in the activation of AChR clustering pathway.

NSC-87877 was then tested on C2C12 myotubes in the presence of purified MuSK total IgG and IgG subclasses. SHP2 inhibition significantly increased MuSK phosphorylation despite the presence of MuSK total IgG and IgG4, and prevented the dispersal of AChR clusters in all the samples. Our experiments further confirmed that inhibition of MuSK activation represents the main pathogenic mechanism of the IgG4 subclass as they block agrin-LRP4 interaction with MuSK. The removal of the physiologic inhibition of SHP2 by NSC-87877 is sufficient to activate the autophosphorylation loop of MuSK directly on its intracytoplasmic domain and, therefore, initiates the phosphorylation cascade resulting in AChR clustering (Figure 15).

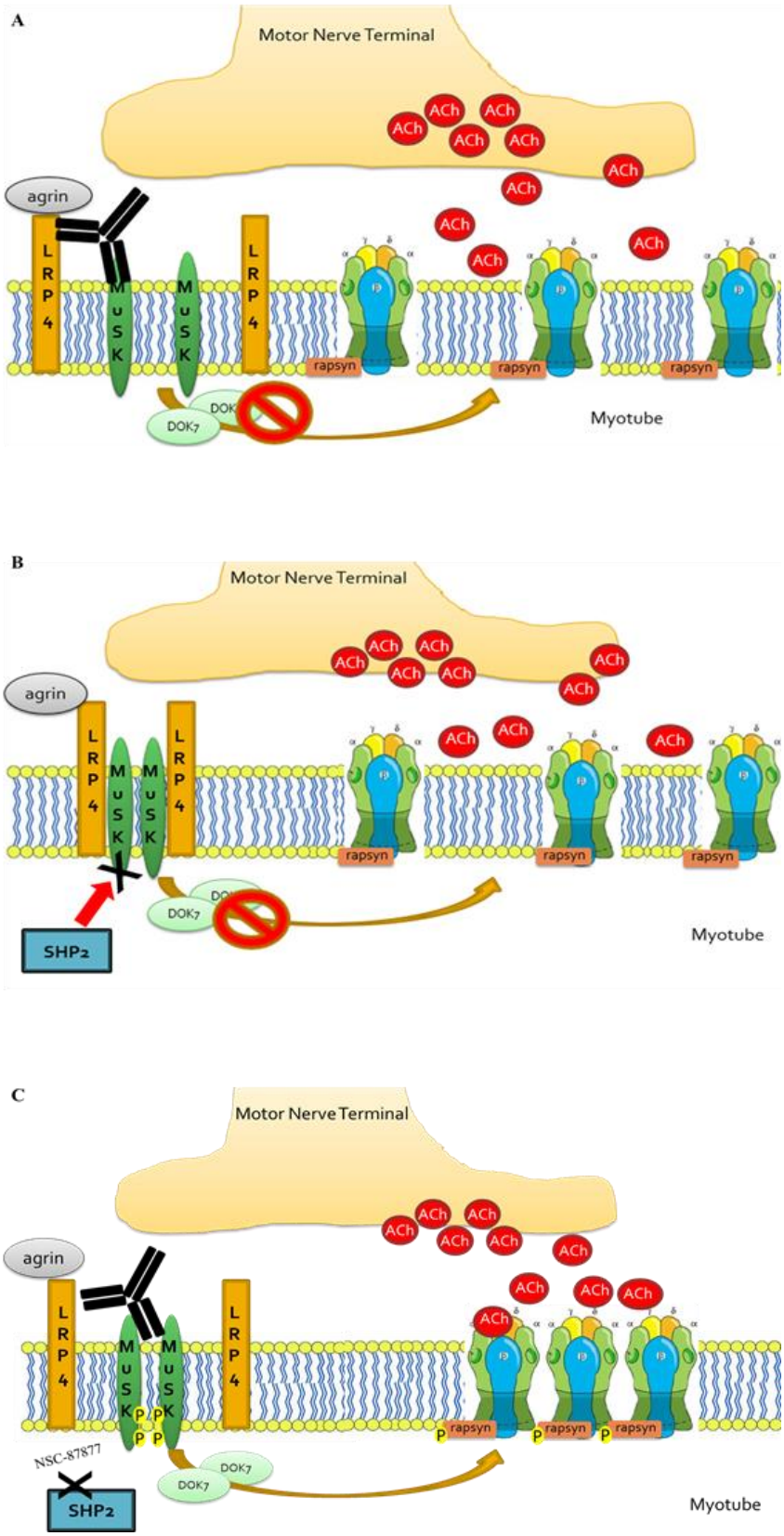

Figure 15. Representation of the effects of SHP2 inhibition by NSC-87877 on the AChR clustering pathway. In A: MuSK antibodies block LRP4-MuSK interaction preventing MuSK phosphorylation and causing the dispersal of AChR clusters. In B: SHP2 physiologically downregulates MuSK activation inducing dispersal of AChR clusters in extrasynaptic sites. In C: NSC-87877 inhibits SHP2 and increases MuSK phosphorylation activating AChR pathway despite the presence of MuSK antibodies.

Consistently with the finding of Koneczny and colleagues, MuSK IgG1-3 also showed pathogenic potential although the mechanism by which they work is still unclear. According to our results, IgG1-3 did to not reduce MuSK phosphorylation although they were still able to disperse AChR clusters. The reliability of these observations on MuSK phosphorylation, however, has to be verified as MuSK immunoprecipitation with IgG1-3 was very difficult to obtain compared to total IgG and IgG4, and only worked well in a minority of the experiments. This could be due in part to a minor affinity of IgG1-3 to MuSK leading to a less stable binding during the immunoprecipitation process. Nevertheless, if IgG1-3 are pathogenic without reducing MuSK phosphorylation, one possible explanation is that, due to their divalent binding, IgG1-3 could restrain MuSK in an abnormal dimer configuration resulting in a pathologically phosphorylated state. This could lead to an abnormal interaction with the downstream players of the AChR pathway, in particular Dok7. Interestingly, a congenital myasthenic syndrome associated with a missense mutation (p.Met835Val) in the MuSK kinase domain has been reported (Ammar et al, 2013). This mutation increases basal MuSK phosphorylation and impaired co-immunoprecipitation of MuSK and Dok7 when both proteins were transfected in HEK 293 cells. Although NSC-87877 did not modify significantly MuSK phosphorylation in the myotubes incubated with MuSK IgG1-3, the drug was still able to prevent the dispersal of AChR clusters induced by the antibodies. It is possible that the inhibition of SHP2 restores a more physiological phosphorylation of MuSK and, therefore, favouring binding and activation of Dok7 with the reactivation of the downstream clustering pathway. Thus, regardless of the IgG subclass of the antibodies, or the mechanisms by which they work, SHP2 inhibition could provide a novel pharmacological treatment for MuSK-MG.

Finally, would NSC-87877 have other “off target” effects that might be detrimental? NSC-87877 represents currently the most specific compound to inhibit selectively SHP2 activity through the binding to its catalytic cleft. However, NSC-87877 inhibits other phosphatases, in particular SHP1 and, with less affinity, DUSP26 (Chen et al, 2006; Song et al, 2009). Nevertheless, it is worth noting that SHP2 expression is readily detected in C2C12 myotubes and its role in AChR clustering is well established (Madhavan et al, 2005; Zhao et al, 2007) whilst neither SHP1 nor DUSP26 have been reported to be involved in

AChR clustering, suggesting that the effects we observed were specific to SHP2 inhibition. The use of this drug in animal models of MuSK-MG is justified as a proof of principle that inhibition of this phosphatase can provide a pharmacological, relatively rapid treatment for MuSK-MG.

Conclusions

MuSK-MG is a treatable disease but, despite the progress of our understanding on its pathogenesis and the advanced multiple ways of treatment, we still lack of a specific therapy able to counteract directly the mechanisms that cause the symptoms. Modulating the activity of the intracellular regulators of AChR clustering pathway could represent an important first step in the development of a specific treatment. In particular, the phosphatase SHP2, that physiologically reduce MuSK activation, could be an effective and potentially safe protein to target.

Our *in vitro* results suggest that inhibition of SHP2 by the drug NSC-87877 is able to cause a dose-dependent increase of both MuSK phosphorylation and AChR clustering. More importantly, these effects are maintained in the presence of MuSK-Abs providing an initial but solid evidence of the potential efficacy of this strategy in the treatment of MuSK-MG.

Our findings open a wide range of possibilities for the future developments of our research. First, it would be important to test SHP2 inhibition in an animal model of MuSK myasthenia in order to verify its efficacy and reliability *in vivo*. Moreover, SHP2 inhibition could be effective also in other disorders that impair neuromuscular transmission (in particular congenital myasthenic syndromes) and therefore its efficacy in models of different diseases should be studied. These steps are fundamental in order to develop specific and safe therapies for use in clinical practice.

Bibliography

Part I

Allen RC, Zoghbi HY, Moseley AB, Rosenblatt HM, Belmont JW. Methylation of HpaII and HhaI sites near the polymorphic CAG repeat in the human androgen-receptor gene correlates with X chromosome inactivation. Am J Hum Genet. 1992 Dec;51(6):1229-39.

Amos-Landgraf JM, Cottle A, Plenge RM, Friez M, Schwartz CE, Longshore J, Willard HF. X chromosome-inactivation patterns of 1,005 phenotypically unaffected females. Am J Hum Genet. 2006 Sep;79(3):493-9. Epub 2006 Jul 27.

Arahata K, Ishihara T, Fukunaga H, Orimo S, Lee JH, Goto K, Nonaka I. Inflammatory response in facioscapulohumeral muscular dystrophy (FSHD): immunocytochemical and genetic analyses. Muscle Nerve Suppl 1995, 2:S56–S66.

Askanas V, Alvarez RB, McFerrin J, et al. Facio-scapulo-humeral (FSH) syndrome with abnormal desmin accumulation. Neurology 1992; 42:22-25.

Balatsouras DG, Korres S, Manta P, Panousopoulou A, Vassilopoulos D. Cochlear function in facioscapulohumeral muscular dystrophy, Otol. Neurotol. 2007, 7–10.

Bergamasco B, Mutani R: Le miopatie. In: La Neurologia di Bergamini. Ed. Libreria Cortina. Torino. 2007. pp: 670-671.

Blewitt ME, Gendrel AV, Pang Z, Sparrow DB, Whitelaw N, Craig JM, Apedaile A, Hilton DJ, Dunwoodie SL, Brockdorff N, Kay GF, Whitelaw E. SmcHD1, containing a structural-maintenance-of-chromosomes hinge domain, has a critical role in X inactivation. Nat Genet. 2008 May;40(5):663-9. doi: 10.1038/ng.142.

Bromberg MB, Scott DM. Single fiber EMG reference values: reformatted in tabular form. AD HOC Committee of the AAEM Single Fiber Special Interest Group.Muscle Nerve. 1994 Jul;17(7):820-1.

Butz M, Koch MC, Muller-Felber W, Lemmers RJ, van der Maarel SM, Schreiber H. Facioscapulohumeral muscular dystrophy. Phenotype-genotype correlation in patients with borderline D4Z4 repeat numbers. J Neurol 2003; 250:932-937.

Chen JC, King OD, Zhang Y, Clayton NP, Spencer C, Wentworth BM, Emerson CP Jr, Wagner KR. Morpholino-mediated Knockdown of DUX4 Toward Facioscapulohumeral Muscular Dystrophy Therapeutics. Mol Ther. 2016 Aug;24(8):1405-11. doi: 10.1038/mt.2016.111.

Chen TH, Lai YH, Lee PL, Hsu JH, Goto K, Hayashi YK. Infantile facioscapulohumeral muscular dystrophy revisited: expansion of clinical phenotypes in patients with a very short EcoRI fragment, Neuromuscul. Disord. 2013, 298–305.

De Greef JC, Lemmers RJ, Camaño P, Day JW, Sacconi S, Dunand M, van Engelen BG, Kiuru-Enari S, Padberg GW, Rosa AL, Desnuelle C, Spuler S, Tarnopolsky M, Venance SL, Frants RR, van der Maarel SM, Tawil R. Clinical features of facioscapulohumeral muscular dystrophy 2. Neurology. 2010 Oct 26;75(17):1548-54. doi: 10.1212/WNL.0b013e3181f96175.

De Greef JC, Lemmers RJ, van Engelen BG, Sacconi S, Venance SL, Frants RR. Common epigenetic changes of D4Z4 in contraction-dependent and contraction-independent FSHD. Hum. Mutat. 2009, 1449–1459.

De Greef JC, Wohlgemuth M, Chan OA, Hansson KB, Smeets D, Frants RR, Weemaes CM, Padberg GW, van der Maarel SM. Hypomethylation is restricted to the D4Z4 repeat array in phenotypic FSHD. Neurology. 2007 Sep 4;69(10):1018-26.

Deidda G, Cacurri S, Piazzo N, Felicetti L. Direct delection of 4q35 rearrangements implicated in Facioscapulohumeral Muscular Dystrophy (FSHD). J Med Genet 1996; 33:361-365.

Dixit M, Ansseau E, Tassin A, Winokur S, Shi R, Qian H, Sauvage S, Matteotti C, van Acker AM, Leo O, Figlewicz D, Barro M, Laudj-Chenivesse S, Belayew A, Coppee F, Chen YW. DUX4, a candidate gene of Facioscapulohumeral

Muscular Dystrophy, encodes a transcriptional activator of PITX1. PNAS 2007; 104: 18157-18162.

Dubowitz V, Sewry CA. Definition of pathological changes seen in muscle biopsies. In: Muscle Biopsy – A pratical approach (third edition). Sounders Elsevier. 2007. pp: 75-123.

Dubowitz V, Sewry CA: Muscular dystrophies and allied disorders V: Facioscapulohumeral, myotonic and oculopharyngeal muscular dystrophy. In: Muscle Biopsy – A pratical approach (third edition). Sounders Elsevier. 2007. pp: 395-399.

Endo T, Nadal-Ginard B. Reversal of myogenic terminal differentiation by SV40 large T antigen results in mitosis and apoptosis. J Cell Sci 1998, 111:1081–1093.

Figlewicz DA, Tawil R. Facioscapulohumeral dystrophy. Gene Reviews 2005. www. ncbi.nlm.nih.gov/

Fisher J, Upadhyaya M. Molecular genetics of facioscapulohumeral muscular dystrophy (FSHD). Neuromusc Disord 1997; 7: 55-62.

Frisullo G, Frusciante R, Nociti V, Tasca G, Renna R, Iorio R, Patanella AK, Iannaccone E, Marti A, Rossi M, Bianco A, Monforte M, Tonali PA, Mirabella M, Batocchi AP, Ricci E. CD8(+) T cells in facioscapulohumeral muscular dystrophy patients with inflammatory features at muscle MRI. J Clin Immunol 2011, 31:155–166.

Gabellini D, Green MR, Tupler R. Inappropriate gene activation in FSHD: a repressor complex binds a chromosomal repeat deleted in dystrophic muscle. Cell 2002; 110:339-348.

Gabriels J, Beckers MC, Ding H, De Vriese A, Paisance S, ven der Maarel SM, Padberg GW, Frants RR, Hewitt JE, Collen D, Belayew A. Nucleotide sequence of the partially deleted D4Z4 locus in a patient with FSHD identifies a putative gene within each 3.3 kb element. Gene 1999; 236: 25-32.

Gendrel AV, Apedaile A, Coker H, Termanis A, Zvetkova I, Godwin J, Tang YA, Huntley D, Montana G, Taylor S, Giannoulatou E, Heard E, Stancheva I, Brockdorff N. Smchd1-dependent and -independent pathways determine developmental dynamics of CpG island methylation on the inactive X chromosome. Dev Cell. 2012 Aug 14;23(2):265-79. doi: 10.1016/j.devcel.2012.06.011.

Geng LN, Yao Z, Snider L, Fong AP, Cech JN, Young JM, van der Maarel SM, Ruzzo WL, Gentleman RC, Tawil R, Tapscott SJ. DUX4 activates germline genes, retroelements, and immune mediators: implications for facioscapulohumeral dystrophy. Dev Cell 2012, 22:38–51.

Gieron MA, Korthals JK, Kousseff BG. Facioscapulohumeral dystrophy with cochlear hearing loss and tortuosity of retinal vessels. Am J Med Genet 1985; 22:143-147.

Gilbert JR, Speer MC, Stajich J, Clancy R, Lewis K, Qiu H, Yamaoka L, Kumar A, Vance J, Stewart C, Rozear M, Roses AD, Pericak-Vance MA. Exclusion mapping of chromosomal regions which cross hybridaze to FSHD1A associated markers in FSHD1B. J Med Genet 1995; 32: 770-773.

Hewitt JF, Lyle R, Clark LN, Valleley EM, Wright TJ, Wijmenga C, Van Deutekom JCT, Francis F, Sharpe PT, Hofker M, Frants RR, Williamson R. Analysis of the tandem repeat locus D4Z4 associated with Facioscapulohumeral Muscular Dystrophy. Hum Mol Genet 1994; 3: 1287-1295.

Hudgson P, Bradley WG, Jenkison M. Familial "mitochondrial" myopathy. A myopathy associated with disordered oxidative metabolism in muscle fibres. 1. Clinical, electrophysiological and pathological findings. J Neurol Sci 1972; 16:343-370.

Jiang G, Yang F, Van Overveld PG, Vedanarayanan V, van der Maarel S, Ehrlich M. Testing the position-effect variegation hypothesis for Facioscapulohumeral muscular dystrophy by analysis of histone modification and gene expression in subtelomeric 4q. Hum Mol Genet 2003; 12: 2909-29021.

Jones TI, Chen JC, Rahimov F, Homma S, Arashiro P, Beermann ML, King OD, Miller JB, Kunkel LM, Emerson CP Jr, Wagner KR, Jones PL. Facioscapulohumeral muscular dystrophy family studies of DUX4 expression: evidence for disease modifiers and a quantitative model of pathogenesis. Hum Mol Genet 2012, 21:4419–4430.

Kilmer DD, Abresch RT, McCrory MA, Carter GT, Fowler WM Jr., Johnson ER, McDonald CM Profiles of neuromuscular diseases. Facioscapulohumeral muscular dystrophy. Am J Phys Med Rehabil 1995; 74:S131-139.

Kissel JT, McDermott MP, Natarajan R, Mendell JR, Pandya S, King WM, Griggs RC, Tawil R. Pilot trial of albuterol in facioscapulohumeral muscular dystrophy. FSH-DY Group. Neurology 1998; 50:1402-1406.

Kowaljow V, Marcowycz A, Ansseau E, Conde CB, Sauvage S, Matteotti C, Arias C, Corona ED, Nunez NG, Leo O, Wattiez R, Figlewicz D, Laoudj-Chenivesse D, Belayew A, Coppee F, Rosa AL. The DUX4 gene at the FSHD1A locus encodes a pro-apoptotic protein. Neuromuscul Disord 2007, 17:611–623.

Landouzy L, Dejerine J: De la myopathie atrophique progressive. Rev Med Franc 1885, 5:81–253.

Larsen M, Rost S, El Hajj N, Ferbert A, Deschauer M, Walter MC, Schoser B, Tacik P, Kress W, Müller CR. Diagnostic approach for FSHD revisited: SMCHD1 mutations cause FSHD2 and act as modifiers of disease severity in FSHD1. Eur J Hum Genet. 2015 Jun;23(6):808-16. doi: 10.1038/ejhg.2014.191.

Lemmers RJ, de Kievit P, Sandkuijl L, Padberg GW, van Ommen GJ, Frants RR, van der Maarel SM. Facioscapulohumeral muscular dystrophy is uniquely associated with one of the two variants of the 4q subtelomere. Nat Genet 2002; 32:235-236.

Lemmers RJ, Tawil R, Petek LM, Balog J, Block GJ, Santen GW, Amell AM, van der Vliet PJ, Almomani R, Straasheijm KR, Krom YD, Klooster R, Sun Y, den Dunnen JT, Helmer Q, Donlin-Smith CM, Padberg GW, van Engelen BG, de Greef JC, Aartsma-Rus AM, Frants RR, de Visser M, Desnuelle C, Sacconi S,

Filippova GN, Bakker B, Bamshad MJ, Tapscott SJ, Miller DG, van der Maarel SM. Digenic inheritance of an SMCHD1 mutation and an FSHD-permissive D4Z4 allele causes facioscapulohumeral muscular dystrophy type 2. Nat Genet 2012, 44:1370–1374.

Lemmers RJ, Tawil R, Petek LM, Balog J, Block GJ, Santen GW. Digenic inheritance of an SMCHD1 mutation and an FSHD-permissive D4Z4 allele causes facioscapulohumeral muscular dystrophy type 2. Nat. Genet. 2012, 1370–1374.

Lemmers RJ, van der Maarel SM, van Deutekom JC, van der Wielen MJ, Deidda G, Dauwerse HG, Hewitt J, Hofker M, Bakker E, Padberg GW, Frants RR: Inter- and intrachromosomal sub-telomeric rearrangements on 4q35: implications for facioscapulohumeral muscular dystrophy (FSHD) aetiology and diagnosis. Hum Mol Genet 1998, 7:1207–1214.

Lemmers RJ, van der Vliet PJ, Klooster R, Sacconi S, Camaño P, Dauwerse JG, Snider L, Straasheijm KR, van Ommen GJ, Padberg GW, Miller DG, Tapscott SJ, Tawil R, Frants RR, van der Maarel SM. A unifying genetic model for facioscapulohumeral muscular dystrophy. Science. 2010, 1650-3.

Lemmers RJ, van der Vliet PJ, van der Gaag KJ, Zuniga S, Frants RR, de Knijff P, van der Maarel SM. Worldwide population analysis of the 4q and 10q subtelomeres identifies only four discrete interchromosomal sequence transfers in human evolution. Am J Hum Genet 2010, 86:364–377.

Lemmers RJ, van der Wielen MJ, Bakker E, Padberg GW, Frants RR, van der Maarel SM. Somatic mosaicism in FSHD often goes undetected. Ann Neurol. 2004 Jun;55(6):845-50.

Lemmers RJ, Wohlgemuth M, van der Gaag KJ, van der Vliet PJ, van Teijlingen CM, de Knijff P. Specific sequence variations within the 4q35 region are associated with facioscapulohumeral muscular dystrophy, Am. J. Hum. Genet. 2007, 884–894.

Leung DG, Carrino JA, Wagner KR, Jacobs MA. Whole-body magnetic resonance imaging evaluation of facioscapulohumeral muscular dystrophy. Muscle Nerve 2015 Jan 16. doi: 10.1002/mus.24569.

Lim JW, Snider L, Yao Z, Tawil R, Van Der Maarel SM, Rigo F, Bennett CF, Filippova GN, Tapscott SJ. DICER/AGO-dependent epigenetic silencing of D4Z4 repeats enhanced by exogenous siRNA suggests mechanisms and therapies for FSHD. Hum Mol Genet. 2015 Sep 1;24(17):4817-28. doi: 10.1093/hmg/ddv206.

Lunt PW, Compston DAS, Harper PS. Estimation of age dependent penetrance in Facioscapulohumeral Muscular Dystrophy by minimizing ascertainment bias. J Med Genet 1989; 26: 755-760.

Lunt PW, Harper PS. Genetic counselling in facioscapulohumeral muscular dystrophy. J Med Genet. 1991 Oct;28(10):655-64.

Lunt PW, Jardina PE, Koch MC, Maynard J, Osborne M, Williams M, Harper PS, Updhyaya M. Correlation between fragment size at D4F104S1 and age at onset or at wheelchair use, with a possible generational effect, accounts for much phenotypic variation in 4q35- Facioscapulohumeral Muscular Dystrophy (FSHD). Hum Mol Genet 1995; 4: 1243-1244.

Mul K, Lassche S, Voermans NC, Padberg GW, Horlings CG, van Engelen BG. What's in a name? The clinical features of facioscapulohumeral muscular dystrophy. Pract Neurol. 2016 Jun;16(3):201-7. doi: 10.1136/practneurol-2015-001353. Epub 2016 Feb 9. Review.

Munsat TL, Piper D, Cancilla P, Mednick J. Inflammatory myopathy with facioscapulohumeral distribution. Neurology 1972; 22:335-347.

Olsen DB, Orngreen MC, Vissing J. Aerobic training improves exercise performance in Facioscapulohumeral Muscular Dystrophy. Neurology 2005; 64: E22.

Padberg G. Facioscapulohumeral muscular dystrophy: a clinician's experience, in: M. Upadhyaya, D.N. Cooper (Eds.), Facioscapulohumeral Muscular Dystrophy.

Clinical Medicine and Molecular Cell Biology, Garland Science/BIOS Scientific Publishers, Oxon, United Kingdom, 2004.

Padberg GW, Brouwer OF, de Keizer RJW, Dijkman G, Wijmenga C, Grote JJ, Frants RR. On the significance of retinal vascular disease and hearing loss in facioscapulohumeral muscular dystrophy. Muscle & Nerve 1995; 2:S73-S80.

Padberg GW, Lunt PW, Koch M, Fardeau M. Diagnostic criteria for facioscapulohumeral muscular dystrophy. Neuromuscul Disord 1991; 1: 231–4.

Padberg GW. Facioscapulohumeral disease. Thesis. University of Leiden, the Netherlands. 1982

Quarantelli M, Lanzillo R, Del Vecchio W, Mollica C, Prinster A, Iadicicco L. Modifications of brain tissue volumes in facioscapulohumeral dystrophy. NeuroImage 2006, 1237–1242.

Ricci G, Scionti I, Sera F, Govi M, D'Amico R, Frambolli I, Mele F, Filosto M, Vercelli L, Ruggiero L, Berardinelli A, Angelini C, Antonini G, Bucci E, Cao M, Daolio J, Di Muzio A, Di Leo R, Galluzzi G, Iannaccone E, Maggi L, Maruotti V, Moggio M, Mongini T, Morandi L, Nikolic A, Pastorello E, Ricci E, Rodolico C, Santoro L, Servida M, Siciliano G, Tomelleri G, Tupler R. Large scale genotype-phenotype analyses indicate that novel prognostic tools are required for families with facioscapulohumeral muscular dystrophy. Brain. 2013 Nov;136(Pt 11):3408-17. doi: 10.1093/brain/awt226. Epub 2013 Sep 11.

Rijkers T, Deidda G, van Koningsbruggen S, van Geel M, Lemmers RJ, van Deutekom JC, Figlewicz D, Hewitt JE, Padberg GW, Frants RR, van der Maarel SM. FRG2, an FSHD candidate gene, is transcriptionally upregulated in differentiating primary myoblast cultures of FSHD patients. J Med Genet 2004, 41:826–836.

Rothstein TL, Carlson CB, Sumi SM. Polymyositis with facioscapulohumeral distribution. Arch Neurol 1971; 25:313-319.

Sacconi S, Lemmers RJ, Balog J, van der Vliet PJ, Lahaut P, van Nieuwenhuizen MP, Straasheijm KR, Debipersad RD, Vos-Versteeg M, Salviati L, Casarin A, Pegoraro E, Tawil R, Bakker E, Tapscott SJ, Desnuelle C, van der Maarel SM. The FSHD2 gene SMCHD1 is a modifier of disease severity in families affected by FSHD1. Am J Hum Genet 2013, 93:744–751.

Sacconi S, Salviati L, Desnuelle C. Facioscapulohumeral muscular dystrophy. Biochim Biophys Acta. 2015, 1852(4):607-614.

Sandri M, El Meslemani AH, Sandri C, Schjerling P, Vissing K, Andersen JL, Rossini K, Carraro U, Angelini C. Caspase 3 expression correlates with skeletal muscle apoptosis in Duchenne and facioscapulo human muscular dystrophy. A potential target for pharmacological treatment? J Neuropathol Exp Neurol. 2001 Mar;60(3):302-12.

Sarpharazi M, Wijmenga C, Upadhayaya M, Weifenbach B, Hyser C, Mathews K, Murray J, Gilbert J, Pericak-Vance M, Lunt P, Frants RR, Jacobsen S, Harper PS, Padberg GW. Regional mapping of Facioscapulohumeral Muscular Dystrophy gene on 4q35-combined analysis of an international consortium. Am J Hum Genet 1992; 51: 396-403.

Scionti I, Fabbri G, Fiorillo C, Ricci G, Greco F, D'Amico R, Termanini A, Vercelli L, Tomelleri G, Cao M, Santoro L, Percesepe A, Tupler R. Facioscapulohumeral muscular dystrophy: new insights from compound heterozygotes and implication for prenatal genetic counselling. J Med Genet. 2012 Mar;49(3):171-8. doi: 10.1136/jmedgenet-2011-100454. Epub 2012 Jan 3.

Scionti I, Greco F, Ricci G, Govi M, Arashiro P, Vercelli L, Berardinelli A, Angelini C, Antonini G, Cao M, Di Muzio A, Moggio M, Morandi L, Ricci E, Rodolico C, Ruggiero L, Santoro L, Siciliano G, Tomelleri G, Trevisan CP, Galluzzi G, Wright W, Zatz M, Tupler R. Large-scale population analysis challenges the current criteria for the molecular diagnosis of fascioscapulohumeral muscular dystrophy. Am J Hum Genet. 2012 Apr 6;90(4):628-35. doi: 10.1016/j.ajhg.2012.02.019.

Semple F, MacPherson H, Webb S, Cox SL, Mallin LJ, Tyrrell C, Grimes GR, Semple CA, Nix MA, Millhauser GL, Dorin JR. Human beta-defensin 3 affects the activity of pro-inflammatory pathways associated with MyD88 and TRIF. Eur J Immunol 2011, 41:3291–3300.

Snider L, Geng LN, Lemmers RJ, Kyba M, Ware CB, Nelson AM, Tawil R, Filippova GN, van der Maarel SM, Tapscott SJ, Miller DG. Facioscapulohumeral dystrophy: incomplete suppression of a retrotransposed gene. PLoS Genet. 2010 Oct 28;6(10):e1001181. doi: 10.1371/journal.pgen.1001181.

Spurlock G, Jim HP, Upadhyaya M. Confirmation that the specific SSLP microsatellite allele 4qA161 segregates with fascioscapulohumeral muscular dystrophy (FSHD) in a cohort of multiplex and simplex FSHD families. Muscle Nerve 2010, 820–821.

Statland JM, McDermott MP, Heatwole C, Martens WB, Pandya S, van der Kooi EL, Kissel JT, Wagner KR, Tawil R. Reevaluating measures of disease progression in facioscapulohumeral muscular dystrophy. Neuromuscul Disord 2013, 23:306–312.

Statland JM, Sacconi S, Farmakidis C, Donlin-Smith CM, Chung M, Tawil R. Coats syndrome in facioscapulohumeral dystrophy type 1: frequency and D4Z4 contraction size. Neurology 2013, 1247–1250.

Stevenson WG, Perloff JK, Weiss JN, Anderson TL. Facioscapulohumeral muscular dystrophy: evidence for selective, genetic electrophysiologic cardiac involvement. J Am Coll Cardiol 1990; 15:292-299

Tasca G, Monforte M, Ottaviani P, Pelliccioni M, Frusciante R, Laschena F, Ricci E. Magnetic Resonance Imaging in a large cohort of facioscapulohumeral muscular dystrophy patients: pattern refinement and implications for clinical trials. Ann Neurol. 2016 Mar 19. doi: 10.1002/ana.24640.

Tawil R, van der Maarel SM, Tapscott SJ. Facioscapulohumeral dystrophy: the path to consensus on pathophysiology. Skelet Muscle 2014, 10;4:12.
Tawil R, Van Der Maarel SM. Facioscapulohumeral muscular dystrophy. Muscle Nerve 2006, 34:1–15.

Thomas NST, Wiseman K, Spurlock G, MacDonald M, Ustek D, Upadhyaya M. A large patient study confirming that Facioscapulohumeral Muscular Dystrophy (FSHD) disease expression is almost exclusively associated with an FSHD locus located on a 4qA-defined 4qter subtelomere. J Med Genet 2007; 44: 215-218.

Tonini MM, Pavanello RC, Gurgel-Giannetti J, Lemmers RJ, van der Maarel SM, Frants RR, Zatz M. Homozygosity for autosomal dominant facioscapulohumeral muscular dystrophy (FSHD) does not result in a more severe phenotype. J Med Genet 2004; 41:e17.

Tonini MMO, Passos-Bueno MR, Cerqueira A, Matioli SR, Pavanello R, Zatz M. Asymptomatic carriers and gender differences in Facioscapulohumeral Muscular Dystrophy (FSHD). Neuromusc Disord 2003; 14; 33-38.

Trevisan CP, Pastorello E, Ermani M, Angelini C, Nante G, Tomelleri G. Facioscapulohumeral muscular dystrophy and occurrence of heart arrhythmia. Eur. Neurol.2006, 1–5.

Tupler R, Berardinelli A, Barbierato L, Frants R, Hewitt JE, Lanzi G. Monosomy of distal 4q does not cause facioscapulohumeral muscular dystrophy. J. Med. Genet. 1996, 366–370.

Upadhayaya M, Maynard J, Osbron M, Jardine P, Harper PS, Lunt P. Germinal mosaicsm in Facioscapulohumeral Muscular Dystrophy (FSHD). Muscle & Nerve 1995; S2:S45-S49.

Upadhyaya M, Lunt PW, Sarfarazi M, Broadhead W, Daniels J, Owen M, Harper PS. DNA marker applicable to presymptomatic and prenatal diagnosis of Facioscapulohumeral disease. Lancet 1990; 336: 1320-1321.

Upadhyaya M, Maynard J, Rogers MT, Lunt PW, Jardine P, Ravine D, Harper PS. Improved molecular diagnosis of facioscapulohumeral muscular dystrophy (FSHD): validation of the differential double digestion for FSHD. J Med Genet 1997; 34:476-479.

Van der Kooi EL, Vogels OJ, van Asseldonk RJ, Lindeman E, Hendriks JC, Wohlgemuth M, van der Maarel SM, Padberg GW. Strength training and albuterol in facioscapulohumeral muscular dystrophy. Neurology 2004; 63:702-708.

Van Deutekom JC, Bakker E, Lemmers RJ, van der Wielen MJ, Bik E, Hofker MH, Padberg GW, Frants RR. Evidence for subtelomeric exchange of 3.3 kb tandemly repeated units between chromosomes 4q35 and 10q26: implications for genetic counselling and etiology of FSHD1. Hum Mol Genet 1996, 5:1997–2003.

Van Deutekom JCT, Lemmers RJLF, Grewal PK, van Geel M, Romberg S, Dauwerse HG, Wright TJ, Padberg GW, Hofker MH, Hewitt JE, Frants RR. Identification of the first gene (FRG1) from the FSHD region on human chromosome 4q35. Hum Mol Genet 1996; 5: 581-590.

Van Deutekom JCT, Wijmenga C, Van Tienhoven EAE, Gruter AM, Frants RR, Hewitt JE, Padberg CW, Van Ommen GJB, Hofker MH. FSHD associated DNA rearrangements are due to deletions of integral copies of a 3.2 Kb tandemly repeated unit. Hum Mol Genet 1993; 2: 2037-2042.

Wallace LM, Garwick SE, Mei W, Belayew A, Coppee F, Ladner KJ, Guttridge D, Yang J, Harper SQ. DUX4, a candidate gene for facioscapulohumeral muscular dystrophy, causes p53-dependent myopathy in vivo. Ann Neurol 2011, 69:540–552.

Wang LH, Tawil R. Facioscapulohumeral Dystrophy. Curr Neurol Neurosci Rep. 2016 Jul;16(7):66. doi: 10.1007/s11910-016-0667-0. Review.

Weiffenbach B, Dubois J, Storvick D, Tawil R, Jacobsen SJ, Gilbert J, Wijmenga C, Mendell JR, Winokur S, Altherr MR, Schultz P, Olandt S, Frants RR, Pericak-

Vance M, Griggs RCTI. Mapping the Facioscapulohumeral Muscular Dystrophy gene is complicated by chromosome-4q35 recombination events. Nat Genet 1993; 4: 165-169.

Wijmenga C, Frants RR, Brouwer OF, Moerer P, Weber JL, Padberg GW. Location of Facioscapulohumeral Muscular Dystrophy gene on chromosome 4. Lancet 1990; 336: 651-653.

Wijmenga C, Padberg GW, Moerer P, Wiegant J, Liem L, Brouwer OF, Milner ECB. Mapping of Facioscapulohumeral Muscular Dystrophy gene to chromosome 4q35-qter by multipoint linkage analysis and in situ hybridization. Genomics 1991; 9: 570-575.

Wijmenga C, Van Deutekom JCT, Hewitt JE, Padberg GW, Van Ommen GJB, Hofker MH, Frants RR. Pulsed-field gel electrophoresis of the D4F104S1 locus reveals the size and the parental origin of the Facioscapulohumeral Muscular Dystrophy (FSHD) – associated deletions. Genomics 1994; 19: 21-26.

Winokur ST, Bengtsson U, Wasmuth JJ, Altherr MR. Mildly repetitive sequences closely linked to the Facioscapulohumeral Muscular Dystrophy gene on distal chromosome 4q cross hybridize to regions of heterochromatin. Cytogenet Cell Genet 1994; 66:231.

Winokur ST, Chen YW, Masny PS, Martin JH, Ehmsen JT, Tapscott SJ, van der Maarel SM, Hayashi Y, Flanigan KM. Expression profiling of FSHD, muscle supports a defects in specific stages of myogenic differentiation. Hum Mol Genet 2003; 12: 2895-2907.

Wohlgemuth M, Lemmers RJ, van der Kooi EL, van der Wielen MJ, van Overveld PG, Dauwerse H, Bakker E, Frants RR, Padberg GW, van der Maarel SM. Possible phenotypic dosage effect in patients compound heterozygous for FSHD-sized 4q35 alleles. Neurology 2003; 61:909-913.

Wohlgemuth M, van der Kooi EL, van Kesteren RG, van der Maarel SM, Padberg GW. Ventilatory support in facioscapulohumeral muscular dystrophy. Neurology 2004 176–178.

Zatz M, Marie SK, Cerqueira A, Vainzof M, Pavanello RC, Passos-Bueno MR. The facioscapulohumeral muscular dystrophy (FSHD1) gene affects males more severely and more frequently than females. Am J Med Genet 1998; 77:155-161.

Zatz M, Marie SK, Passos-Bueno MR, Vainzof M, Campiotto S, Cerqueira A, Wijmenga C, Padberg G, Frants R. High proportion of new mutations and possible anticipation in Brazilian facioscapulohumeral muscular dystrophy families. Am J Hum Genet 1995; 56:99-105.

Part II

Aarli JA, Skeie GO, Mygland A, Gilhus NE. Muscle striation antibodies in myasthenia gravis. Diagnostic and functional significance. Ann N Y Acad Sci. 1998 May 13;841:505-15. Review.

Aarli JA. Myasthenia gravis in the elderly: Is it different? Ann N Y Acad Sci. 2008;1132:238-43. doi: 10.1196/annals.1405.040.

Aharonov A, Abramsky O, Tarrab-Hazdai R, Fuchs S. Humoral antibodies to acetylcholine receptor in patients with myasthenia gravis. Lancet. 1975 Aug 23;2(7930):340-2.

Alahgholi-Hajibehzad M, Yilmaz V, Gülsen-Parman Y, Aysal F, Oflazer P, Deymeer F, Saruhan-Direskeneli G. Association of HLA-DRB1∗14, -DRB1∗16 and -DQB1∗05 with MuSK-MG gravis in patients from Turkey. Hum Immunol. 2013 Dec;74(12):1633-5. doi: 10.1016/j.humimm.2013.08.271. Epub 2013 Aug 28.

Alonso A, Sasin J, Bottini N, Friedberg I, Friedberg I, Osterman A, Godzik A, Hunter T, Dixon J, and Mustelin T. Protein tyrosine phosphatases in the human genome. Cell. 2004. 117:699–711.

Antonio-Santos AA, Eggenberger ER. Medical treatment options for ocular myasthenia gravis. Curr Opin Ophthalmol. 2008 Nov;19(6):468-78. doi: 10.1097/ICU.0b013e328310da18. Review.

Arber S, Burden SJ, Harris AJ. Patterning of skeletal muscle. Curr Opin Neurobiol. 2002; 12:100–103.

Bartoccioni E, Scuderi F, Augugliaro A, Chiatamone Ranieri S, Sauchelli D, Alboino P, Marino M, Evoli A. HLA class II allele analysis in MuSK-positive myasthenia gravis suggests a role for DQ5. Neurology. 2009 Jan 13;72(2):195-7. doi: 10.1212/01.wnl.0000339103.08830.86.

Bedlack RS, Sanders DB. On the concept of myasthenic crisis. J Clin Neuromuscul Dis. 2002 Sep;4(1):40-2.

Ben Ammar A, Soltanzadeh P, Bauché S, Richard P, Goillot E, Herbst R, Gaudon K, Huzé C, Schaeffer L, Yamanashi Y, Higuchi O, Taly A, Koenig J, Leroy JP, Hentati F, Najmabadi H, Kahrizi K, Ilkhani M, Fardeau M, Eymard B, Hantaï D. A mutation causes MuSK reduced sensitivity to agrin and congenital myasthenia. PLoS One. 2013;8(1):e53826. doi: 10.1371/journal.pone.0053826. Epub 2013 Jan 9. Erratum in: PLoS One. 2013;8(9). doi: 10.1371/annotation/3ff2b918-c83c-4c6f-a2e2-4d91294ec92f.

Benatar M, Sanders DB, Wolfe GI, McDermott MP, Tawil R. Design of the efficacy of prednisone in the treatment of ocular myasthenia (EPITOME) trial. Ann N Y Acad Sci 2012; 1275**:** 17–22.

Bentires-Alj M, Paez JG, David FS, Keilhack H, Halmos B, Naoki K, Maris JM, Richardson A, Bardelli A, Sugarbaker DJ, Richards WG, Du J, Girard L, Minna JD, Loh ML, Fisher DE, Velculescu VE, Vogelstein B, Meyerson M, Sellers WR, Neel BG. Activating mutations of the noonan syndrome-associated SHP2/PTPN11 gene in human solid tumors and adult acutemyelogenou s leukemia. Cancer Res. 2004 Dec 15;64(24):8816-20.

Benveniste O, Hilton-Jones D. The role of rituximab in the treatment of myasthenia gravis. Eur Neurol Rev 2010; 5: 95–100.

Bergamin E, Hallock PT, Burden SJ, Hubbard SR. The cytoplasmic adaptor protein Dok7 activates the receptor tyrosine kinase MuSK via dimerization. Mol Cell. 2010; 39:100–109.

Blalock A, Harvey AM, Ford FR, Lilienthal JL. The treatment of myasthenia gravis by removal of the thymus gland. JAMA. 1941; 117:1529–33.

Borges LS, Ferns M. Agrin-induced phosphorylation of the acetylcholine receptor regulates cytoskeletal anchoring and clustering. J Cell Biol 2001 Apr 02;153(1):1-12.

Bromberg MB, Wald JJ, Forshew DA, Feldman EL, Albers JW. Randomized trial of azathioprine or prednisone for initial immunosuppressive trea tment of myasthenia gravis. J Neurol Sci. 1997 Sep 1;150(1):59-62.

Buckley C, Newsom-Davis J, Willcox N, Vincent A. Do titin and cytokine antibodies in MG patients predict thymoma or thymoma recurrence? Neurology. 2001 Nov 13;57(9):1579-82.

Bunda S, Burrell K, Heir P, Zeng L, Alamsahebpour A, Kano Y, Raught B, Zhang ZY, Zadeh G, Ohh M. Inhibition of SHP2-mediated dephosphorylation of Ras suppresses oncogenesis. Nat Commun. 2015 Nov 30;6:8859. doi: 10.1038/ncomms9859.

Burden SJ. Building the vertebrate neuromuscular synapse. J Neurobiol. 2002; 53:501–511.

Burges J, Wray DW, Pizzighella S, Hall Z, Vincent A. A myasthenia gravis plasma immunoglobulin reduces miniature endplate potentials at human endplates in vitro. Muscle Nerve. 1990 May;13(5):407-13.

Carr AS, Cardwell CR, McCarron PO, McConville J. A systematic review of population based epidemiological studies in Myasthenia Gravis. BMC Neurol. 2010 Jun 18;10:46. doi: 10.1186/1471-2377-10-46.

Chen F, Qian L, Yang ZH, Huang Y, Ngo ST, Ruan NJ, Wang J, Schneider C, Noakes PG, Ding YQ, Mei L, Luo ZG. Rapsyn interaction with calpain stabilizes AChR clusters at the neuromuscular junction. Neuron. 2007;55:247–260

Chen L, Sung SS, Yip ML, Lawrence HR, Ren Y, Guida WC, Sebti SM, Lawrence NJ, Wu J. Discovery of a novel shp2 protein tyrosine phosphatase inhibitor. Mol Pharmacol. 2006 Aug;70(2):562-70. Epub 2006 May 22.

Chen WH, Chiu HC, Hseih RP. Association of HLA-Bw46DR9 combination with juvenile myasthenia in Chinese. J Neurol Neurosurg Psychiatry. 1993;56:382–85.

Chung, W. S. & Barres, B. A. Selective remodeling: refining neural connectivity at the neuromuscular junction. PLoS Biol. 7, e1000185 (2009).

Cole RN, Ghazanfari N, Ngo ST, Gervásio OL, Reddel SW, Phillips WD. Patient autoantibodies deplete postsynaptic musclespecific kinase leading to disas sembly of the ACh receptor scaffold and myasthenia gravis in mice. J Physiol. 2010 Sep 1;588(Pt 17):3217-29. doi: 10.1113/jphysiol.2010.190298. Epub 2010 Jul 5.

Compston DAS, Vincent A, Newsom-Davis J, Batchelor JR. Clinical, pathological, HLA antigen and immunological evidence for disease heterogeneity in myasthenia gravis. Brain. 1980;103:579–601.

Cossins J, Belaya K, Zoltowska K, Koneczny I, Maxwell S, Jacobson L, Leite MI, Waters P, Vincent A, Beeson D.
The search for new antigenic targets in myasthenia gravis. Ann N Y Acad Sci. 2012 Dec;1275:123-8. doi: 10.1111/j.1749-6632.2012.06833.x. Review.

Coutinho A, Chapman K. The anti-inflammatory and immunosuppressive effects of glucocorticoids, recent developments and mechanistic insights. Mol Cell Endocrinol. 2011 Mar 15; 335(1): 2–13. doi: 10.1016/j.mce.2010.04.005

Cunnick JM, Mei L, Doupnik CA, and Wu J. Phosphotyrosines 627 and 659 of Gab1 constitute a bisphosphoryl tyrosine-based activation motif (BTAM) conferring binding and activation of SHP2. J Biol Chem. 2001. 276:24380–24387.

Deb TB, Wong L, Salomon DS, Zhou G, Dixon JE, Gutkind JS, Thompson SA, and Johnson GR. A common requirement for the catalytic activity and both SH2 domains of SHP-2 in mitogen-activated protein (MAP) kinase activation by the

ErbB family of receptors. A specific role for SHP-2 in map, but not c-Jun aminoterminal kinase activation. J Biol Chem. 1998. 273:16643–16646.

Drachman DB, Angus CW, Adams RN, Michelson JD, Hoffman GJ. Myasthenic antibodies cross-link acetylcholine receptors to accelerate degradation. N. Engl. J. Med., 298 (1978), pp. 1116-1122

E Kerty, A Elsais, Z Argov, A Evoli, NE Gilhus. EFNS/ENS guidelines for the treatment of ocular myasthenia gravis. Eur J Neurol, 21 (2014), pp. 687-693

Evoli A, Tonali PA, Padua L, Monaco ML, Scuderi F, Batocchi AP, Marino M, Bartoccioni E. Clinical correlates with anti-MuSK-Abs in generalized seronegative myasthenia gravis. Brain. 2003 Oct;126(Pt 10):2304-11. Epub 2003 Jun 23.
Evoli A. Clinical aspects of neuromuscular transmission disorders. Acta Neurol Scand Suppl. 2006;183:8-11. Review.4

Finn AJ, Feng G, Pendergast AM. Postsynaptic requirement for Abl kinases in assembly of the neuromuscular junction. Nat Neurosci 2003 Jul;6(7):717-23.

Flanagan-Steet, H., Fox, M. A., Meyer, D. & Sanes, J. R. Neuromuscular synapses can form in vivo by incorporation of initially aneural postsynaptic specializations. Development 132, 4471–4481 (2005).

Gajdos P, Chevret S, Toyka K. Plasma exchange for myasthenia gravis. Cochrane Database Syst Rev 2002, (4):CD002275.

Gallardo E, Martínez-Hernández E, Titulaer MJ, Huijbers MG, Martínez MA, Ramos A, Querol L, Díaz-Manera J, Rojas-García R, Hayworth CR, Verschuuren JJ, Balice-Gordon R, Dalmau J, Illa I. Cortactin autoantibodies in myasthenia gravis. Autoimmun Rev. 2014 Oct;13(10):1003-7. doi: 10.1016/j.autrev.2014.08.039. Epub 2014 Sep 3.

Gasperi C, Melms A, Schoser B, Zhang Y, Meltoranta J, Risson V, Schaeffer L, Schalke B, Kröger S. Anti-agrin autoantibodies in myasthenia gravis. Neurology. 2014 Jun 3;82(22):1976-83. doi: 10.1212/WNL.0000000000000478. Epub 2014 May 2.

Giraud M, Taubert R, Vandiedonck C, Ke X, Lévi-Strauss M, Pagani F, Baralle FE, Eymard B, Tranchant C, Gajdos P, Vincent A, Willcox N, Beeson D, Kyewski B, Garchon HJ. An IRF8-binding promoter variant and AIRE control CHRNA1 promiscuous expression in thymus. Nature. 2007 Aug 23;448(7156):934-7.

Giraud M, Vandiedonck C, Garchon HJ. Genetic factors in autoimmune myasthenia gravis. Ann N Y Acad Sci. 2008;1132:180–92.

Glass DJ, Bowen DC, Stitt TN, Radziejewski C, Bruno J, Ryan TE, Gies DR, Shah S, Mattsson K, Burden SJ, et al. Agrin acts via a MuSK receptor complex. Cell. 1996; 85:513–523.

Grob D, Brunner N, Namba T, Pagala M. Lifetime course of myasthenia gravis. Muscle Nerve. 2008;37:141–49.

Gronseth GS, Barohn RJ: Practice parameter: thymectomy for autoimmune myasthenia gravis (an evidence-based review): report of the Quality Standards Subcommittee of the American Academy of Neurology. Neurology 2000, 55:7–15.

Grosskopf S, Eckert C, Arkona C, Radetzki S, Böhm K, Heinemann U, Wolber G, von Kries JP, Birchmeier W, Rademann J. Selective inhibitors of the protein tyrosine phosphatase SHP2 block cellular motility and growth of cancer cells in vitro and in vivo. ChemMedChem. 2015 May;10(5):815-26. doi: 10.1002/cmdc.201500015. Epub 2015 Apr 15.

Guptill JT, Sanders DB, Evoli A. Anti-MuSK-Ab myasthenia gravis: clinical findings and response to treatment in two large cohorts. Muscle Nerve. 2011;44(1):36–40. doi: 10.1002/mus.22006.

Hallock PT, Xu CF, Park TJ, Neubert TA, Curran T, Burden SJ. Dok-7 regulates neuromuscular synapse formation by recruiting Crk and Crk-L. Genes Dev 2010 Nov 1;24(21):2451-61.

Heinemann S, Bevan S, Kullberg R, Lindstrom J, Rice J. Modulation of acetylcholine receptor by antibody against the receptor. Proc Natl Acad Sci U S A. 1977 Jul;74(7):3090-4.

Heldal AT, Owe JF, Gilhus NE, Romi F. Seropositive myasthenia gravis: a nationwide epidemiologic study. Neurology. 2009 Jul 14;73(2):150-1. doi: 10.1212/WNL.0b013e3181ad53c2.

Herbst R, Burden SJ. The juxtamembrane region of MuSK has a critical role in agrin-mediated signaling. EMBO J. 2000; 19:67–77.

Higuchi O, Hamuro J, Motomura M, Yamanashi Y. Autoantibodies to low-density lipoprotein receptor-related protein 4 in myasthenia gravis. Ann Neurol. 2011 Feb;69(2):418-22. doi: 10.1002/ana.22312.

Hoch W, McConville J, Helms S, Newsom-Davis J, Melms A, Vincent A. Auto-antibodies to the receptor tyrosine kinase MuSK in patients with myasthenia gravis without acetylcholine receptor antibodies. Nat Med. 2001 Mar;7(3):365-8.
Hoffacker V, Schultz A, Tiesinga JJ, Gold R, Schalke B, Nix W, Kiefer R, Muller-Hermelink HK, Marx A. Thymomas alter the T-cell subset composition in the blood: a potential mechanism for thymoma-associated autoimmune disease. Blood. 2000;96:3872–3879.

Huda S, Waters P, Woodhall M, Leite MI, Jacobson L, De Rosa A, Maestri M, Ricciardi R, Heckmann JM, Maniaol A, Evoli A, Cossins J, Hilton-Jones D, Vincent A. IgG-specific cell-based assay detects potentially pathogenic MuSK-

Ab-Abs in seronegative MG. Neurol Neuroimmunol Neuroinflamm. 2017 Jun 5;4(4):e357. doi: 10.1212/NXI.0000000000000357. eCollection 2017 Jul.

Hughes T. The early history of myasthenia gravis. Neuromuscul Disord. 2005 Dec;15(12):878-86. Epub 2005 Nov 9. Review.

Huijbers MG, Zhang W, Klooster R, Niks EH, Friese MB, Straasheijm KR, Thijssen PE, Vrolijk H, Plomp JJ, Vogels P, Losen M, Van der Maarel SM, Burden SJ, Verschuuren JJ.

MuSK IgG4 autoantibodies cause myasthenia gravis by inhibiting binding betwee n MuSK and LRP4. Proc Natl Acad Sci U S A. 2013 Dec 17;110(51):20783-8. doi: 10.1073/pnas.1313944110. Epub 2013 Dec 2.

Jacob S, Viegas S, Leite MI, Webster R, Cossins J, Kennett R, Hilton-Jones D, Morgan BP, Vincent A.
Presence and pathogenic relevance of antibodies to clustered acetylcholine recepto r in ocular and generalized myastheniagravis. Arch Neurol. 2012 Aug;69(8):994 1001. doi: 10.1001/archneurol.2012.437.

Janer M, Cowland A, Picard J, Campbell D, Pontarotti P, Newsom-Davis J, Bunce M, Welsh K, Demaine A, Wilson AG, Willcox N.
A susceptibility region for myasthenia gravis extending into the HLA-class I sector telomeric to HLA-C. Hum Immunol. 1999 Sep;60(9):909-17.

Jaretzki A 3rd, Barohn RJ, Ernstoff RM, Kaminski HJ, Keesey JC, Penn AS, Sanders DB. Myasthenia gravis: recommendations for clinical research standards. Task Force of the Medical Scientific Advisory Board of the Myasthenia Gravis Foundation of America. Ann Thorac Surg. 2000 Jul;70(1):327-34.

Keesey JC. Clinical evaluation and management of myasthenia gravis. Muscle Nerve. 2004 Apr;29(4):484-505. Review.

Keesey, J.C. 2002. “Crisis” in myasthenia gravis: an historical perspective. Muscle Nerve. 26:1-3.

Kerty E, Elsais A, Argov Z, Evoli A, Gilhus NE. EFNS/ENS guidelines for the treatment of ocular myasthenia gravis. Eur J Neurol; 2014: 21**:** 687–93.

Keung B, Robeson KR, DiCapua DB, Rosen JB, O'Connor KC, Goldstein JM, Nowak RJ. Long-term benefit of rituximab in MuSK autoantibody myasthenia gravis patients. J Neurol Neurosurg Psychiatry. 2013 Dec;84(12):1407-9. doi: 10.1136/jnnp-2012-303664. Epub 2013 Jun 12

Klein R, Marx A, Ströbel P, Schalke B, Nix W, Willcox N. Autoimmune associations and autoantibody screening show focused recognition in patient subgroups with generalized myasthenia gravis. Hum Immunol. 2013 Sep;74(9):1184-93. doi: 10.1016/j.humimm.2013.06.020. Epub 2013 Jun 18.

Klooster R, Plomp JJ, Huijbers MG, Niks EH, Straasheijm KR, Detmers FJ, Hermans PW, Sleijpen K, Verrips A, Losen M, Martinez-Martinez P, De Baets MH, van der Maarel SM, Verschuuren JJ. Muscle-specific kinase myasthenia gravis IgG4 autoantibodies cause severe neuromuscula r junction dysfunction in mice. Brain. 2012 Apr;135(Pt 4):1081-101. doi: 10.1093/brain/aws025. Epub 2012 Mar 6.

Koneczny I, Cossins J, Waters P, Beeson D, Vincent A. MuSK myasthenia gravis IgG4 disrupts the interaction of LRP4 with MuSK but both IgG4 and IgG1-3 can disperse preformedagrin-independent AChR clusters. PLoS One. 2013 Nov 7;8(11):e80695. doi: 10.1371/journal.pone.0080695. eCollection 2013.

Koneczny I, Stevens JA, De Rosa A, Huda S, Huijbers MG, Saxena A, Maestri M, Lazaridis K, Zisimopoulou P, Tzartos S, Verschuuren J, van der Maarel SM, van Damme P, De Baets MH, Molenaar PC, Vincent A, Ricciardi R, Martinez-Martinez P, Losen M. IgG4 autoantibodies against muscle-specific kinase undergo

Fab-arm exchange in myasthenia gravis patients. J Autoimmun. 2017 Feb;77:104-115. doi: 10.1016/j.jaut.2016.11.005. Epub 2016 Dec 10.

Küçükerden M, Huda R, Tüzün E, Yılmaz A, Skriapa L, Trakas N, Strait RT, Finkelman FD, Kabadayı S, Zisimopoulou P, Tzartos S, Christadoss P. MuSK induced experimental autoimmune myasthenia gravis does not require IgG1 antibody to MuSK. J Neuroimmunol. 2016 Jun 15;295-296:84-92. doi: 10.1016/j.jneuroim.2016.04.003. Epub 2016 Apr 11.

Kummer TT, Misgeld T, Sanes JR. Assembly of the postsynaptic membrane at the neuromuscular junction: paradigm lost. Curr Opin Neurobiol. 2006; 16:74–82.
Lee WY, Free CR, Sine SM. Binding to gating transduction in nicotinic receptors: Cys-loop energetically couples to pre-M1 and M2-M3 regions. J Neurosci 2009 Mar 11;29(10):3189-99.

Lee Y, Rudell J, Ferns M. Rapsyn interacts with the muscle acetylcholine receptor via alpha-helical domains in the alpha, beta, and epsilon subunit intracellular loops. Neuroscience 2009 Sep 29;163(1):222-32.

Leite MI, Jacob S, Viegas S, Cossins J, Clover L, Morgan BP, Beeson D, Willcox N, Vincent A. IgG1 antibodies to acetylcholine receptors in 'seronegative' myasthenia gravis. Brain. 2008 Jul;131(Pt 7):1940-52. doi: 10.1093/brain/awn092. Epub 2008 May 31.

Lennon VA, Lambert EH. Monoclonal autoantibodies to acetylcholine receptors: evidence for a dominant idiotype and requirement of complement for pathogenicity. Ann N Y Acad Sci. 1981;377:77-96.

Lin W, Dominguez B, Yang J, Aryal P, Brandon EP, Gage FH, Lee KF. Neurotransmitter acetylcholine negatively regulates neuromuscular synapse formation by a Cdk5-dependent mechanism. Neuron. 2005 May 19;46(4):569-79.

Maddison P, McConville J, Farrugia ME, Davies N, Rose M, Norwood F, Jungbluth H, Robb S, Hilton-Jones D. The use

of rituximab in myasthenia gravis and Lambert-Eaton myasthenic syndrome. J Neurol Neurosurg Psychiatry. 2011 Jun;82(6):671-3. doi: 10.1136/jnnp.2009.197632. Epub 2010 Apr 14.

Marx A, Pfister F, Schalke B, Saruhan-Direskeneli G, Melms A, Ströbel P. The different roles of the thymus in the pathogenesis of the various myasthenia gravis subtypes. Autoimmun Rev. 2013 Jul;12(9):875-84. doi: 10.1016/ j.autrev.2013.03.007. Epub 2013 Mar 25. Review.

Marx A, Schultz A, Wilisch A, Helmreich M, Nenninger R, Müller-Hermelink HK. Paraneoplastic autoimmunity in thymus tumors. Dev Immunol. 1998;6(1-2):129-40.

Matsui N, Nakane S, Nakagawa Y, Kondo K, Mitsui T, Matsumoto T, Arisawa K, Kaji R. Increasing incidence of elderly onset patients with myasthenia gravis in a local area of Japan. J Neurol Neurosurg Psychiatry. 2009 Oct;80(10):1168-71. doi: 10.1136/jnnp.2008.152637.

Matsuki K, Juji T, Tokunaga K, Takamizawa M, Maeda H, Soda M, Nomura Y, Segawa M. HLA antigens in Japanese patients with myasthenia gravis. J Clin Invest. 1990 Aug;86(2):392-9.

Matthews I, Chen S, Hewer R, McGrath V, Furmaniak J, Rees Smith B. Muscle-specific receptor tyrosine kinase autoantibodies—a new immunoprecipitation assay. Clin. Chim. Acta, 348 (2004), pp. 95-99

McConville J, Farrugia ME, Beeson D, Kishore U, Metcalfe R, Newsom-Davis J, VincentA.Detection and characterization of MuSK-
Abs in seronegative myasthenia gravis. Ann Neurol. 2004 Apr;55(4):580-4.

Meriggioli MN, Rowin J, Richman JG, Leurgans S. Mycophenolate mofetil for myasthenia gravis: a double-blind, placebocontrolled pilot study. Ann N Y Acad Sci 2003, 998:494–499.

Meriggioli MN, Sanders DB. Autoimmune myasthenia gravis: emerging clinical and biological heterogeneity. Lancet Neurol. 2009 May;8(5):475-90. doi: 10.1016/S1474-4422(09)70063-8. Review.

Misgeld T, Kummer TT, Lichtman JW, Sanes JR. Agrin promotes synaptic differentiation by counteracting an inhibitory effect of neurotransmitter. Proc Natl Acad Sci U S A. 2005 Aug 2;102(31):11088-93. Epub 2005 Jul 25

Mishina M, Takai T, Imoto K, Noda M, Takahashi T, Numa S, et al. Molecular Distinction between Fetal and Adult Forms of Muscle Acetylcholine-Receptor. Nature 1986 May 22;321(6068):406-11

Mittaud P, Marangi PA, Erb-Vogtli S, Fuhrer C. Agrin-induced activation of acetylcholine receptor-bound Src family kinases requires Rapsyn and correlates with acetylcholine receptor clustering. J Biol Chem 2001 Apr 27;276(17):14505-13.

Mori S, Kubo S, Akiyoshi T, Yamada S, Miyazaki T, Hotta H, Desaki J, Kishi M, Konishi T, Nishino Y, Miyazawa A, Maruyama N, Shigemoto K. Antibodies against musclespecific kinase impair both presynaptic and postsynapti c functions in a murine model of myasthenia gravis. Am J Pathol. 2012 Feb;180(2):798-810. doi: 10.1016/j.ajpath.2011.10.031. Epub 2011 Dec 3.

Morsch M, Reddel SW, Ghazanfari N, Toyka KV, Phillips WD. Pyridostigmine but not 3,4-diaminopyridine exacerbates ACh receptor loss and myasthenia induced in mice by muscle-specific kinase autoantibody. J Physiol. 2013 May 15;591(10):2747-62. doi: 10.1113/jphysiol.2013.251827. Epub 2013 Feb 25.

Mukhtasimova N, Lee WY, Wang HL, Sine SM. Detection and trapping of intermediate states priming nicotinic receptor channel opening. Nature 2009 May 21;459(7245):451-4.

Nations SP, Wolfe GI, Amato AA, Jackson CE, Bryan WW, Barohn RJ. Distal myasthenia gravis. Neurology 1999;52:632–34.

Neel BG, Gu H, and Pao L (2003) The 'Shp'ing news: SH2 domain-containing tyrosine phosphatases in cell signaling. Trends Biochem Sci 28:284–293.

Nishimune H, Valdez G, Jarad G, Moulson CL, Müller U, Miner JH, Sanes JR. Laminins promote postsynaptic maturation by an autocrine mechanism at the neuromuscular junction. J Cell Biol. 2008 Sep 22;182(6):1201-15. doi: 10.1083/jcb.200805095. Epub 2008 Sep 15.

Niks EH, Kuks JB, Roep BO, Haasnoot GW, Verduijn W, Ballieux BE, De Baets MH, Vincent A, Verschuuren JJ. Strong association of MuSK antibody-positive myasthenia gravis and HLA-DR14-DQ5. Neurology. 2006 Jun 13;66(11):1772-4.

Oger J, Kaufman R, Berry K. Acetylcholine receptor antibodies in myasthenia gravis: use of a qualitative assay for diagnostic purposes. Can J Neurol Sci, Aug 1987. 14 (3) pp. 297-302

Pakzad Z, Aziz T, Oger J. Increasing incidence of myasthenia gravis among elderly in British Columbia, Canada. Neurology. 2011;76(17):1526–1528. doi: 10.1212/WNL.0b013e318217e735.

Palace J, Newsom-Davis J, Lecky B. A randomized double-blind trial of prednisolone alone or with azathioprine in myasthenia gravis. *Neurology* 1998; 50: 1778–83.

Panzer, J. A., Song, Y. & Balice-Gordon, R. J. *In vivo* imaging of preferential motor axon outgrowth to and synaptogenesis at prepatterned acetylcholine receptor clusters in embryonic zebrafish skeletal muscle. J Neurosci. 2006 Jan 18;26(3):934-47.

Pasnoor M, Wolfe GI, Nations S, Trivedi J, Barohn RJ, Herbelin L, McVey A, Dimachkie M, Kissel J, Walsh R, Amato A, Mozaffar T, Hungs M, Chui L, Goldstein J, Novella S, Burns T, Phillips L, Claussen G, Young A, Bertorini T,

Oh S. Clinical findings in MuSK-antibody positive myasthenia gravis: a U.S. experience. Muscle Nerve. 2010 Mar;41(3):370-4. doi: 10.1002/mus.2153

Patel V, Oh A, Voit A, Sultatos LG, Babu GJ, Wilson BA, Ho M, McArdle JJ. Altered active zones, vesicle pools, nerve terminal conductivity,and morphology d uring experimental MuSK myastheniagravis. PLoS One. 2014 Dec 1;9(12):e110571. doi: 10.1371/journal.pone.0110571. eCollection 2014.

Patrick J, Lindstrom J, Culp B, McMillan J. Studies on purified eel acetylcholine receptor and anti-acetylcholine receptor antibody. Proc Natl Acad Sci 1973; U S A, 70 (12), pp. 3334-3338

Pearce JM. Mary Broadfoot Walker (1888-1974): a historic discovery in myasthenia gravis. Eur Neurol. 2005;53(1):51-3. Epub 2005 Mar 1.

Pevzner A, Schoser B, Peters K, Cosma NC, Karakatsani A, Schalke B, Melms A, Kröger S. Anti-LRP4 autoantibodies in AChR- and MuSK-antibody-negative myasthenia gravis. J Neurol. 2012 Mar;259(3):427-35. doi: 10.1007/s00415-011-6194-7. Epub 2011 Aug 5.

Phillips LH 2nd, Torner JC. Epidemiologic evidence for a changing natural history of myasthenia gravis. Neurology. 1996 Nov;47(5):1233-8.

Plomp JJ, Van Kempen GT, De Baets MB, Graus YM, Kuks JB, Molenaar PC. Acetylcholine release in myasthenia gravis: regulation at single end-plate level. Ann Neurol. 1995 May;37(5):627-36.

Qian YK, Chan AW, Madhavan R, Peng HB. The function of Shp2 tyrosine phosphatase in the dispersal of acetylcholine receptor clusters. BMC Neurosci. 2008 Jul 23;9:70. doi: 10.1186/1471-2202-9-70.

Qureshi AI, Choudhry MA, Akbar MS, Mohammad Y, Chua HC, Yahia AM, Ulatowski JA, Krendel DA, Leshner RT. Plasma exchange versus intravenous

immunoglobulin treatment in myasthenic crisis. Neurology. 1999 Feb;52(3):629-32.

Rodolico C, Toscano A, Autunno M, Messina S, Nicolosi C, Aguennouz M, Laurà M, Girlanda P, Messina C, Vita G. Limb-girdle myasthenia: clinical, electrophysiological and morphological features in fa milial and autoimmune cases. Neuromuscul Disord. 2002 Dec;12(10):964-9.

Rodríguez Cruz PM, Al-Hajjar M, Huda S, Jacobson L, Woodhall M, Jayawant S, Buckley C, Hilton-Jones D, Beeson D, Vincent A, Leite MI, Palace J. Clinical Features and Diagnostic Usefulness of Antibodies to Clustered Acetylcho line Receptors in the Diagnosis of Seronegative Myasthenia Gravis. JAMA Neurol. 2015 Jun;72(6):642-9. doi: 10.1001/jamaneurol.2015.0203

Ronager J, Ravnborg M, Hermansen I, Vorstrup S. Immunoglobulin treatment versus plasma exchange in patients with chronic moderate to severe myasthenia gravis. Artif Organs 2001, 25:967–973.

Ruff RL, Lennon VA. End-plate voltage-gated sodium channels are lost in clinical and experimental myasthenia gravis. Ann Neurol. 1998 Mar;43(3):370-9.
Sanders DB, El-Salem K, Massey JM, McConville J, Vincent A. Clinical aspects of MuSK-Ab positive seronegative MG. Neurology. 2003 Jun 24;60(12):1978-80.

Sanders DB, Stalberg EV. AAEM minimonograph # single fiber EMG, Don sanders and Erik V stalberg. Muscle nerve. 1996;19:1069–83.

Sarrigiannis PG, Kennett RP, Read S, Farrugia ME. Single fiber EMG with a concentric needle electrode validation in myasthenia gravis. Muscle Nerve. 2006;33:61–5.

Schneeberger VE, Ren Y, Luetteke N, Huang Q, Chen L, Lawrence HR, Lawrence NJ, Haura EB, Koomen JM, Coppola D, Wu J.

Inhibition of Shp2 suppresses mutant EGFR-induced lung tumors in transgenic mouse model of lung adenocarcinoma. Oncotarget. 2015 Mar 20;6(8):6191-202.

Shen C, Lu Y, Zhang B, Figueiredo D, Bean J, Jung J, Wu H, Barik A, Yin DM, Xiong WC, Mei L. Antibodies against low-density lipoprotein receptor-related protein 4 induce myasthenia gravis. J Clin Invest. 2013 Dec;123(12):5190-202. doi: 10.1172/JCI66039. Epub 2013 Nov 8.

Shigemoto K, Kubo S, Maruyama N, Hato N, Yamada H, Jie C, Kobayashi N, Mominoki K, Abe Y, Ueda N, Matsuda S. Induction of myasthenia by immunization against muscle-specific kinase. J Clin Invest. 2006 Apr;116(4):1016-24. Epub 2006 Mar 23.

Skeie GO, Apostolski S, Evoli A, Gilhus NE, Illa I, Harms L, Hilton-Jones D, Melms A, Verschuuren J, Horge HW; European Federation of Neurological Societies. Guidelines for treatment of autoimmune neuromuscular transmission disorders. Eur J Neurol. 2010 Jul;17(7):893-902. doi: 10.1111/j.1468-1331.2010.03019.x. Epub 2010 Apr 12.

Skjei KL, Lennon VA, Kuntz NL. Muscle specific kinase autoimmune myasthenia gravis in children: a case series. *Neuromuscul Disord* 2013; 23**:** 874-82.

Slater CR. The functional organization of motor nerve terminals. Prog Neurobiol. 2015 Nov;134:55-103. doi: 10.1016/j.pneurobio.2015.09.004. Epub 2015 Oct 9. Review.

Somnier FE. Increasing incidence of late-onset anti-AChR antibody seropositive myasthenia gravis. Neurology. 2005 Sep 27;65(6):928-30.

Song M, Park JE, Park SG, Lee DH, Choi HK, Park BC, Ryu SE, Kim JH, Cho S. NSC-87877, inhibitor of SHP-1/2 PTPs, inhibits dual-specificity phosphatase 26 (DUSP26). Biochem Biophys Res Commun. 2009 Apr 17;381(4):491-5. doi: 10.1016/j.bbrc.2009.02.069. Epub 2009 Feb 20.

Stiegler AL, Burden SJ, Hubbard SR. Crystal structure of the agrin-responsive immunoglobulin-like domains 1 and 2 of the receptor tyrosine kinase MuSK. J Mol Biol. 2006; 364:424–433.

Strobel P, Chuang WY, Chuvpilo S, Zettl A, Katzenberger T, Kalbacher H, Rieckmann P, Nix W, Schalke B, Gold R, Muller-Hermelink HK, Peterson P, Marx A. Common cellular and diverse genetic basis of thymoma-associated myasthenia gravis: role of MHC class II and AIRE genes and genetic polymorphisms. Ann NY Acad Sci. 2008;1132:143–156. doi: 10.1196/annals.1405.018

Suzuki S, Baba A, Kaida K, Utsugisawa K, Kita Y, Tsugawa J, Ogawa G, Nagane Y, Kuwana M, Suzuki N. Cardiac involvements in myasthenia gravis associated with anti-Kv1.4 antibodies. Eur J Neurol. 2014 Feb;21(2):223-30. doi: 10.1111/ene.12234. Epub 2013 Jul 5.

Tan CS, Koralnik IJ. Progressive multifocal leukoencephalopathy and other disorders caused by JC virus: clinical features and pathogenesis. Lancet Neurol. 2010 Apr;9(4):425-37. doi: 10.1016/S1474-4422(10)70040-5. Review.

Tartaglia M and Gelb BD. Germ-line and somatic PTPN11 mutations in human disease. Eur J Med Genet. 2005. 48:81–96.

Thiruppathi M, Rowin J, Ganesh B, Sheng JR, Prabhakar BS, Meriggioli MN. Impaired regulatory function in circulating CD4(+)CD25(high)CD127(low/−) T cells in patients with myasthenia gravis. Clin Immunol. 2012;145:209–223. doi: 10.1016/j.clim.2012.09.012.

Till JH, Becerra M, Watty W, Lu Y, Ma Y, Neubert TA, Burden SJ, Hubbard SR. Crystal structure of the MuSK tyrosine kinase: insights into receptor autoregulation. Structure. 2002; 10:1187–1196.

Tindall RS, Phillips JT, Rollins JA, Wells L, Hall K. A clinical therapeutic trial of cyclosporine in myasthenia gravis. Ann N Y Acad Sci. 1993 Jun 21;681:539-51.

Tüzün E, Christadoss P. Complement associated pathogenic mechanisms in myasthenia gravis.Autoimmun Rev. 2013 Jul;12(9):904-11. doi: 10.1016/j.autrev.2013.03.003. Epub 2013 Mar 26. Review.

Viegas S, Jacobson L, Waters P, Cossins J, Jacob S, Leite MI, Webster R, Vincent A. Passive and active immunization models of MuSK-Ab positive myasthenia: electrophysiological evidence for pre and postsynaptic de fects. Exp Neurol. 2012 Apr; 234(2):506-12. doi: 10.1016/j.expneurol.2012.01.025. Epub 2012 Feb 3.

Vincent A, Clover L, Buckley C, Grimley Evans J, Rothwell PM; UK Myasthenia Gravis Survey. Evidence of underdiagnosis of myasthenia gravis in older people. J Neurol Neurosurg Psychiatry. 2003 Aug;74(8):1105-8.

Vincent A, Leite MI Neuromuscular junction autoimmune disease: muscle specific kinase antibodies and treatments for myasthenia gravis. Curr Opin Neurol. 2005. 18(5):519–525

Vincent A, Leite MI, Farrugia ME, Jacob S, Viegas S, Shiraishi H, Benveniste O, Morgan BP, Hilton-Jones D, Newsom-Davis J, Beeson D, Willcox N. Myasthenia gravis seronegative for acetylcholine receptor antibodies. Ann N Y Acad Sci. 2008;1132:84-92. doi: 10.1196/annals.1405.020.

Vincent A. Unravelling the pathogenesis of myasthenia gravis. Nat Rev Immunol. 2002 Oct;2(10):797-804. Review.

Weidoff PM Jr, McNamee MG, Wilson BW. Alteration of acetylcholine receptor and acetylcholinesterase metabolism by actinomycin D in cultured muscle cells. Can J Physiol Pharmacol. 1981 Jun;59(6):580-5.

Wendell LC, Levine JM. Myasthenic crisis. Neurohospitalist. 2011 Jan;1(1):16-22. doi: 10.1177/1941875210382918.

Weston C, Gordon C, Teressa G, Hod E, Ren XD, Prives J. Cooperative regulation by Rac and Rho of agrin-induced acetylcholine receptor clustering in muscle cells. J Biol Chem 2003 Feb 21;278(8):6450-5.

Willcox N, Leite MI, Kadota Y, Jones M, Meager A, Subrahmanyam P, Dasgupta B, Morgan BP, Vincent A. Autoimmunizing mechanisms in thymoma and thymus. Ann NY Acad Sci. 2008;1132:163–173. doi: 10.1196/annals.1405.021.

Wolfe GI, Kaminski HJ, Cutter GR. Randomized Trial of Thymectomy in Myasthenia Gravis. N Engl J Med. 2016 Nov 17;375(20):2006-2007. doi: 10.1056/NEJMc1611704.

Wyatt, R. M. & Balice-Gordon, R. J. Activity-dependent elimination of neuromuscular synapses. J. Neurocytol. 32, 777–794 (2003).

Ye B, Tantai JC, Li W, Ge XX, Feng J, Cheng M, Zhao H. Video-assisted thoracoscopic surgery versus robotic-assisted thoracoscopic surgery in the surgical treatment of Masaokastage I thymoma. World J Surg Oncol. 2013 Jul 17;11:157. doi: 10.1186/1477-7819-11-157.

Yi JS, Decroos EC, Sanders DB, Weinhold KJ, Guptill JT. Prolonged B-cell depletion in MuSK myasthenia gravis following rituximab treatment. Muscle Nerve. 2013 Dec;48(6):992-3. doi: 10.1002/mus.24063. Epub 2013 Oct 7.

Yu YL, Hawkins BR, Ip MS, Wong V, Woo E: Myasthenia gravis in Hong Kong Chinese: Epidemiology and adult disease**.** *Acta Neurol Scand* 1992, 86(2):113-119.

Yumoto, N., Kim, N. & Burden, S. J. LRP4 is a retrograde signal for presynaptic differentiation at neuromuscular synapses. Nature 489, 438–442 (2012).

Zambelis T, Kokotis P, Karandreas N. Repetitive nerve stimulation of facial and hypothenar muscles: relative sensitivity in different myasthenia gravis subgroups. Eur Neurol. 2011;65(4):203-7. doi: 10.1159/000324915. Epub 2011 Mar 17.

Zhang B, Luo S, Wang Q, Suzuki T, Xiong WC, Mei L. LRP4 serves as a coreceptor of agrin. Neuron. 2008 Oct 23;60(2):285-97. doi: 10.1016/j.neuron.2008.10.006.

Zhang B, Tzartos JS, Belimezi M, Ragheb S, Bealmear B, Lewis RA, Xiong WC, Lisak RP, Tzartos SJ, Mei L. Autoantibodies to lipoprotein-related protein 4 in patients with double-seronegative myasthenia gravis. Arch Neurol. 2012 Apr;69(4):445-51. doi: 10.1001/archneurol.2011.2393. Epub 2011 Dec 12.

Zhang X, Yang M, Xu J, Zhang M, Lang B, Wang W, Vincent A. Clinical and serological study of myasthenia gravis in HuBei Province, China.J N eurol Neurosurg Psychiatry. 2007 Apr;78(4):386-90. Epub 2006 Nov 6.

Zhang B, Shen C, Bealmear B, Ragheb S, Xiong WC, Lewis RA, Lisak RP, Mei L. Autoantibodies to agrin in myasthenia gravis patients. PLoS One. 2014 Mar 14;9(3):e91816. doi: 10.1371/journal.pone.0091816. eCollection 2014.

Zhang, W, Coldefy AS, Hubbard SR, Burden SJ. Agrin binds to the N-terminal region of LRP4 protein and stimulates association between LRP4 and the first immunoglobulin-like domain in muscle-specific kinase (MuSK). J. Biol. Chem. 286, 40624–40630 (2011).

Zhao XT, Qian YK, Chan AW, Madhavan R, Peng HB. Regulation of ACh receptor clustering by the tyrosine phosphatase Shp2. Dev Neurobiol. 2007 Nov;67(13):1789-801.

Zinman L, Ng E, Bril V: IV immunoglobulin in patients with myasthenia gravis: a randomized controlled trial. Neurology 2007. 68:837–841.

Zisimopoulou P, Evangelakou P, Tzartos J, Lazaridis K, Zouvelou V, Mantegazza R, Antozzi C, Andreetta F, Evoli A, Deymeer F, Saruhan-Direskeneli G, Durmus H, Brenner T, Vaknin A, Berrih-Aknin S, Frenkian Cuvelier M, Stojkovic T, DeBaets M, Losen M, Martinez-Martinez P, Kleopa KA, Zamba-Papanicolaou E, Kyriakides T, Kostera-Pruszczyk A, Szczudlik P, Szyluk B, Lavrnic D, Basta I, Peric S, Tallaksen C, Maniaol A, Tzartos SJ. A comprehensive analysis of the epidemiology and clinical characteristics of anti-LRP4 in myasthenia gravis. J Autoimmun. 2014 Aug;52:139-45. doi: 10.1016/j.jaut.2013.12.004. Epub 2013 Dec 24.

Zoltowska Katarzyna M, Belaya K, Leite M, Patrick W, Vincent A, Beeson D. Collagen Q--a potential target for autoantibodies in myasthenia gravis. J Neurol Sci. 2015 Jan 15;348(1-2):241-4. doi: 10.1016/j.jns.2014.12.015. Epub 2014 Dec 18.

Zong Y, Zhang B, Gu S, Lee K, Zhou J, Yao G, Figueiredo D, Perry K, Mei L, Jin R. Structural basis of agrin-LRP4-MuSK signaling. Genes Dev. 2012; 26:247–258.

Zuber B, Unwin N. Structure and superorganization of acetylcholine receptorrapsyn complexes. Proc Natl Acad Sci U S A 2013 Jun 25;110(26):10622-7.